NEUTRONS FOR SOCIETY

INSTITUT LAUE-LANGEVIN

Annual Report 2021

Annual Report 2021

INSTITUT LAUE-LANGEVIN


© ILL/Kaptis

Contents

Publishing information

Editors:
Giovanna Cicognani and Jacques Jestin

Production team:
Giovanna Cicognani and Virginie Guerard

Scientific advisors:
Markus Appel, Ketty Beauvois, Ursula Bengaard Hansen, Laura Cañadillas-Delgado, Orsolya Czakkel, Lukas Helfen, Olga Matsarskaia, Caterina Michelagnoli, Tatiana Morozova, Jacques Ollivier.

Design:
Morton Ward Limited

Photography:
S. Claisse – ILL (unless otherwise specified), and C. Tresca (ILL's Directors' portraits)

Further copies can be obtained from:
Institut Laue-Langevin
Communication Unit
CS 20156, F-38042 Grenoble Cedex 9
communication@ill.eu
www.ill.eu

FOREWORD


© L. Thion

ON 31 August 2021, the ILL reached the remarkable landmark of 50 years of science and innovation providing sustained and outstanding service to the global neutron community. During this period, the ILL's large, diverse and dynamic user community has been able to solve many of nature's mysteries and make important contributions to societal challenges, thanks to the unique exploratory capacities of neutrons. On behalf of the ILL Steering Committee, we congratulate the ILL! Over these 50 years the Institute has been a truly worthwhile investment for science and innovation and a beacon for collaboration in Europe.

And the Institute is still going strong! The re-qualification of the reactor vessel was an important milestone for the operation of the high-flux reactor and was successfully completed on 19 January 2021. Despite the pandemic, three reactor cycles providing 176 days of beamtime were run, with the ILL having ensured that everything was in place to allow the experiments to be performed with remote access.

The long shutdown that began in the autumn of 2021 will continue through most of 2022. This is part of the ILL2023 programme to make the ILL fit for the future by maintaining and upgrading the neutron source, meeting the latest safety standards and completing the Endurance programme. It includes replacing key reactor components such as the reactor chimney, renewing the H1–H2 beam tube and completing several major Endurance guide and instrument projects. Our Associates have made a major effort to support the Endurance programme, but that this programme can be carried out in all its scope despite difficult financial conditions is only possible thanks to the continued support of our Scientific Member countries, which between them now contribute about a quarter of the ILL budget. We look forward to a rejuvenated flagship when this ambitious maintenance and modernisation programme is completed.

An important and long-prepared event occurred on 15 September, when the governments of France, Germany and the UK signed a formal agreement to extend the original 1971 inter-governmental Convention for a further 10 years. This is clear recognition that the ILL, with its high-flux reactor and instrument modernisation programmes, remains at the forefront of neutron research. With this extension, the partners demonstrate the crucial importance to their countries of research with neutrons and the contribution it has made to solving the most pressing problems facing society. When the ongoing work under the ILL2023 programme is completed, a rejuvenated ILL will be able to focus on delivering neutrons to science, with regular reactor operations and much more powerful instrumentation, so that the investments made in recent years pay off scientifically.

A new management team will lead the ILL into this approaching phase of boosted scientific productivity. With Paul Langan as Director of the ILL, Jacques Jestin as Head of the Science Division, Andreas Meyer as Associate Director leading the Projects and Techniques Division, and Jérôme Estrade as Associate Director at the head of the Reactor Division, the ILL has a team of excellent scientists for these important responsibilities. Our great thanks go to the departing directors, Helmut Schober and Mark Johnson, who have handed the ILL over in excellent condition. For the benefit of the entire neutron community, we especially wish Helmut Schober the best of luck as the new Director General of the ESS.

Finally, on behalf of the entire Steering Committee, we would like to express our sincere gratitude to the ILL's staff for their commitment and dedication under the difficult pandemic conditions, and to the scientific users throughout Europe for the support they have given to the ILL.

Thomas Brückel & **Astrid Lambrecht**
ILL Steering Committee Chairs in 2021

WE are moving into an exciting new transitional phase for the ILL, and what we do in the next three years will be decisive in shaping our future. During this phase, the ILL will begin completing and pivoting away from two decades of large campaigns of reactor and instrument improvements, and turn towards fully exploiting our modern scientific infrastructure and collaborative research environment in order to deliver the most exciting and impactful science. The ILL that we build today will provide future researchers with unprecedented capabilities for neutron science at a safe, reliable and sustainable high-flux reactor, for the decade to come and beyond.

Two important developments in 2021 signalled our advance into this phase. First, completion of the third reactor cycle in October heralded the start of a carefully planned, 14-month-long, reactor shutdown. This long shutdown is required for both a large and complex programme of work (referred to as ILL2023) to maintain and improve the reactor, and to complete the Endurance instrument upgrade programme. Work is progressing well due to our growing excellence in project management and execution, and to the full engagement of ILL personnel especially. Second, in September the governments of Associate countries France, Germany and the UK signed a 6th protocol that extends the original 1971 convention to operate the ILL to 2033. Its signing reflects the Associates' strong belief in the importance of neutron science. It also ensures that researchers will fully benefit from the large increases in instrument performance delivered by the Millennium and Endurance programmes in their continuing quest for breakthrough discoveries. We now have a clear long-term perspective to map out our future science strategy.

That future science strategy must align with the construction in Lund of the European Spallation Source (ESS), which will provide much-needed additional neutron scattering capabilities that are expected to eventually match or exceed some of those of the ILL. We will offer our scientific and technical expertise, as well as 50 years of operational experience, to help the ESS deliver those capabilities to researchers as soon as possible. However, we must also recognise that over the period of the newly signed protocol the ILL will have one of the most powerful suites of upgraded neutron instruments that Europe has seen so far. I believe that our biggest challenge is to be ready to fully seize the opportunity that lies ahead to deliver the best science possible with this instrument suite.

In 2021, despite the pandemic, our personnel safely operated the ILL over the largest numbers of neutron days and supported the largest number of experiments in a decade. The scientific highlights in this report illustrate important types of scientific information that can only be provided by neutron experiments. Those experiments were driven by an innovative and creative research community motivated by the desire to advance knowledge across broad areas of science. They were enabled by personnel from various ILL services and benefitted from the collaboration of our scientific staff.

Some of the highlights in this report reflect a growing emphasis in modern science on multidisciplinary teams using a variety of complementary experimental, computational and analytical techniques to solve increasingly complex problems. As we adapt to this changing scientific environment, we can position the ILL so that it continues to thrive as an exciting and dynamic part of an extended, collaborative, European research infrastructure, ready to tackle the most challenging problems we face in areas such as health, clean and efficient energy, and green technologies.

Finally, the achievements highlighted in this report reflect the commitment and professionalism of all ILL services and personnel, working under additional burdens, constraints and uncertainties imposed by the COVID-19 pandemic. By way of example, I would like to mention the work of staff from our medical centre who stepped up to administer hundreds of COVID-19 tests and doses of vaccines in their relentless efforts to keep us safe. Our staff have given a lot over the past year, and I greatly look forward to a time in the future when we can pause as an organisation and take the opportunity to celebrate and reward those outstanding contributions.

Paul Langan
ILL Director


© L. Thion

WHAT IS THE ILL

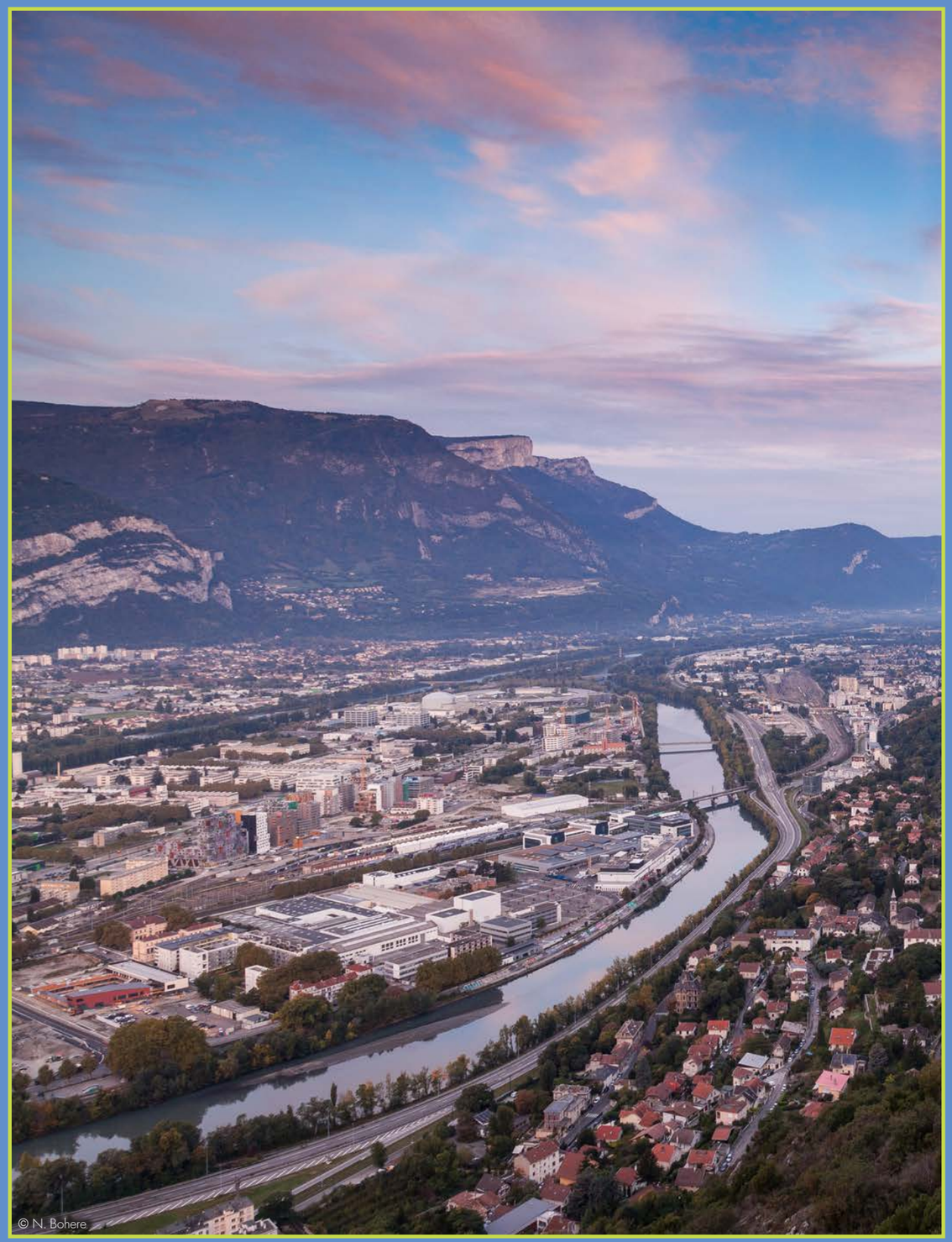

© N. Bohere

About the ILL

The Institut Laue Langevin (ILL) is an international research centre providing world-leading facilities in neutron science and technology. Neutrons are used at the ILL to probe the microscopic structure and dynamics of a broad range of materials at molecular, atomic and nuclear level.

The ILL operates the most intense neutron source in the world, a 58.3 MW nuclear reactor designed for high brightness. The reactor normally functions round-the-clock for four 50-day cycles per year, supplying neutrons to a suite of 40 high-performance instruments constantly maintained at the highest state of the art.

The ILL is owned by its three founding countries—France, Germany and the UK. These three Associate countries contributed some 72 M€ to the Institute in 2021, a sum enhanced by significant contributions from the ILL's Scientific Member countries—Austria, Belgium, the Czech Republic, Denmark, Italy, Poland, Slovakia, Slovenia, Spain, Sweden and Switzerland. As a result, the ILL's overall budget in 2021 amounted to about 105 M€.

As a service institute, the ILL makes its facilities and expertise available to visiting scientists. It has a global user community of about 2 000 researchers from almost 40 countries who come to work at the ILL every year. The 850 experiments they perform annually are pre-selected by a scientific review committee. Between 550 and 600 scientific papers are published annually, following the treatment and interpretation of data obtained from the use of our facilities. Of these articles, 139 were published in high-impact journals in 2021.

NEUTRONS AND SOCIETY

The scope of the research carried out at the ILL is very broad, embracing condensed matter physics, chemistry, biology, materials and earth sciences, engineering, and nuclear and particle physics. Much of it impacts on many of the challenges facing society today, from sustainable sources of energy, better healthcare and a cleaner environment, to new materials for information and computer technology.

PREPARING FOR THE FUTURE

To maintain its status as leader in neutron science, the Institute has continually upgraded its instruments, infrastructure and scientific equipment over the last 50 years. The latest modernisation—the Endurance programme—was launched in 2016 and is currently in its second phase (2020—2023). Endurance is part of a major programme of maintenance and upgrade work covering the Reactor Division and other projects, called ILL2023. When completed, the ILL will effectively be a brand-new installation offering future researchers unprecedented capabilities for neutron science at a safe, reliable, and sustainable high flux reactor, for the decade to come and beyond.

Why neutron scattering is useful

When used to probe small samples of materials, neutron beams have the power to reveal what is invisible using other forms of radiation. Neutrons can appear to behave as particles, waves or microscopic magnetic dipoles; with these very specific properties they can provide information that is often impossible to obtain using other techniques. Below are a few of the special characteristics of neutrons.

WAVELENGTHS OF TENTHS OF NANOMETRES

Neutrons have wavelengths varying from 0.01 to 100 nanometres. This makes them an ideal probe of atomic and molecular structures whether composed of single atomic species or complex biopolymers.

ENERGIES OF MILLI-ELECTRONVOLTS

The milli-electronvolt energies associated with neutrons are of the same magnitude as the diffusive motions of atoms and molecules in solids and liquids, the coherent waves in single crystals (phonons and magnons) and the vibrational modes in molecules. Any energy exchange, therefore, of between 1μeV (or even 1 neV with neutron spin-echo techniques) and 1 eV between the incoming neutron and the sample is easy to detect.

MICROSCOPICALLY MAGNETIC

Neutrons possess a magnetic dipole moment, which makes them sensitive to the magnetic fields generated by unpaired electrons in materials. They therefore play an important role in investigations of the magnetic behaviour of materials at the atomic level. In addition, as the neutron scattering effect of the atomic nuclei in a sample depends on the orientation of the spin of both the neutron and the atomic nuclei, neutron scattering techniques are ideal for detecting nuclear spin order.

ELECTRICALLY NEUTRAL

As neutrons are electrically neutral they can penetrate far into matter without doing damage. They are therefore precious allies in research into biological samples or engineering components under extreme conditions of pressure, temperature or magnetic field, or within chemical-reaction vessels.

HIGH SENSITIVITY AND SELECTIVITY

The scattering from nucleus to nucleus in a sample varies in a quasi-random manner, even for different isotopes of the same atom. This means that light atoms remain visible in the presence of heavy atoms, and atoms close to each other in the periodic table can be clearly distinguished. This makes it possible to use isotopic substitution in order to vary the contrast in certain samples and thus highlight specific structural features. Neutrons are also particularly sensitive to hydrogen atoms and are therefore essential for research into hydrogen-storage materials, organic molecular materials, and biomolecular samples or polymers.

SCIENTIFIC HIGHLIGHTS

The scientific highlights presented in this annual report demonstrate how research with neutrons continues to push back the frontiers of science.

KEEP **UP-TO-DATE**:

facebook.com/ILLGrenoble
twitter.com/ILLGrenoble
linkedin.com/company/institut-laue-langevin

544
ILL PUBLICATIONS
RECORDED IN 2021
OF WHICH **139** PUBLISHED
IN HIGH-IMPACT JOURNALS

15
PRESS
RELEASES
WERE PRODUCED IN 2021

When viewed in the context of the ongoing public health situation, 2021 was a fantastic year for the ILL—and for the neutron community at large—with the completion of three reactor cycles providing no fewer than 172 days of operation and enabling the impressive figure of almost fifteen hundred experiments to be carried out. Despite the considerably reduced number of users on site (30–40 % fewer than in normal circumstances), the ILL was able to successfully overcome this challenge, thanks to the exceptional commitment of the staff of the Science Division whose scientists and technicians worked flat out to prepare samples; and to the invaluable assistance of the various support laboratories (chemistry lab, D-lab, PSCM and PSB), which managed and optimised the experiments. Strong support was also provided by the User Office, which shipped samples and guaranteed efficient communication with users. The Scientific Computing group played an important role with the deployment of Mantid for data reduction on the different classes of instruments and the offer of add-ons for numerical simulations. Recent developments have shown the potential of new software for autonomous instrument configuration and optimising data acquisition. The Sample Environment group, for its part, increased the capacity of the fast-cooling mode on high-temperature controllers, upgraded cryostats, cryo-furnaces and gas handling systems for dilution inserts, equipped high-pressure regulators with reliable controllers and deployed fast sample changers (SANS, cryostats, etc.). The Theory group was also actively involved, working in close collaboration with the instrument scientists, in helping to interpret the results of neutron experiments.

As illustrated by the subject of the 2021 Nobel Prize in physics, complexity has been driving research into increasingly complex systems, techniques and environments over the last decade. Applications and theories require multi-component, multi-responsive, multi-functional materials whose structure, dynamics and magnetic properties must be investigated using a combination of analytical methods. Converting such experiments into publications demands more time, more effort and more collaboration, but ultimately results in more reliable and higher impact science. The ILL's scientific output has been constant over the last decade, standing at around 550–600 publications per year. Publication efficiency and impact, on the other hand, are rising constantly, demonstrating the Institute's exceptional capacity to adapt not only to complex science but also to the ever-changing regulations governing reactor operation and, finally, to the exceptional challenges of COVID-19. This is amply demonstrated by the wide range of scientific highlights presented in this year's Annual Report. SARS-CoV-2 research is beginning to bear fruit, with the publication of important results made possible thanks to the tremendous efforts of the ILL's Science groups, who have been working with major collaborators since the very start of the public health crisis.

In addition to delivering science, 2021 was a period of intense organisational work to prepare for the 14-month long shutdown in 2022. The successful completion of this vast programme of work under the constraints of an extremely tight schedule will involve mobilising everyone at the ILL to take on tasks in addition to their regular duties.

In order to strengthen the ILL's position, we also need to consolidate the collaborations and partnerships already established on the EPN campus and increase our involvement in European projects and programmes in collaboration with industrial partners. A recent example of success in this area was the signing in 2021 of the Memorandum of Understanding to create a 'battery hub' in Grenoble. This will make the ILL, the ESRF and the CEA key players in battery-related research by 2030.

The skills and know-how available at the ILL, the commitment and dedication of ILL staff, the restart of the user programme at the end of 2022/beginning of 2023 and the successful completion of the Endurance programme in 2024 will all be key factors in establishing the ILL as the world's reference centre for neutron scattering and maximising scientific output to address both fundamental and societal challenges in the coming decade.

Jacques Jestin
Associate Director,
Head of Science Division

COLLEGE INTRODUCTIONS

COLLEGE 1 – APPLIED MATERIALS SCIENCE, INSTRUMENTATION AND TECHNIQUES

L. Helfen (College 1 secretary)

College 1 accepts proposals from applied physics, materials science and industry-related research, as well as those on new instrumentation and methods in neutron scattering, including scientific computing. As a consequence, this college deals with proposals from a very diverse user community, with scientific topics ranging from metallurgy and applied neutron scattering to cultural heritage and neutron imaging.

Although all the ILL instruments are accessible *via* College 1, most of the proposals it received in 2021 were for beamtime at the imaging instrument NeXT (which became part of the ILL instrument suite in 2020) or on the strain scanner SALSA. Additive manufacturing continues to play an important role not only for SALSA but also in NeXT proposals. Beamtime at NeXT was often requested for geomaterials and for energy-related research. In 2021, NeXT was also accessible for the first time *via* an alternative access scheme created by the recently founded NI-Matters consortium (composed of Université Grenoble Alpes, the Helmholtz-Zentrum Berlin and the ILL). This new consortium can assign about a quarter of NeXT's beamtime, particularly to geomaterials and to energy-related science topics.

COLLEGE 2 – THEORY

T. Morozova (College 2 secretary)

College 2 is dedicated to theoretical modelling in the fields of electronic structure, magnetism and soft matter. The college pursues its own line of research while also benefitting from fruitful collaborations with theoreticians and experimentalists inside and outside the Institute.

Although our long-standing tradition of hosting visiting researchers has been hampered by the pandemic, we have been able to conduct remote collaborations successfully. For instance, in collaboration with scientists from other ILL colleges and German colleagues, some of our group members have been awarded a research grant to investigate possible mechanisms in the phase behaviour of intrinsically disordered proteins. Other scientists in the college have released open-source code for calculating magnetic integrals and local excitations. In addition, postdoctoral fellows who recently joined us have been engaging in collaborative projects and participating in neutron experiments at the ILL. During the year, group members also participated in scientific exchanges in seminars and conferences held mostly online.

COLLEGE 3 – NUCLEAR AND PARTICLE PHYSICS

C. Michelagnoli (College 3 secretary)

College 3 is dedicated to nuclear and particle physics research. Many experiments and projects were run in 2021: PF2 users tested the quantum weak equivalence principle, refined the neutron lifetime value, searched for mirror neutrons and measured scattering cross sections of sD2. In parallel, future UCN technology was tested, experimental concepts validated and PF2 benchmark tests performed with the aim of enabling new-generation experiments at an improved PF2 in 2023.

With regard to other instruments, SuperSUN has been assembled and commissioning begun; S18 demonstrated that a much larger and more sensitive interferometer set-up is feasible, using two independent, fine-adjusted crystals; and the ALDEN campaign at PF1B measured yield and parameters of delayed neutrons in neutron-induced fission. Furthermore, in a new configuration of PF1B, neutron capture cross sections as a function of energy were measured. Elsewhere, nuclear spectroscopy experiments at PN1/LOHENGRIN studied excited states of neutron-rich nuclides *via* conversion electron spectroscopy and fast timing experiments; at FIPPS, nuclear shape coexistence was investigated after neutron capture on rare targets; and an actinide target irradiation in V4 produced Cf, Es and Fm isotopes used for high-resolution laser spectroscopy at Mainz University.

COLLEGE 4 – MAGNETIC EXCITATIONS

U. Bengaard Hansen (College 4 secretary)

College 4 concentrates on the study of magnetic excitations in ordered and disordered magnets, superconductors and frustrated systems. In particular, there has been strong interest in the field of low-dimensional magnetism, especially for studies of magnetic excitations in triangular, kagome and pyrochlore lattices.

Not surprisingly, 2021 was a demanding year. Major effort went into performing as many College 4 experiments as possible before the long shutdown—including experiments with challenging sample environments such as low-temperature, high-magnetic field or high-pressure environments—with a limited number of users on site. At the cold three-axis instrument ThALES, a new machine-learning-based approach for optimising data acquisition continues to be tested and represents a new way of performing a three-axis experiment. The algorithm has been developed in a collaboration with the ILL's Computing for Science Group and the Berkeley Lab. Finally, for the thermal time-of-flight instrument PANTHER, the Cu-monochromator has been commissioned and can now be used in addition to the graphite monochromator already in place.

COLLEGE 5A – CRYSTALLOGRAPHY

L. Cañadillas-Delgado (College 5A secretary)

College 5A focuses on crystallographic studies investigating relationships between the structure and properties of materials. These studies are performed on single-crystal and powder samples, and mainly on diffraction instruments. Neutron diffraction is a powerful tool for determining crystalline structures and is often used in combination with other types of radiation from which complementary information can be obtained.

The College 5A user community is made up of experienced groups of scientists from the fields of chemistry and solid-state and condensed-matter physics. These research groups are from ILL member countries, although many also involve international collaborations with non-member countries. The range of materials investigated includes perovskites, zeolites, organic/inorganic hybrid materials, minerals, inorganic materials and pure organic compounds. There has also recently been increasing interest in more applied studies, for example on gas-storage materials, solar-cell materials including perovskites for photovoltaic applications, ionic conductors, *in situ* and/or *in operando* measurements on battery materials and superconducting materials.

COLLEGE 5B – MAGNETIC STRUCTURES

K. Beauvois (College 5B secretary)

College 5B is dedicated to the study of magnetic structures, making use of polarised and unpolarised neutron powder and single-crystal diffraction, small-angle neutron scattering and neutron reflectometry.

The community is becoming increasingly interested in the discovery of new frustrated magnetic systems with completely novel topologies. Other topics include molecular magnets, double perovskite compounds, superconductors, multipolar orders, and functional materials such as multiferroics, magnetocaloric compounds and materials for spintronics. There has also been a slight increase in nanoparticle, permanent magnet and battery technology studies; these have strengthened our links with industry. Polarised neutron reflectometry is used to resolve the magnetic structure arising from decreased layer thickness, proximity effects and exchange coupling in thin films and multilayers. The materials and structures involved are diverse, with a trend towards superconducting layers, insulating magnetic oxides and topological materials. Many experiments additionally seek information on lateral arrangements and the behaviour of magnetic moments from off-specular scattering. This work typically concerns fabricated magnetic patterns and magnetic domain formation, and has been expanded upon by attempts to determine the spin configuration in thin film skyrmion systems.

COLLEGE 6 – STRUCTURE AND DYNAMICS OF DISORDERED SYSTEMS

M. Appel (College 6 secretary)

'Disorder' is the common denominator of proposals received by College 6. A large proportion of the college's proposed experiments aim to tackle problems in the fundamental science domain, such as the underlying mechanism of glass forming or the enduring mystery of the behaviour of simple water.

Some studies also have relevance to questions in energy and battery research, related, for example, to dynamics and conduction in electrolytes. Both dynamics and structure are of interest, with similar volumes of requests for beamtime on diffraction instruments (D3, D16, D20 and especially D4) as on spectrometers (IN5, IN16B, PANTHER and WASP). While most proposals deal with glasses and amorphous materials in the bulk state, continuous and considerable interest has been noted in the domain of confined and porous systems.

COLLEGE 7 – SPECTROSCOPY IN SOLID-STATE PHYSICS & CHEMISTRY

J. Ollivier (College 7 secretary)

The field of non-magnetic excitations in solid-state materials studied by inelastic neutron scattering—the purpose of College 7—has been dominated by studies of the dynamics of materials relating to clean energy, ranging from thermoelectric materials and materials for batteries to solar cells and solid oxide fuel cells.

The rather high number of proposals in College 7 in 2021 resulted in high demand for beamtime on the inelastic instrument suite, in particular IN1, IN8, IN5, IN16B and the fully commissioned PANTHER, thereby necessitating a stringent selection process. Looking at the proposed experiments, hybrid lead-halide perovskites remain objects of scrutiny, whether with respect to deciphering the role of phonon instabilities or to investigating the remarkable steadiness of the photo-generated excitons that give these organic materials their exceptional yield. There is also interest in water–polymer interactions using inelastic neuron scattering, given the need for clean and sustainable methods for splitting water into H_2 and O_2. Molecular hydrogen as an energy vector to replace fossil-based fuels requires innovative production methods to be viable. One of these is the solar-powered splitting of water using organic porous polymer photocatalysts; this has led to studies of water–polymer interactions using inelastic neuron scattering.

COLLEGE 8 – STRUCTURE AND DYNAMICS OF BIOLOGICAL SYSTEMS

O. Matsarskaia (College 8 secretary)

With its unique ability to locate hydrogen atoms, neutron crystallography (D19, LADI and DALI) is a vital tool for investigating biological structures, including viruses such as SARS-CoV-2. We have been performing solution studies using our unique set of SANS instruments (D11, D22 and D33). Selective deuteration—often carried out in collaboration with the ILL's Deuteration Laboratory (D-Lab)—and contrast-matching are crucial for analysing biomolecular complexes. The reflectometers FIGARO and D17 and the diffractometer D16 are being used to investigate model lipids and their interactions with biomolecules. This is of particular interest for studies of lipid-based drug delivery vehicles and vaccines. The spectrometers IN15, IN13 and IN11 provide insight into the dynamics of biological systems over a large range of time and Q. In addition, we have access to a wide variety of complementary techniques for further characterising samples, through the EMBL, the PSB platform and the PSCM.

COLLEGE 9 – STRUCTURE AND DYNAMICS OF SOFT CONDENSED MATTER

O. Czakkel (College 9 secretary)

The field of soft condensed matter includes a broad range of common systems highly relevant to our daily life: health and beauty products, detergents, lubricants, food emulsions, foams, and many others. Given this diversity, College 9 has long held a prominent position in the ILL user programme, accounting for 20 % of proposals submitted in 2021—the second largest number of applications received by any college.

As in previous years, the proposals in 2021 covered both fundamental and applied science, very often at the interface of physics, chemistry and biology. About 17 % of them focused on the dynamics of systems, whilst the majority sought to explore the structure of 'soft' materials on different length scales, using small-angle neutron scattering (SANS) or diffraction. A significant number of the proposed experiments (25 %) were dedicated to the study of soft matter assemblies at liquid and solid interfaces by neutron reflectivity, focusing on both static and time-dependent structures under varying thermodynamic conditions and tailored intermolecular interactions. The chemistry and PSCM laboratories fully supported our users, who very often need to prepare their samples just before their experiment. Four new PhD students started their theses on soft matter-related subjects in 2021, three of whom were recruited under the InnovaXN programme.

More information on the support facilities mentioned above can be found on p.106.

ILL IN THE PRESS 2020–2021

1. Published in *Drug Discovery World* on 26 July 2021
2. Published in *Lab Manager* in March 2021
3. Published in *Research Features* on 18 February 2021
4. Published in *LABMATE* on 4 February 2021

More articles at

https://www.ill.eu/news-press-events/press-corner/ill-in-the-media/

1.

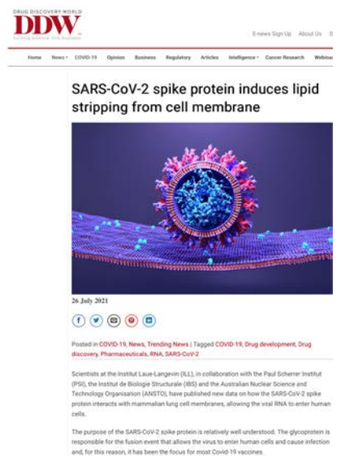

DRUG DISCOVERY WORLD

DDW

SARS-CoV-2 spike protein induces lipid stripping from cell membrane

26 July 2021

Posted in COVID-19, News, Trending News | Tagged COVID-19, Drug development, Drug discovery, Pharmaceuticals, RNA, SARS-CoV-2

Scientists at the Institut Laue-Langevin (ILL), in collaboration with the Paul Scherrer Institut (PSI), the Institut de Biologie Structurale (IBS) and the Australian Nuclear Science and Technology Organisation (ANSTO), have published new data on how the SARS-CoV-2 spike protein interacts with mammalian lung cell membranes, allowing the viral RNA to enter human cells.

The purpose of the SARS-CoV-2 spike protein is relatively well-understood. The glycoprotein is responsible for the fusion event that allows the virus to enter human cells and cause infection and, for this reason, it has been the focus for most Covid-19 vaccines.

2.

Lab Manager

March 2021 Volume 16 • Number 2

Run Your Lab Like a Business

FROM OCEANS TO INDUSTRIES, THE APPLICATIONS KEEP EXPANDING

CALORIMETRY

by Mike May, PhD

Millions of tons of microplastics—pieces less than five millimeters long—pollute the world's oceans, and differential scanning calorimetry (DSC) can identify that debris. In fact, DSC can be used in a range of studies of polymers and plastics. Effectively applying DSC, though, depends on a combination of hardware and software. Today's platforms offer many advances, including higher sensitivity, which allows measurements on smaller samples, built-in autosamplers that provide automation, and various analytical packages.

One example of DSC used is the study of microplastics is research conducted by scientists in Egypt, in which the technology was applied to water samples from the Mediterranean coast. With their DSC-based screening method, the researchers identified 10 types of microplastics in the samples. Similarly, scientists in Brazil analyzed hospital waste with DSC and found that polymers made up almost 99 percent of the waste produced from medical devices. These studies provide just a dozens of how DSC can be used.

an example, Mettler Toledo's STARe software provides six methods for determining a sample's specific heat capacity. Some vendors even run training sessions on making the most of their software packages.

In addition, commercial software packages can be enhanced with add-ons. As an example, TA Instruments (a Waters company) developed its TRIOS software for DSC, and the company offers various add-ons for thermal kinetics, such as a rheology polymer library. Some DSC software also focuses on simplification. With Hitachi's NEXTA DSC platform, for example, the software guides users through the process to make it easy even for beginners when using standard methods of DSC.

Still, some scientists prefer to develop their own analytical tools. At the Institut Laue-Langevin in Grenoble, France, for example, scientific coordinator of the Partnership of Soft Condensed Matter PSCM Leonardo Chiappisi and Aline Cova, a PhD student in his group, created their own DSC software called pyDSC to handle a large amount of data in a short time. This sounds Python-based script

3.

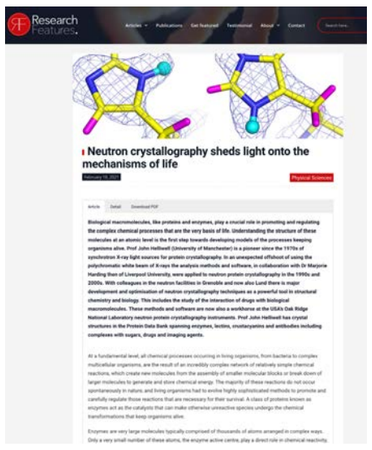

Research features

Articles Publications Get featured Testimonial About Contact

Neutron crystallography sheds light onto the mechanisms of life

Physical Sciences

Biological macromolecules, like proteins and enzymes, play a crucial role in promoting and regulating the complex chemical processes that are the very basis of life. Understanding the structure of these molecules at an atomic level is the first step towards developing models of the processes keeping organisms alive. Prof John Helliwell (University of Manchester) is a pioneer since the 1970s of synchrotron X-ray light sources for protein crystallography. In an unexpected offshoot of using the polychromatic white beam of X-rays the analysis methods and software, in collaboration with Dr Marjorie Harding then of Liverpool University, were applied to neutron protein crystallography in the 1990s and 2000s. With colleagues in the neutron facilities in Grenoble and now also Lund there is major development and optimisation of neutron crystallography techniques as a powerful tool in structural chemistry and biology. This includes the study of the interaction of drugs with biological macromolecules. These methods and software are now also a workhorse at the USA's Oak Ridge National Laboratory neutron protein crystallography instruments. Prof John Helliwell has crystal structures in the Protein Data Bank spanning enzymes, lectins, crustacyanins and antibodies including complexes with sugars, drugs and imaging agents.

At a fundamental level, all chemical processes occurring in living organisms, from bacteria to complex multicellular organisms, are the result of an incredibly complex network of relatively simple chemical reactions, which create new molecules from the assembly of smaller molecular blocks or break down of larger molecules to generate and store chemical energy. The majority of these reactions do not occur spontaneously in nature, and living organisms had to evolve highly sophisticated methods to promote and carefully regulate those reactions that are necessary for their survival. A class of proteins known as enzymes act as the catalysts that can make otherwise unreactive species undergo the chemical transformations that keep organisms alive.

Enzymes are very large molecules typically comprised of thousands of atoms arranged in complex ways. Only a very small number of these atoms, the enzyme active centre, play a direct role in chemical reactivity.

4.

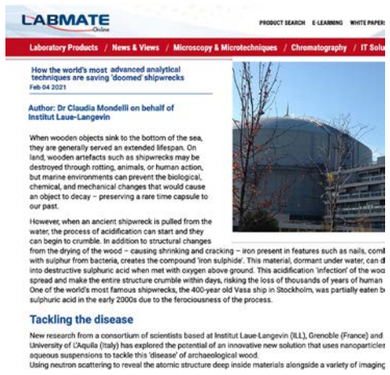

LABMATE Online

PRODUCT SEARCH E-LEARNING WHITE PAPER

Laboratory Products / News & Views / Microscopy & Microtechniques / Chromatography / IT Solu

How the world's most advanced analytical techniques are saving 'doomed shipwrecks

Feb 04 2021

Author: Dr Claudia Mondelli on behalf of Institut Laue-Langevin

When wooden objects sink to the bottom of the sea, they are generally served an extended lifespan. On land, wooden artefacts such as shipwrecks may be destroyed through rotting, animals, or human action, but marine environments can prevent the biological, chemical, and mechanical changes that would cause an object to decay – preserving a rare time capsule to our past.

However, when an ancient shipwreck is pulled from the water, the process of acidification can start and they can begin to crumble. In addition to structural changes from the drying of the wood – causing shrinking and cracking – iron present in features such as nails, comb with sulphur from bacteria, creates the compound 'iron sulphide'. This material, dormant under water, can d into destructive sulphuric acid when met with oxygen above ground. This acidification 'infection' of the woo spread and make the entire structure crumble within days, risking the loss of thousands of years of human One of the world's most famous shipwrecks, the 400-year old Vasa ship in Stockholm, was partially eaten b sulphuric acid in the early 2000s due to the ferociousness of the process.

Tackling the disease

New research from a consortium of scientists based at Institut Laue-Langevin (ILL), Grenoble (France) and University of (Aquila (Italy) has explored the potential of an innovative new solution that uses nanoparticles aqueous suspensions to tackle this 'disease' of archaeological wood.

Using neutron scattering to reveal the atomic structure deep inside materials alongside a variety of imaging

5.

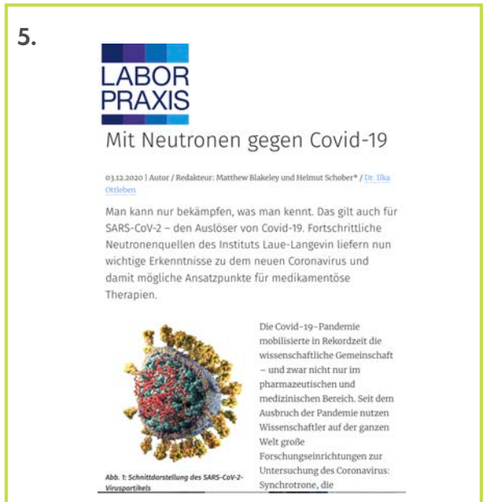

LABOR PRAXIS

Mit Neutronen gegen Covid-19

03.12.2020 | Autor / Redakteur: Matthew Blakeley und Helmut Schober* / Dr. Ilka Ottleben

Man kann nur bekämpfen, was man kennt. Das gilt auch für SARS-CoV-2 – den Auslöser von Covid-19. Fortschrittliche Neutronenquellen des Instituts Laue-Langevin liefern nun wichtige Erkenntnisse zu dem neuen Coronavirus und damit mögliche Ansatzpunkte für medikamentöse Therapien.

Abb. 1: Schnittdarstellung des SARS-CoV-2-Virusportikels

Die Covid-19-Pandemie mobilisierte in Rekordzeit die wissenschaftliche Gemeinschaft – und zwar nicht nur im pharmazeutischen und medizinischen Bereich. Seit dem Ausbruch der Pandemie nutzen Wissenschaftler auf der ganzen Welt große Forschungseinrichtungen zur Untersuchung des Coronavirus: Synchrotrone, die

6.

CURRENT Archaeology

BRITAIN'S FAVOURITE ARCHAEOLOGY MAGAZINE

Science Notes – A new approach to wood preservation

December 3, 2020 · 6 mins read

Wood samples were taken from this 2nd century BC Gallo-Roman ship discovered in Lyon, France, near the River Saône. CREDIT: ARC-Nucléart

7.

Research Industry Report

Slovenia Joins the World's Flagship Neutron Facility, ILL

Forging a partnership

8.

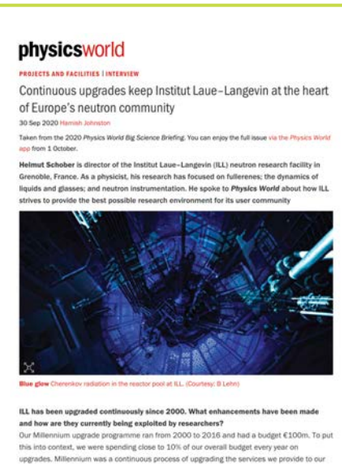

physicsworld

PROJECTS AND FACILITIES | INTERVIEW

Continuous upgrades keep Institut Laue-Langevin at the heart of Europe's neutron community

30 Sep 2020 Hamish Johnston

Taken from the 2020 *Physics World Big Science Briefing*. You can enjoy the full issue via the Physics World app from 1 October.

Helmut Schober is director of the Institut Laue–Langevin (ILL) neutron research facility in Grenoble, France. As a physicist, his research has focused on fullerenes; the dynamics of liquids and glasses; and neutron instrumentation. He spoke to ***Physics World*** about how ILL strives to provide the best possible research environment for its user community

Blue glow Cherenkov radiation in the reactor pool at ILL. (Courtesy: B Lehn)

ILL has been upgraded continuously since 2000. What enhancements have been made and how are they currently being exploited by researchers?

Our Millennium upgrade programme ran from 2000 to 2016 and had a budget €100m. To put this into context, we were spending close to 10% of our overall budget every year on upgrades. Millennium was a continuous process of upgrading the services we provide to our

5. Published in *Labor Praxis* on 3 December 2020
6. Published in *Current Archaeology* on 3 December 2020
7. Published in *Labmate* on 6 November 2020
8. Published in *physicsworld* on 30 September 2020

MAGNETISM

Matthew Coak. British
University of Warwick, UK

'My work focuses on the tuning of low-dimensional quantum magnet systems and materials that exhibit exotic phases like unconventional superconductivity through hydrostatic pressure, low temperatures and ultra-high magnetic fields. I use pressure to squeeze 2D materials towards becoming fully 3D crystals—controlling dimensionality like this allows us to discover new, functional quantum behaviours and states, and thus inform the targeted design of new materials.'

Emergent magnetic phases in pressure-tuned van der Waals antiferromagnet $FePS_3$

High-intensity two-axis diffractometer with variable resolution D20

Through record-breaking high-pressure measurements at the ILL, it has been possible to track directly the evolution of magnetism through the insulator-to-metal transition in an exciting family of low-dimensional compounds. Such materials, in which magnetic interaction is broadly constrained to the two-dimensional planes of transition metal ions, provide a versatile playground in which to explore both the fundamental properties of magnetism and electrical conduction, as well as exhibiting a range of behaviour useful for the development of future devices [1]. Applying external pressure to these systems is a uniquely powerful method of tuning. The interactions between the isolated layers are gradually, controllably, strengthened as they are pushed together. The new functional quantum phases discovered and understanding gained can then be used to design new materials that exhibit these effects in the absence of external conditions.

AUTHORS
M.J. Coak (University of Warwick, UK)
D.M. Jarvis, **A.R. Wildes** and **T.C. Hansen** (ILL)
C. Liu, **C.R.S. Haines** and **S.S. Saxena** (University of Cambridge, UK)
H. Hamidov (Navoi State Mining Institute, Uzbekistan)
S. Klotz (Sorbonne Université, France)
J.A.M. Paddison (Oak Ridge National Laboratory, USA)

ARTICLE FROM
Phys. Rev. X (2021)—doi: 10.1103/PhysRevX.11.011024

REFERENCES

[1] M.J. Coak, D.M. Jarvis, H. Hamidov, C.R.S. Haines, P.L. Alireza, C. Liu, S. Son, I. Hwang, G.I. Lampronti, D. Daisenberger, P. Nahai-Williamson, A.R. Wildes, S.S. Saxena and J.-G. Park, J. Phys. Condens. Matter 32 (2019) 124003
[2] C.R.S. Haines, M.J. Coak, A.R. Wildes, G.I. Lampronti, C. Liu, P. Nahai-Williamson, H. Hamidov, D. Daisenberger and S.S. Saxena, Phys. Rev. Lett. 121 (2018) 266801
[3] S. Klotz, Th. Strässle, B. Lebert, M. d'Astuto and Th. Hansen, High Press. Res. 36 (2016) 73
[4] Y. Wang, Z. Zhou, T. Wen, Y. Zhou, N. Li, F. Han, Y. Xiao, P. Chow, J. Sun, M. Pravica, A.L. Cornelius, W. Yang and Y. Zhao, J. Am. Chem. Soc. 138 (2016) 15751

Through high-pressure powder neutron diffraction at the ILL, we have unveiled the evolution of magnetic ordering in $FePS_3$ through its insulator–metal transition into an unconventional metallic state. The newly discovered high-pressure magnetic phase is certain to form either a precursor or a disruption to the high-pressure superconductivity recently found in these important materials.

$FePS_3$ is a 2D material, similar to graphite in that it is a layered compound that can be delaminated down to a single monolayer. It differs from graphene in that it is intrinsically magnetic, presenting some intriguing physical properties and technological possibilities. Previous experiments have shown that as pressure is applied to $FePS_3$, the material undergoes a series of structural transitions [2]. The highest-pressure phase ('HP-II') involves a collapse of the inter-planar spacing, causing the material to move towards a more three-dimensional nature. It is this transition that drives the material from being electrically insulating to becoming metallic.

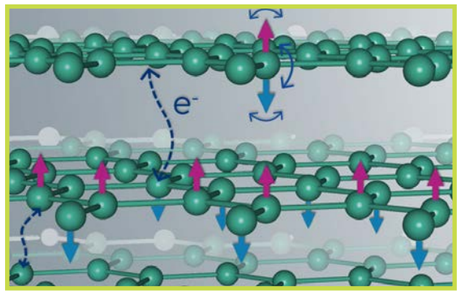

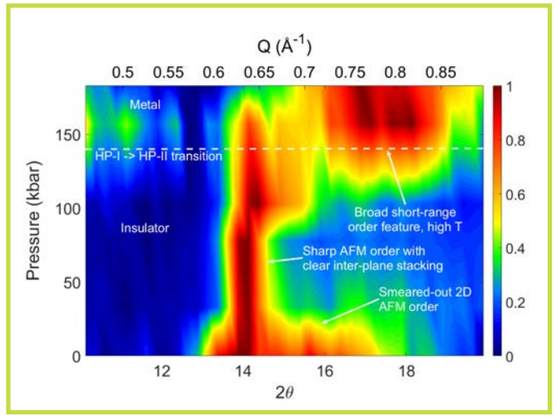

Figure 1
Magnetic peaks at 80 K for increasing pressures—colour represents normalised intensity. At ambient pressure, the magnetic order is characterised by an asymmetric feature of both 0 1 0 and 0 1 $\frac{1}{2}$ contributions. This feature then sharpens into a sharp 0 1 0 peak by 20 kbar. At the 140 kbar HP-I to HP-II structural transition, the magnetism instead shows a broad feature at higher Q that persists above room temperature.

Up until now, it has only been possible to probe the question of what happens to the long-range magnetic order in the system as the material metallises using indirect techniques. Answering the scientific question posed here required pushing new techniques and limits. Thus, we used specially designed double-toroidal sintered diamond anvils on the D20 instrument at the ILL [3] to perform low-temperature neutron diffraction measurements up to a maximum pressure of 18.3 GPa (183 kbar), *i.e.* more than double that previously accessible to users.

We followed the evolution of the magnetism through the magnetic scattering. First, we observed a switching of the inter-planar coupling from antiferro- to ferro-magnetic; then, with the collapse of the inter-planar spacing, long-range order was replaced with a previously unobserved form of short-range magnetic order.

This result is of particular interest because of the recent discovery of superconductivity under pressure in the related compound $FePSe_3$. Previous indirect measurements on both compounds by X-ray emission spectroscopy reported a crossover to a zero-spin, non-magnetic state accompanying metallisation [4]. The contradiction raised by the direct observations in our neutron study raises questions regarding the coexistence of magnetism and superconductivity in these low-dimensional materials, or the potential for such superconductivity to be magnetically mediated—or disrupted.

The stunning success of the measurements marks the excellent ongoing progress in instrumentation at the ILL and demonstrates the viability of this high-pressure set-up for widespread use in scattering experiments at the Institute.

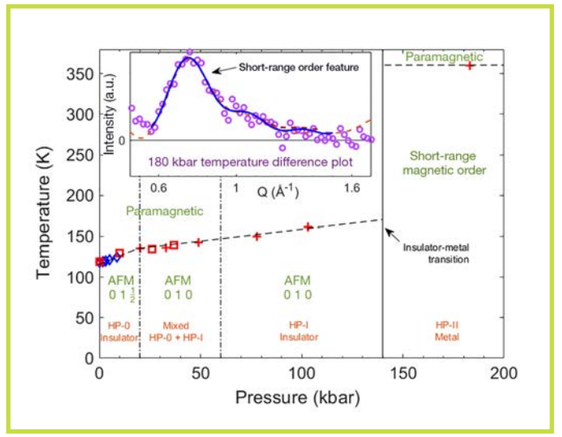

Figure 2
Resulting pressure–temperature phase diagram for $FePS_3$. Data points display extracted temperatures of magnetic transitions plotted against pressure. Blue points are extracted from magnetisation measurements, red from neutron powder patterns. Vertical lines on the phase diagram designate the pressures at which structural transitions occur. The **inset** shows the result of subtracting the 300 K data from the 80 K at 183 kbar, showing the SRO magnetic feature. The lines show Reverse Monte Carlo fit to this feature, used to extract the spin correlations in this state.

MAGNETISM

Jonathan Alaria. French
University of Liverpool, UK

'I am a senior lecturer in the Physics Department and Stephenson Institute for Renewable Energy at the University of Liverpool. My group research focuses on the growth of single crystals, epitaxial thin films and measurement of the physical properties of functional inorganic materials such as (i) complex magnetic structures (multiferroics, magnetocalorics and low-dimensional magnets), (ii) thermoelectrics and (iii) transparent conductors.'

Structure and magnetism of the lacunar spinel $GaMo_4Se_8$, a skyrmion candidate material

High-resolution two-axis diffractometer D2B

Materials possessing exotic magnetic textures are technologically important as they could be implemented in next generation, high-density data-storage media. In this context, magnetic skyrmions have been part of extensive research for more than a decade now as they present a range of extraordinary behaviours such as topological stability, low-current mobility and small domain size. Controlling the size of the individual skyrmions and their field and temperature stability is fundamental for practical applications. In the family of lacunar spinel compounds, $GaMo_4Se_8$ stands out because it features smaller skyrmions due to enhanced spin–orbit interactions.

AUTHORS
J. Alaria (University of Liverpool, UK)
S. Savvin and P. Vir (ILL)

ARTICLE FROM
Chem. Mater. (2021)—doi.org/10.1021/acs.chemmater.1c01448

REFERENCES

[1] S.S.P. Parkin *et al.*, Science 320 (2008) 190
[2] A. Fert *et al.*, Nat. Nanotechnol. 8 (2013) 152
[3] U.K. Rößler *et al.*, Nature 442 (2006) 797
[4] L. Wang *et al.*, Nat. Mater. 14 (2015) 1116
[5] D.I. Khomskii *et al.*, Chem. Rev. 121 (2021) 2992

Using powder neutron diffraction we observe that, unlike other skyrmion hosts, $GaMo_4Se_8$ undergoes a phase separation at the structural transition resulting in two coexisting phases with different crystal structures. The subtle structural distortions and strain resulting from the phase coexistence below T_c stabilise Néel skyrmions in $GaMo_4Se_8$ under a wide range of temperatures and magnetic fields, as demonstrated by bulk magnetic measurements.

Conventional semiconductor data storage technologies are reaching their saturation limits. The unprecedented amount of newly/daily generated data therefore requires the development of alternative devices using new physics concepts. Taking advantage of the spin properties of electrons in lieu of charge can provide an additional degree of freedom. This emergent field of research has been coined 'spintronics'. Among numerous exciting ideas proposed in the last couple of decades for designing innovative, high-density memory, one of the most prominent is *skyrmions racetrack memory*, which employs topological, vortex-like spin structures known as skyrmions [1, 2]. Skyrmions are stabilised by various competing magnetic interactions, such as the Heisenberg exchange interaction, the Dzyaloshinskii–Moriya interaction and the Zeeman effect. As the existence of these exotic spin textures depends upon specific crystal symmetries, they have only been observed in certain classes of materials [3]. In order to help unearth the underlying properties of skyrmions it is therefore vital to discover/study new skyrmion-hosting materials.

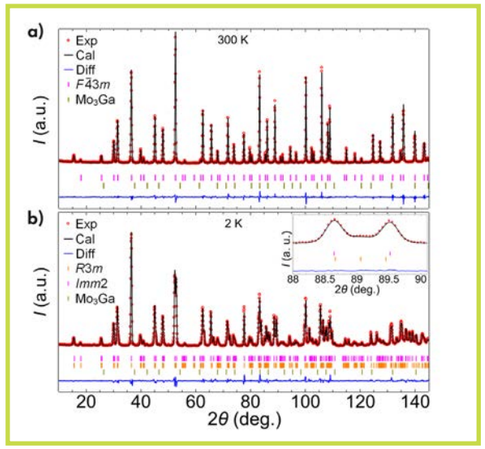

Figure 1

The observed (red open circles) and calculated (black solid line) powder neutron diffraction patterns measured at **a)** 300 K, high-temperature phase ($F\bar{4}3m$), and **b)** 2 K, low-temperature phases (*R3m* and *Imm2* Bragg reflections in magenta and orange vertical lines, respectively; Bragg peaks associated with the trace impurity Ga_3Mo, grey vertical lines). The blue line is the difference plot. The **inset in b)** highlights the region around the cubic (408) peak, which splits through the Jahn–Teller transition with contributions from both *R3m* and *Imm2* phases visible.

Figure 2

Schematic of structural transitions in $GaMo_4Se_8$ induced by Jahn–Teller distortions. The two low-temperature structures are displayed in pseudo-cubic cells (indicated by blue solid lines) and on their own. Γ_1, Γ_3, and Γ_4 are the distortion modes.

Lacunar spinel compounds are very compelling to the magnetic scientific community in this regard, as their low-temperature structure is rhombohedral with C_{3v} symmetry. Their empirical formula is $A_{0.5}B_2X_4 \approx AB_4X_8$, which is a derivative of the conventional spinel compound AB_2X_4, in which half of the A-sites are vacant. The members of this family are known to show structural transition at low temperatures and to display various emergent physical properties such as multiferroicity and pressure-induced superconductivity [4, 5]. The most common structural transition observed is from the high-temperature cubic phase ($F\bar{4}3m$) to the low-temperature rhombohedral phase (*R3m*), due to the Jahn–Teller distortion. Having a non-centrosymmetric crystal structure (*R3m*, C_{3v} symmetry) allows for the non-zero Dzyaloshinskii–Moriya interaction, which can in turn stabilise skyrmions [3].

$GaMo_4Se_8$ belongs to this family; and among all the family's known members it has one of the largest spin–orbit couplings (SOCs), due mainly to the presence of Mo and Se atoms. As the size of skyrmions depends upon the SOC, $GaMo_4Se_8$ can probably host skyrmions of quite small size. A complete structural investigation using the high-resolution neutron powder diffractometer D2B was carried out, and the results of the Rietveld refinements are presented in **figure 1**. At 300 K, the compound crystallises in the non-centrosymmetric space group $F\bar{4}3m$ (**figure 1a**). Cooling the sample to below T_{JT} = 51 K (structural transition temperature) results in the splitting of several high-intensity peaks (**figure 1b**), indicating the expected structural distortion. However, refinement of the low-temperature diffraction pattern in the *R3m* phase only, shows several unindexed peaks (**figure 1b inset**). This indicates the possibility of another coexisting phase. Indeed, including another phase in the *Imm2* space group results in extremely good refinement. The phase ratio of *R3m* to *Imm2* below T_{JT} is found to be 70:30.

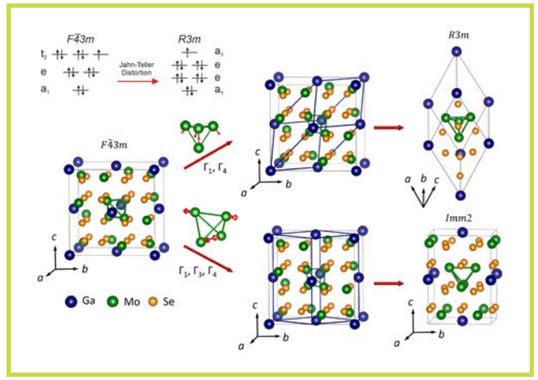

In **figure 2**, the relation of low-temperature phases (*R3m* and *Imm2*) to the high-temperature phase ($F\bar{4}3m$) is presented for the compound $GaMo_4Se_8$. For the *R3m* phase the distortion is along [111] and is compressive, resulting in the formation of a polar space group with C_{3v} symmetry. In this case, the cell volume is reduced to a quarter of cubic volume and the new cell edge is $a_r = a_c/\sqrt{2}$, the subscripts referring to the rhombohedral and cubic cells, respectively. Conversely, for the *Imm2* the distortions occur along the [100] and [010] directions and change the symmetry to C_{2v}. The resulting cell volume is halved and the new cell edges become, $a_o = a_c/2$, $b_o = b_c/2$, and $c_o = c_c$, the subscripts referring to the orthorhombic and cubic cells, respectively.

Due to the presence of C_{3v} symmetry, the type of skyrmion that can be found in $GaMo_4Se_8$ is Néel-type [3]. **Figure 3a** presents a schematic of the internal spin arrangement of Néel-type skyrmions. In contrast to the Bloch-type commonly observed in chiral compounds, wherein spins from core to periphery follow a helical motion, in Néel-type skyrmions the rotation fashion is cycloid-like, as depicted by the radial cut. **Figure 3b** shows the magnetic phase diagram obtained from dM/dT curves of a single crystal. The low-field region (light blue) is expected to be cycloid, while the red region is expected to be skyrmions.

Our study reveals that $GaMo_4Se_8$ is a unique compound with coexisting structural phases at low temperatures. Additionally, the indication of complex magnetism should stimulate the magnetism community to further investigate this compound as a skyrmions host.

Figure 3

a) A schematic of the spin arrangement in Néel-type skyrmions, below which is a representation of the radial cut of the skyrmion which resembles a cycloid spin structure. **b)** Magnetic phase diagram of $GaMo_4Se_8$ obtained by $(\partial m/\partial T)H$ for various magnetic fields.

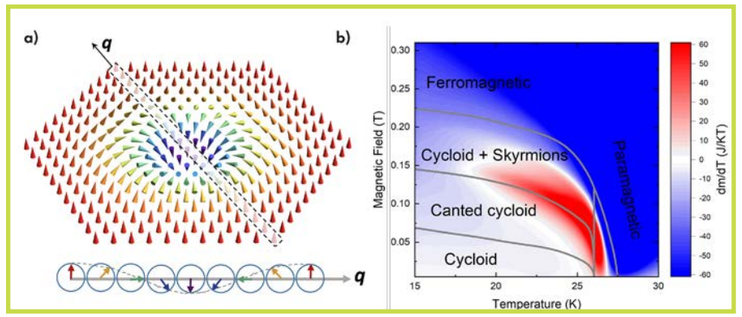

Jannis Willwater. German
Institut für Physik der Kondensierten Materie, TU Braunschweig, Germany

'I am in the third year of my PhD studies at the TU Braunschweig. My main field of research is the experimental investigation of strongly correlated electron systems, in particular using large-scale research facilities.'

Crystallographic and magnetic structure of $UNi_4{}^{11}B$

High-resolution two-axis diffractometer D2B, single-crystal 4-circle diffractometer D10 and Laue single-crystal diffractometer CYCLOPS

Frustrated metallic f-electron magnets have been the focus of extensive research efforts in recent years. A prominent example is the metallic f-electron magnet UNi_4B. We have used a combination of various neutron diffraction techniques at the ILL to investigate the crystallographic and magnetic properties of $UNi_4{}^{11}B$. For this material a highly unusual form of partial antiferromagnetic ordering was proposed, which in turn carries a magnetic toroidal moment [1]. This type of magnetic order might thus lead to novel types of magnetoelectric effects [2]. We have fully refined the crystallographic and magnetic structure of $UNi_4{}^{11}B$ at low temperatures and established the experimental basis for future studies of toroidal order in condensed matter.

AUTHORS

J. Willwater and **S. Süllow** (TU Braunschweig, Germany)
M. Reehuis and **R. Feyerherm** (HZB, Germany)
H. Amitsuka (Hokkaido University, Japan)
B. Ouladdiaf and **E. Suard** (ILL, France)
M. Klicpera, **M. Vališka**, **J. Pospíšil** and **V. Sechovský** (Charles University, Czech Republic)

ARTICLE FROM

Phys. Rev. B (2021)—doi:10.1103/PhysRevB.103.184426

REFERENCES

[1] S. Mentink *et al.*, Phys. Rev. Lett. 73 (1994) 1031
[2] H. Saito *et al.*, J. Phys. Soc. Jpn 87 (2018) 033702
[3] C. Tabata *et al.*, J. Phys. Soc. Jpn 90 (2021) 064601
[4] R. Movshovich *et al.*, Phys. Rev. Lett. 83 (1999) 1031

The metallic f-electron magnet UNi_4B has been reported to exhibit a highly unusual form of partial antiferromagnetic ordering below T_N = 19.5 K, with only two out of three uranium magnetic moments participating in long-range magnetic order [1]. In effect, it forms a vortex-like magnetic structure that carries magnetic toroidal order [2]. This could lead to novel types of magnetoelectric effects, such as the observed current-dependent magnetisation in UNi_4B [2]. This proposition relies on the correct characterisation of the crystallographic symmetry. Recently, however, X-ray diffraction experiments have indicated that the crystallographic symmetry of UNi_4B is lower than the originally proposed hexagonal one [3]. In response to this situation, we carried out neutron diffraction experiments on powder and single-crystalline samples to fully characterise the crystallographic and magnetic structure of UNi_4B.

A high-quality $UNi_4{}^{11}B$ single crystal was prepared using the floating zone method. A part of the ingot was ground into a powder and then investigated using the D2B instrument. This initial phase of the study demonstrated that UNi_4B crystallises in an orthorhombic crystal

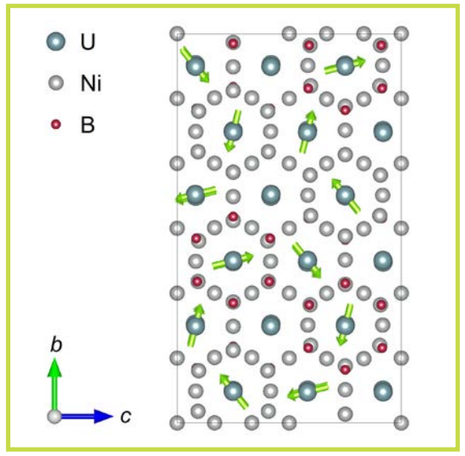

Figure 1
Magnetic unit cell of UNi_4B refined from the D10 data. The arrows represent the magnetic moments.

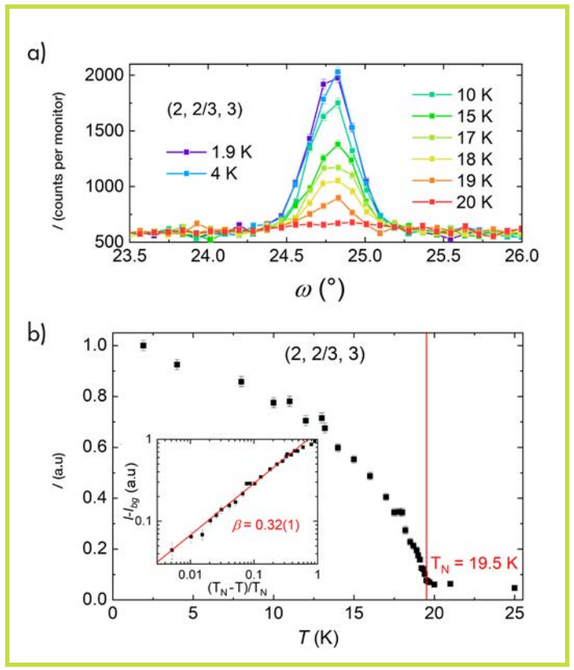

Figure 2
a) ω-scans of the magnetic (2, 2/3, 3) Bragg peak. **b)** Temperature dependence of the integrated intensities of the magnetic reflection at (2, 2/3, 3). **Inset)** Double logarithmic plot of the integrated intensity *vs* $(T_N - T)/T_N$ to derive the critical behaviour.

structure. To obtain a full crystal structure analysis of UNi_4B, we subsequently carried out neutron diffraction experiments on single-crystalline material using the D10 instrument. A basic refinement of this data was produced consistent with the space group *Cmcm*, as proposed by X-ray diffraction [3]. However, various reflections forbidden to this space group were also detected. We identified the lower-symmetry space groups that accommodate these reflections and found that the space group *Pmm*2 (No. 25) properly describes our measured data. Thus, we have established that $UNi_4{}^{11}B$ crystallises in an orthorhombic lattice of space group *Pmm*2.

Next, a set of magnetic reflections was measured on D10 to determine the magnetic structure. The propagation vector was established at **k** = (0, 2/3, 0), leading to a magnetic unit cell with the dimensions a × 1.5b × c based on simplified *Cmcm* symmetry. We consequently validated the partial magnetic ordering and the vortex-like moment configuration with an ordered magnetic moment of μ_{ord} = 0.99(1) μ_B/(U atom). The refinement is improved if a slight canting of ~15 ° is allowed within the plane of the vortex (**figure 1**).

We then investigated the nature of the magnetic transition in more detail. To do this, we carried out ω-scans of magnetic reflections as a function of temperature, as depicted for the (2, 2/3, 3) reflection in **figure 2a**.

From the data, the transition temperature was determined to be T_N = 19.5 K. Furthermore, the integrated intensities shown in **figure 2b** allowed us to analyse the critical behaviour of the magnetic transition. A corresponding power law fit yielded a critical exponent β = 0.32(1) (**figure 2b inset**). Comparing this against theory classifies the material as a 3D-Ising-like antiferromagnet. Given its noncollinear magnetic structure, UNi_4B might therefore be a realisation of the noncollinear Ising model.

Finally, we investigated the low-temperature magnetism of UNi_4B using D10 and the neutron Laue instrument CYCLOPS. In a previous study, a maximum in the specific heat was observed at 330 mK and tentatively attributed to the ordering of the remaining U moments [4]. However, in our experiments we observed no additional magnetic reflections below 330 mK, nor did the intensity of the magnetic and nuclear reflections change. Therefore, our findings disprove the proposed second magnetic phase transition with ordering of the remaining U moments at low temperatures.

In summary, we have established UNi_4B as a rare example of an Ising-like, frustrated, metallic f-electron magnet with a partially ordered magnetic ground state. We have fully characterised the crystal and magnetic structure of UNi_4B down to the lowest temperatures by, in particular, harnessing the different elemental contrast (here regarding ^{11}B) between neutron scattering and X-ray diffraction.

MAGNETISM

Oksana Zaharko. Swiss
Paul Scherrer Institut, PSI, Switzerland
'After a PhD in solid state chemistry at the Lviv State University (Ukraine), I worked in a number of research centres in Poland, Germany and Switzerland. In 1998 I joined PSI as a postdoc, and since 2002 I have been working there as a senior scientist, co-responsible for the single-crystal thermal neutron diffractometer Zebra. My main research interests are frustrated magnetic systems, especially those with non-trivial topological properties.'

A fractional antiferromagnetic skyrmion lattice induced by anisotropic couplings

Three-axis spectrometer Thales, single-crystal diffractometer D23 (ILL), single-crystal diffractometer Zebra (PSI) and three-axis spectrometer PANDA (MLZ)

Topology, although a purely mathematical discipline for many years, has since revolutionised our understanding of electronic and magnetic correlations in condensed matter physics. Among topological entities, magnetic skyrmions—nanometre-sized, swirling spin configurations—have garnered enormous interest due to their potential as magnetic information carriers. Until recently, skyrmions were discovered mostly in ferromagnetic materials. Our work endorses theoretical ideas that skyrmions can also be found in antiferromagnets. Using neutron scattering experiments and Monte Carlo modelling, we find evidence for a fractional antiferromagnetic lattice in the $MnSc_2S_4$ spinel and propose a mechanism for its stabilisation.

AUTHORS
O. Zaharko, **S. Gao**, **G. Kaur**, **T. Fennell** and **Ch. Ruegg**
(Paul Scherrer Institute, PSI, Villigen, Switzerland)
H.D. Rosales, **F.A. Gomez Albarracin** and **D.C. Cabra**
(IFLYSIB, UNPL-CONICET, La Plata, Argentina)
V. Tsurkan (University of Augsburg, Germany)
P. Steffens and **M. Boehm** (ILL)
E. Ressouche (Université Grenoble Alpes, CEA, INAC-MEM, Grenoble, France)
P. Cermak and **A. Schneidewind** (Jülich Centre for Neutron Science, Garching, Germany)

ARTICLE FROM
Nature (2020)—doi:10.1038/s41586-020-2716-8

REFERENCES
[1] N. Nagaosa and Y. Tokura, Nat. Nanotechnol. 8 (2013) 899
[2] T. Okubo, S. Chung and H. Kawamura, Phys. Rev. Lett. 108 (2012) 017206
[3] S. Gao *et al.*, Nat. Phys. 13 (2017) 157

Both fundamental and applied aspects of topological magnetism are currently undergoing impressive development. Materials hosting topologically protected spin textures such as skyrmions or merons in real-space, or exhibiting Dirac or Weyl quasiparticles in their momentum-space band structure, are inspiring new theoretical ideas and concepts for information technologies.

We are looking for new materials with topologically non-trivial structures. In relatively well-studied non-centrosymmetric B20 compounds such as MnSi and Cu_2OSeO_3 [1], ferromagnetic skyrmion lattices (F-SkL) form through the interplay of ferromagnetic nearest-neighbour coupling, the Dzyaloshinskii–Moriya interaction and cubic magnetocrystalline anisotropy. Frustrated antiferromagnetic interactions and enhanced spin fluctuations are predicted to play an important role in the formation of antiferromagnetic skyrmion lattices (AF-SkR) [2]. Here we show that anisotropy can also be significant for the formation of AF-SkR.

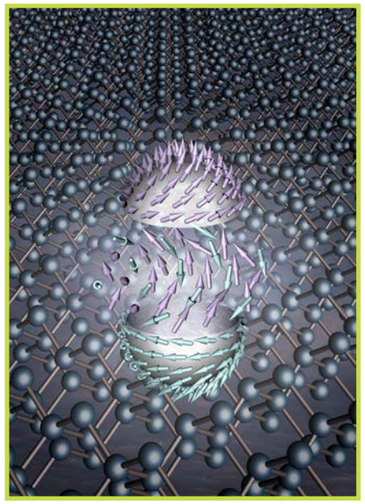

Our study focused on the cubic spinel $MnSc_2S_4$, in which the magnetic Mn^{2+} ions form a bipartite diamond lattice. In previous neutron diffraction work on this material [3] we observed the existence of a spiral spin-liquid state as a result of frustrated ferromagnetic nearest-neighbour J_1 and antiferromagnetic next-nearest neighbour J_2 couplings above the ordering temperature T_N = 2.3 K. From this highly degenerate state, multiple domains of a helical long-range ordered state with the propagation vector **q** = (3/4 3/4 0) emerge through a series of transitions. In an applied magnetic field these domains rearrange into a triple-**q** phase.

Our current neutron scattering experiments and Monte Carlo simulations establish this triple-**q** phase as a fractional antiferromagnetic skyrmion lattice stabilised by anisotropic spin couplings and weak single-ion anisotropy.

Our single-crystal inelastic neutron scattering experiments reveal broad excitations (**figure 1**) reaching a maximal energy of 0.9 meV, which suggests the appearance of multiple magnon bands. These data could be modelled using linear spin-wave theory with up to third-neighbour couplings. In order to establish the mechanism of the triple-**q** formation, we explored various perturbations using Monte Carlo simulations and found that anisotropic spin couplings and weak single-ion anisotropy stabilise this phase. We have inspected the resulting triple-**q** structure by layers in which the Mn^{2+} ions form a triangular lattice. Disentangling the triangular lattice into three sublattices (**figure 2**) identifies whorls with opposite winding directions. Because of the short distance between the centres of the whorls, skyrmions fractionalise into pairs of incipient merons and antimerons.

Our work shows that antiferromagnets can host topologically non-trivial spin textures and suggests a new mechanism for their formation.

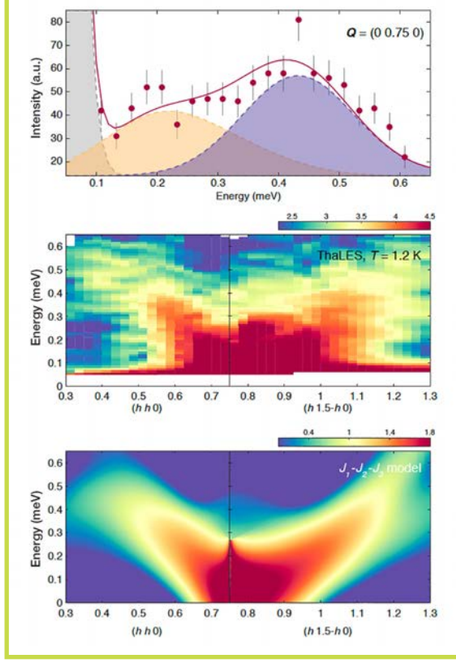

Figure 1
Representative inelastic neutron scattering spectra collected at T = 1.2 K and Q = (0 3/4 0) (**top**), and experimental (**middle**) and calculated (**bottom**) (Q,E) map.

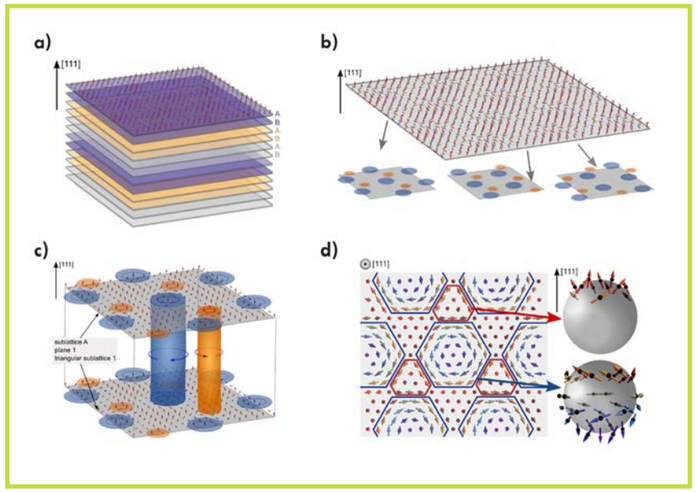

Figure 2
Fractional antiferromagnetic skyrmion lattice in $MnSc_2S_4$.
a) A-B-C stacking of triangular lattice layers.
b) Disentanglement of a representative A-layer into three sublattices.
c) Cylinders of fractional skyrmions along [111].
d) Spin texture of a representative sublattice. Fractional skyrmions are represented by two spheres.

Marta Crisanti. Italian
TU Delft, Netherlands
@martacris42

'I am a postdoc working in the Neutron and Positron Methods for Materials group in TU Delft in the Netherlands. My research focuses on the study of the skyrmion state's characteristics in bulk materials in relation to high pressure and macroscopic features of the samples. Recently, I have been working on low-temperature skyrmions and other novel magnetic states stabilised by magnetic anisotropies.'

Position-dependent stability and lifetime of the skyrmion state in nickel-substituted Cu_2OSeO_3

Small-angle scattering instrument D33 and strain analyser for engineering applications SALSA

Skyrmions are magnetic vortices that can carry information in spintronic devices. These nano-sized spin whirls are stable only under strict conditions of temperature and applied magnetic fields. For the successful technological development of skyrmion devices, it is necessary to loosen these constraints on stability. In this work we study the effects that the macroscopic shape of the sample has on the stability of the skyrmion state, revealing a new way of manipulating its characteristics.

AUTHORS
M. Crisanti (TU Delft, Netherlands)
R. Cubitt (ILL)

ARTICLE FROM
Phys. Rev. B (2020)—doi:10.1103/PhysRevB.102.224407

REFERENCES

[1] K. Everschor-Sitte *et al.*, J. Appl. Phys. 124 (2018) 240901
[2] M. Crisanti *et al.*, Phys. Rev. B 102 (2020) 224407
[3] T. Nakajima *et al.*, J. Phys. Soc. Jpn 87 (2018) 094709
[4] L. Peng *et al.*, Nano Lett. 18 (2018) 7777

Skyrmions are magnetic spin whirls constituting a new topological state of the magnetisation. They are attracting a lot of interest because of their possible application as information carriers in spintronic devices [1]. A Bloch-type skyrmion is depicted in **figure 1a**. In bulk materials, the skyrmion state is usually stable over a small range of applied magnetic fields and temperatures just below the ordering temperature T_C, commonly referred to as the skyrmion pocket (**figure 1b**) [2]. In these materials, skyrmions are arranged in hexagonal lattices and elongate like tubes along the direction of the applied field. Given the small extent of the skyrmion pocket, research efforts have focused on manipulation of its size and position across the H-T phase diagram. Our study takes advantage of the ILL's highly brilliant neutron source to show how demagnetisation effects are of crucial importance when considering the stability of the skyrmion state, indicating how the shape of bulk macroscopic samples influences the size of the skyrmion pocket and the structure of the skyrmion lattice.

Small-angle neutron scattering (SANS) allows for the explicit identification of long-range magnetic structures present in a sample through the analysis of the scattering patterns they produce. Specifically, the skyrmion lattice, having a hexagonal symmetry, results in a six-fold scattering pattern when the magnetic field is applied along the same direction as the neutron beam (**figure 1c**).

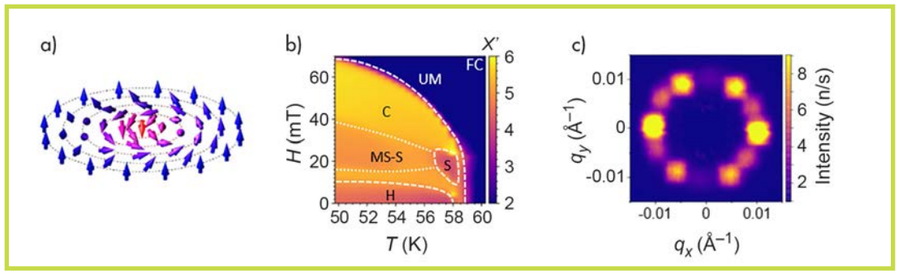

Figure 1
a) Bloch-type skyrmion, the arrows representing magnetic moments. **b)** H-T phase diagram of the sample used in our experiment: Ni-substituted Cu_2OSeO_3[2]. The letters denote the different magnetic states of the sample: 'C' for the conical state, 'H' for the helical, 'S' for skyrmion, 'M-S' for metastable skyrmion, 'UM' for uniformly magnetised. The phase diagram has been measured field cooled (FC). **c)** Scattering pattern of the skyrmion lattice [2].

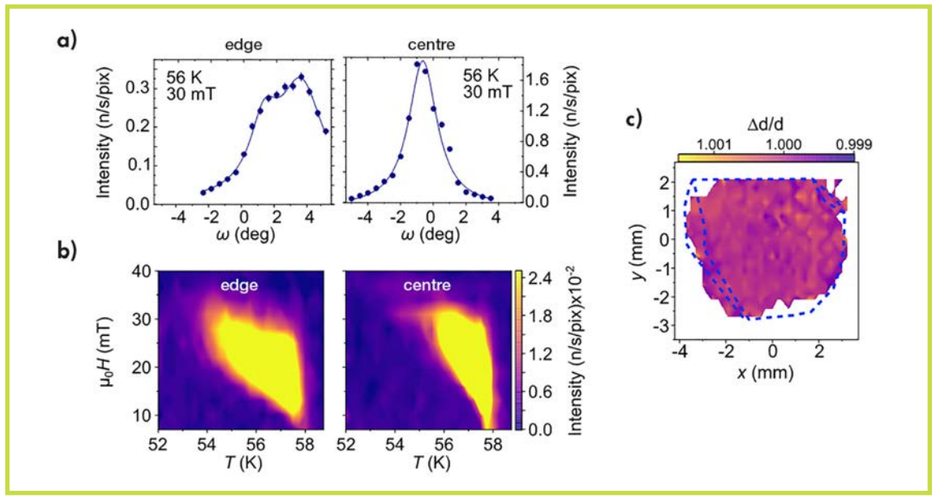

Figure 2
a) Rocking curves collected at the edge and at the centre of the sample. **b)** H-T phase diagram of the skyrmion pocket measured at the edge and at the centre of the sample. **c)** A d-spacing variation map of the sample obtained *via* diffraction measurements on SALSA.

Furthermore, it is possible to collect information on the extent of the Bragg reflections outside the detector plane, in the direction of the magnetic field, using rocking scans.

These scans are performed by rotating the sample and the applied field around the axis perpendicular to the incoming neutron beam, on the detector plane. In our study we recorded the scattered intensity as a function of rotating angle, *i.e.* the rocking curves. From their careful analysis we were able to measure the average correlation length of the skyrmion tubes along the direction of the applied field.

Thanks to the highly brilliant source that the ILL provides on the D33 instrument, we were able to select a small (1 mm) aperture for the neutron beam in front of the sample without incurring measurement times that would be too long to be feasible during a typical experiment. This allowed us to perform spatially resolved measurements across a large Ni-substituted, Cu_2OSeO_3 single crystal.

We established the presence of at least two skyrmion domains. At the centre of the sample, the skyrmion lattice is characterised by rocking curves peaking sharply in the magnetic field's direction; conversely, at the edge of the sample the rocking curves are wider, have multiple peaks and tilt away from the direction of the applied field (**figure 2a**). This corresponds to a well-ordered skyrmion lattice being present at the centre of the sample, while at the edge the lattice appears distorted and is characterised by a shorter correlation length. Moreover, the extent of the skyrmion pocket differed between the two skyrmion domains, as shown in **figure 2b**. The skyrmion pocket at the edge of the sample is characterised by a wider temperature range than that of the pocket at the centre, while both share the same magnetic field range.

One possible explanation for this behaviour is the presence of strain across the sample. This could be responsible for modifying the temperature range of the skyrmion pocket, as has been demonstrated elsewhere [3]. To investigate this possibility, we performed neutron diffraction measurements on the SALSA instrument. With these measurements we were able to characterise the underlying crystal structure of the sample and prove its uniformity, as shown in **figure 2c** displaying the d-spacing variation across the single crystal. Other possible explanations regarding the non-uniformity of Ni content in the sample could be ruled out by our finding of the same ordering temperature in both regions of interest.

We identify the demagnetisation effects induced by the complex shape of the sample edge as being the main cause of the bent and misaligned skyrmion tubes in this area. Moreover, as the demagnetisation additionally induces a field gradient at the edge of the sample, we expect the coexistence in this area of the skyrmion and conical states, inducing a local disorder of the skyrmion lattice and resulting in increased stability as has been shown to occur in FeGe lamellae [4].

In conclusion, we have provided evidence of the effect of demagnetisation on the structure of the skyrmion lattice, as well as evidence of the sensitivity of skyrmion stability on the local ordering of the lattice itself.

Alexander Petsch. German
University of Bristol, UK

'I am a physics PhD student who employs neutron and X-ray scattering techniques to study magnetic and structural excitations, as well as orderings, with a specific focus on quantum magnetism and the implications for coupling and pairing symmetries in unconventional superconductors.'

Reduction of spin susceptibility in the superconducting state of Sr_2RuO_4 observed by polarised neutron scattering

Three-axis spectrometer IN20 with polarisation analysis

The gap function of a superconductor can take on a variety of symmetries, depending on the pairing mechanism and the material's properties. Pairing symmetries can be distinguished in even- and odd-parity, which differ in their magnetic bulk responses or spin susceptibilities, respectively. We used polarised neutron scattering to probe the spin susceptibility in the unconventional superconductor Sr_2RuO_4. Our results lead us to reject a previously accepted odd-parity state and put constraints on the possible pairing symmetries.

AUTHORS

A.N. Petsch, **M. Zhu** and **S.M. Hayden** (University of Bristol)
M. Enderle and **U.B. Hansen** (ILL)
Z.Q. Mao (Pennsylvania State University)
Y. Maeno (University of Kyoto)

ARTICLE FROM

Phys. Rev. Lett. (2020)—doi:10.1103/PhysRevLett.125.217004

REFERENCES

[1] K. Ishida, H. Mukuda, Y. Kitaoka, K. Asayama, Z.Q. Mao, Y. Mori and Y. Maeno, Nature 396 (1998) 658
[2] J.A. Duffy, S.M. Hayden, Y. Maeno, Z. Mao, J. Kulda and G.J. McIntyre, Phys. Rev. Lett. 85 (2000) 5412
[3] A. Pustogow, Y. Luo, A. Chronister, Y.-S. Su, D.A. Sokolov, F. Jerzembeck, A.P. Mackenzie, C.W. Hicks, N. Kikugawa, S. Raghu, E.D. Bauer and S.E. Brown, Nature 574 (2019) 72
[4] A.T. Rømer, D.D. Scherer, I.M. Eremin, P.J. Hirschfeld and B.M. Andersen, Phys. Rev. Lett. 123 (2019) 247001

Sr_2RuO_4 is an unconventional superconductor with T_c = 1.44 K and H_{c2} = 1.5 T. It was considered to be a solid-state analogue of the superfluid ^{3}He A-phase, which inheres in an odd-parity chiral spin-triplet state. Odd-parity states such as *p-wave* states are special in that their gap functions are described by a **d**-vector, rather than by a scalar as even-parity states such as *d-wave* states are. A consequence of this is that a change in or suppression of spin susceptibility is only observed for magnetic fields applied parallel to the **d**-vector; furthermore, some states show only partial suppressions instead of the complete isotropic suppression usually expected in *even-parity superconductors*. However, probing the spin susceptibility in superconductors using most techniques, such as SQUID magnetometry, is hindered by the appearance of diamagnetic supercurrents. The two techniques that can probe spin susceptibility in superconductors are as follows: 1) nuclear magnetic resonance (NMR), which probes the shift in nuclear resonances due to hyperfine interaction

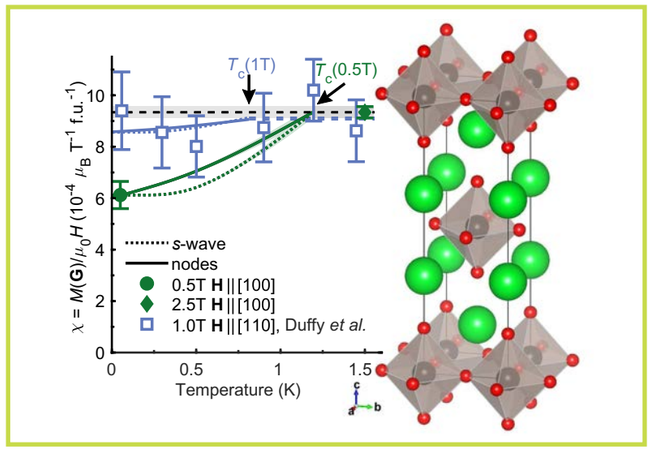

Figure 1

Results from the first experiment (green) compared with the results at 1 T from [2] (blue), with modelled temperature dependencies and the structure of Sr_2RuO_4.

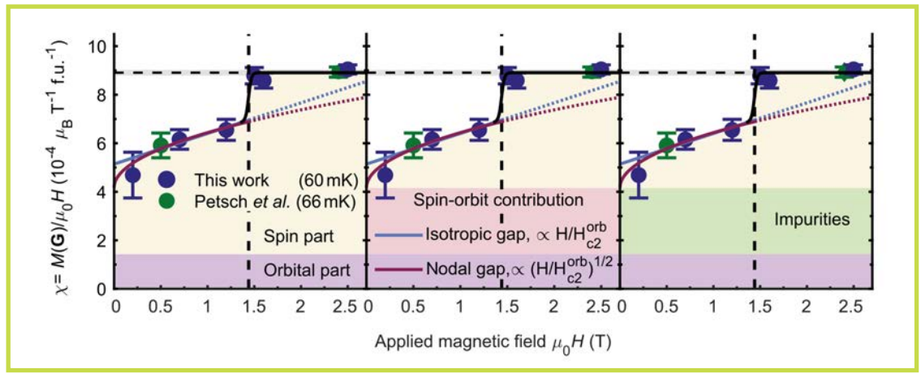

Figure 2

Three theories that might explain the results: (i) an odd-parity state; (ii) spin-triplet contributions due to SOC; or (iii) impurity scattering.

The solid lines denote plausible *H*-dependencies with the dotted lines as their theoretical continuations towards H*corb*.

and which is known as the Knight shift; and 2) polarised neutron diffraction (PNS), which probes magnetisation density through the scattering of neutrons with polarisation parallel and anti-parallel to the applied field and which is related to the ratio of nuclear-to-magnetic Bragg scattering.

Early NMR measurements [1] with a magnetic field applied in the *xy*-plane revealed no change in the Knight shift *K* between the normal and the superconducting state, while a PNS study [2] could observe no drop in susceptibility below T_c either (**figure 1**). At the time, these findings were interpreted as evidence of an odd-parity spin-triplet state with an out-of-plane **d**-vector. A recent NMR study [3] nonetheless observed a change in *K* below the superconducting transition when the field was also applied in-plane and found that the earlier NMR study had suffered from sample heating. This challenged the previous picture of an odd-parity state with an out-of-plane **d**-vector, and raised the question of whether a change in PNS might also be observed if sample heating was insignificant.

We repeated the PNS from [2], again using an Sr_2RuO_4 single crystal, on the polarised three-axis spectrometer IN20 modified as an effective, polarised, two-axis diffractometer. The sample was cooled to 60 mK in a dilution refrigerator and the fields were applied along [100]. The flipping ratio *R* was measured on the (011) Bragg reflection where magnetic contributions primarily arise from the Ru-sides. By applying a weaker magnetic field of 0.5 T rather than the 1 T used in [2], and by improving the statistical error bar considerably, we established that susceptibility at 0.5 T is reduced to about two-thirds of normal state susceptibility, although this does include orbital contributions; we further concluded that the previous study suffered from relatively large error bars (**figure 1**). The statistical error is very difficult to reduce because the required sensitivity is excessive: the flipping ratios are extremely small ($R\text{-}1 \approx 10^{-4}\text{-}10^{-3}$). We further deduced that the spin susceptibility might remain finite.

We recently continued this project on IN20 across various field strengths and with an improved experimental set-up. This was achieved by replacing the usual monitor and detector with faster ones, which allowed for normalisation on flux rather than on time and for better corrections of systematic errors induced by variations in the flux or the reactor power, respectively. The new results show a large jump in susceptibility near H_{c2} due to a first-order transition induced by Pauli pair-breaking. Additionally, we find clear evidence of a large residual susceptibility in the zero-field and zero-temperature limit (**figure 2**). This could be due either to a very large orbital contribution, which is unlikely, however; to pair-breaking impurity scattering, which requires a very unstable superconducting order; or to properties intrinsic to the superconducting state itself.

If the quasiparticle density of states is entirely suppressed, a finite residual spin susceptibility is conventionally understood as the signature of an odd-parity state with an in-plane **d**-vector where only partial suppression is expected. However, Sr_2RuO_4 also exhibits strong spin–orbit coupling (SOC), known to significantly affect the normal-state Fermi surfaces and, as recently suggested, could lead to spin-triplet contributions in even-parity states and thus also to a finite residual spin susceptibility [4].

In that sense, our results are consistent with an odd-parity state with in-plane **d**-vector, or with an even-parity state with residual spin susceptibility which includes recent proposals such as $\{s', d_{x^2-y^2}\}, \{s', d_{xy}\}, \{d_{x^2-y^2}, g_{xy(x^2-y^2)}\}$-wave states [4].

Roman Schlem. German
University of Muenster, Germany

'This work forms a major part of my doctoral thesis, which mainly focuses on structure–property relationships in rare-earth superionic conductors. Combining techniques such as X-ray, synchrotron and neutron diffraction as well as electrochemical impedance spectroscopy, we try to shed light on the influence of different synthesis techniques on resulting chemical structures and link this to observed electrochemical performance. We also provide guidance on attempts to improve lithium- and sodium-based superionic conductors.'

AUTHORS
R. Schlem, A. Banik and W.G. Zeier (University of Muenster, Germany)
E. Suard (ILL)
S. Ohno (Kyushu University, Japan)

ARTICLE FROM
Chem. Mater. (2021)—doi:10.1021/acs.chemmater.0c04352

REFERENCES
[1] M. Gombotz and H.M.R. Wilkening, ACS Sustain. Chem. Eng. 9 (2021) 743
[2] T. Asano, A. Sakai, S. Ouchi, M. Sakaida, A. Miyazaki and S. Hasegawa, Adv. Mater. 30 (2018) 1803075

Insights into the lithium sub-structure of superionic conductors Li_3YCl_6 and Li_3YBr_6

High-resolution two-axis diffractometer D2B

Rare-earth, superionic lithium-ion conductors have been put forward as promising candidates for application in new, solid-state battery design. The underlying lithium sub-structure plays a key role in the electrochemical performance of such materials and, alongside first insights into possible diffusion behaviour, can be studied by high-resolution neutron diffraction and are of paramount value in driving further improvement of such superionic materials.

Using Li_3YBr_6 as an example, we were able to introduce an experimentally confirmed lithium distribution along different octahedral sites and propose an additional tetrahedral co-ordination of lithium ions by bromide anions [1]. The resulting neutron diffraction pattern and structure obtained at room temperature (space group C2/m) are shown in **figure 1**. The structural backbone can be described as a face-centred arrangement of isolated YBr_6^{3-} octahedral on the 001 planes (**figure 1c–e**), with $LiBr_6^{5-}$ octahedra occupying the resulting voids and sharing edges along the ab-plane and in c-direction (**figure 1b–e**).

Interestingly, the synthesis method employed (high-temperature ampoule synthesis *vs* mechanochemical milling) has a significant influence on the resulting disorder, lithium ion distribution and ionic transport properties in rare-earth halides [2]. In the case of Li_3YBr_6 we were able to show that the occupancy of lithium ions on the tetrahedral site strongly depends on the synthesis method employed (**figure 2a**). Furthermore, using the cryo-furnace in the measurement set-up of the D2B diffractometer it was possible to map the influence of temperature. A first insight into the directional preference of lithium-ion diffusion was gained by analysing the anisotropic, temperature-dependent atomic displacement parameters (**figure 2b**). A direct correlation with the adjacent yttrium-ion occupancy was indicated, based on electrostatic interactions (**figure 2c**).

Thus, knowledge of the exact lithium-ion distribution and the influence of the synthesis method employed are important parameters when it comes to designing strategies to improve electrochemical performance that can involve either element-substitution approaches or tweaking of the (micro)structure.

Acknowledgements: The research was supported by Deutsche Forschungsgemeinschaft (DFG) under grant number ZE 1010/4-1. AB acknowledges the Alexander von Humboldt Foundation for its financial support through a postdoctoral fellowship.

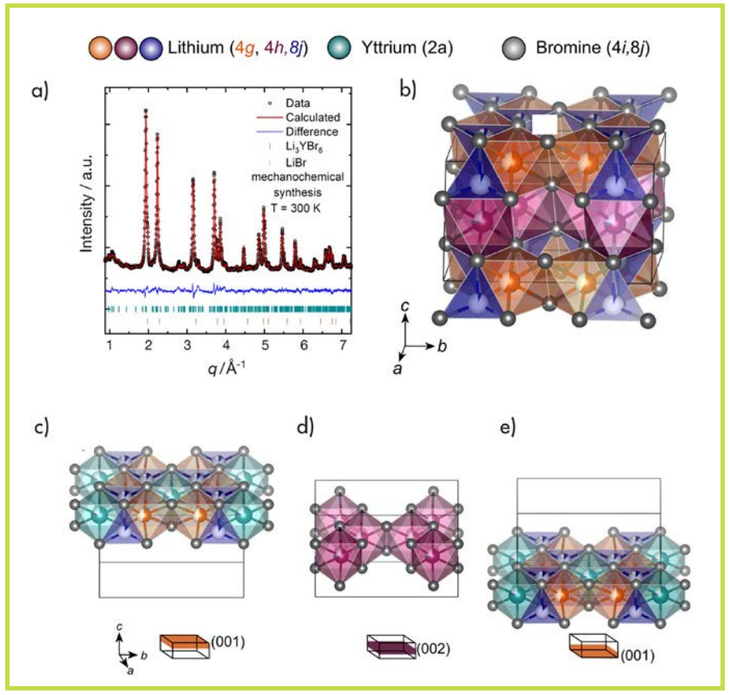

Figure 1

Representative room-temperature neutron diffraction pattern of the mechanochemically synthesised Li_3YBr_6 sample.
a) A monoclinic unit cell (space group C2/m) is used to describe the structure **b)** that consists of YBr_6^{3-} and $LiBr_6^{5-}$ octahedra (teal and orange/red), as well as $LiBr_4^{3-}$ tetrahedra (blue). The polyhedra can be found in different layers **(c–e)**.

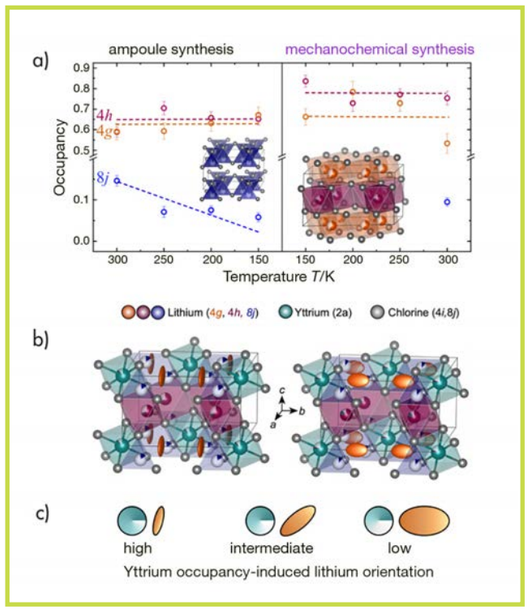

Figure 2

a) Comparison of the two different synthesis approaches with resulting partial occupancies of lithium ions on the various possible sites (blue = tetrahedral; orange/red = octahedral). For both syntheses, the higher occupancies on octahedral sites suggest better stability in this co-ordination, with no severe temperature influence observed. **b)** Structural representations. **c)** Anisotropic displacement ellipsoids for lithium ions on one octahedral site, indicating a different directional preference, based on the synthesis employed and yttrium occupancy.

David Portehault. French Laboratory of Condensed Matter of Paris (LCMCP), France
@DavidPortehault

'I am research director at the CNRS, hosted by Lab LCMCP at Sorbonne University. I explore synthesis pathways at the edge of solid-state and solution chemistry in order to discover nanomaterials based on oxide, boride and silicide chemistry for energy-related properties.'

Hydroxyapatites as versatile inorganic hosts of unusual pentavalent manganese cations

High-resolution two-axis diffractometer D2B

Manganese is a ubiquitous element of life, especially of photosynthesis in which high-valence Mn species, especially the rare Mn(V) oxidation state, are involved. These rare electronic states are accompanied by specific properties, especially in catalysis and energy conversion. Most synthesised Mn(V) compounds are unstable, except in fully inorganic solids. However, the latter are so rare that it has been difficult up until now to draw up guidelines for the design of stable Mn(V) solids and materials. In this work we employed neutron diffraction, first to highlight some key design concepts and then to initiate a paradigm shift towards a new family of Mn(V) materials.

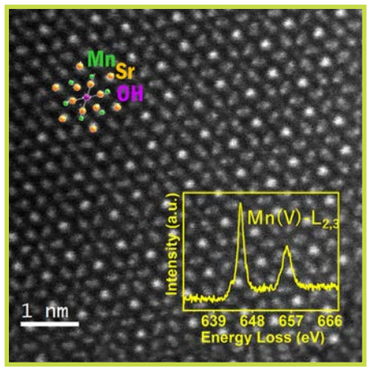

Scanning transmission electron micrograph with atomic number contrast, superimposed with the crystal structure of Mn(V) hydroxyapatites and the specific electron energy loss spectrum of Mn(V) compounds.

AUTHORS

D. Portehault (Laboratory of Condensed Matter of Paris – LCMCP, France)
M.T. Fernández-Diaz (ILL)
M. Parras (Universidad Complutense de Madrid)

ARTICLE FROM

Chem. Mater. (2021)—doi:10.1021/acs.chemmater.0c03673

REFERENCES

[1] M.T. Weller and S.J. Skinner, Acta Crystallogr. Sect. C Cryst. Struct. Commun. 55 (1999) 154
[2] T. Funahashi, A. Mineshige, H. Yoshioka, K. Kobayashi, Y. Matsushita, Y. Katsuya, M. Tanaka, O. Sakata and T. Yazawa, Solid State Ion. 289 (2016) 106

Very few Mn(V)-oxides are known [1]. Up until now, the stabilisation of this unusual oxidation state appeared to be concomitant with the presence of Ba^{2+} in the cationic sublattice. Using soft aqueous chemistry we have managed to design new Sr/Mn(V) hydroxyapatites and their corresponding fluoride-doped compounds, thereby establishing that Ba^{2+} is not essential to stabilise Mn(V). These apatites showed significant anionic conductivity, opening the way to new functional materials built from high-oxidation-state manganese cations.

The first compounds we synthesised have the formula $Sr_5[(Mn_{1-x}Si_x)O_4]_3(OH)_{1-3x}$ ($0 < x < 0.058$) and an apatite structure built from isolated $Mn^{V}O_4^{3-}$ tetrahedra that organise into hexagonal channels running along the *c*-axis and occupied by OH^-/F^- anions (**figure 1a**). Powder neutron diffraction was necessary to determine the crystal structures and compositions accurately. By performing measurements on the high-resolution D2B diffractometer at room temperature, we were able to calculate the Mn/Si ratio in the tetrahedral units of the hydroxyapatite structure due to the different scattering factors (b_{Mn} = -3.73 fm, b_{Si} = 4.149 fm). Thanks to the high hydrogen-sensitivity of neutron diffraction, we succeeded in quantifying and specifying the crystallographic position of the OH groups along the *c*-axis in these Sr-based apatites by using difference Fourier maps (**figures 1b and 1c**).

We subsequently fluorinated these hydroxyapatites to assess how fluoride anions trigger structural transformations and how they can modify anionic conduction. In order to preserve the apatite structure, we fluorinated the hydroxyapatites (using polytetrafluoroethylene as the fluorinating agent) at low temperature. F and O atoms could not be distinguished by neutron diffraction (ND) due to their similar scattering lengths. To overcome this challenge, we again moved

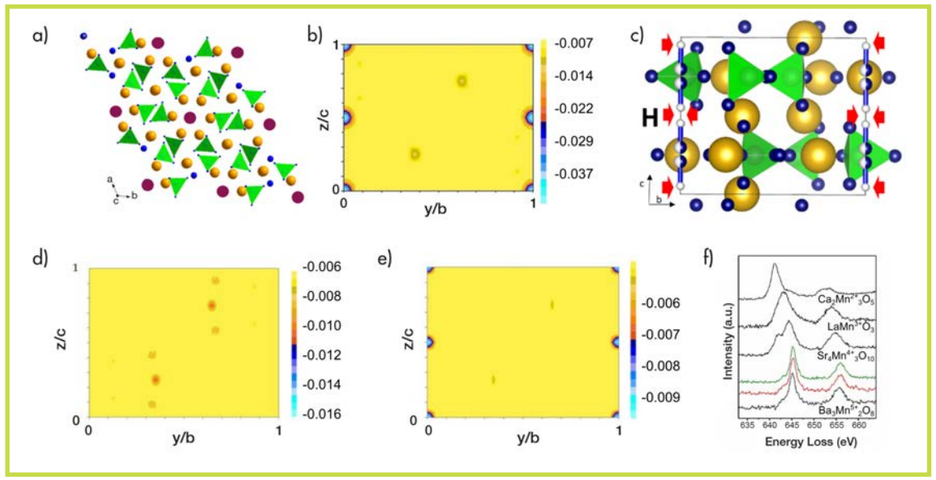

Figure 1

Crystal structure representation for apatite-type structure along **a)** [001] and **c)** [1-10] directions (Sr = orange, Mn = green, OH/F = purple, O = blue). Difference Fourier maps (excluding hydroxyl H) of the section x = 0 for **b)** hydroxyapatites, for **c)**, **d)** Si-doped and **e)** Si-free fluorapatite, respectively. The maps show the positions in which the most prominent negative scattering density appears. The hydrogen atoms of the OH groups should be located at these positions. **f)** The Mn-$L_{2,3}$ EELS spectrum for Si-doped hydroxyapatite (green line) and Si-doped fluorapatite (red line) corresponds to Mn(V) when compared with spectra of reference samples (black lines).

to H detection by neutron diffraction in order to explore the possible substitution of OH^- ions by smaller F^- ones. Difference Fourier maps generated from ND data for the Si-doped hydroxyapatite showed no negative scattering in the section x = 0 (**figure 1d**), thus ruling out the presence of OH groups in the channels of the apatite structure. Hence, the OH^- ions were fully substituted by F^- ions, leading to $Sr_5[(Mn_{0.942(3)}Si_{0.058(3)})O_4]_3F_{0.83(1)}$. In contrast, the difference Fourier map for the Si-free sample exhibited negative scattering density at z ~0 and ~0.5 in the section x = 0 associated with the proton of the OH groups (**figure 1e**). From this ND refinement, the $Sr_5(MnO_4)_3F_{0.90(2)}(OH)_{0.10(2)}$ crystallographic formula could be determined.

Based on the accurate assessment of chemical compositions and crystal structures, we were able to ascertain the sole presence of Mn(V) and use the as-obtained compounds to record, for the first time, electron energy loss spectra (EELS) Mn-$L_{2,3}$ of manganese with oxidation state (V) (**figure 1f**). Our samples exhibit conductivity values of the order 10^{-4} S cm^{-1} and low corresponding activation energies at 500 °C, in agreement with O^{2-} conduction and comparable with oxyapatite-type lanthanum silicates [2].

The accurate structure we obtained from neutron diffraction data was essential in identifying the anionic conduction paths from calculated Bond Valence Energy Landscape maps (BVEL). Two different conductions paths were identified: through the O^{2-} ions (**figure 2a**) of the tetrahedral units; and through the hydroxyl or F^- anions (**figure 2b**) in the channels of the apatite structure. These rare-earth-free materials constitute a novel approach to the design of materials for solid oxide fuel cells.

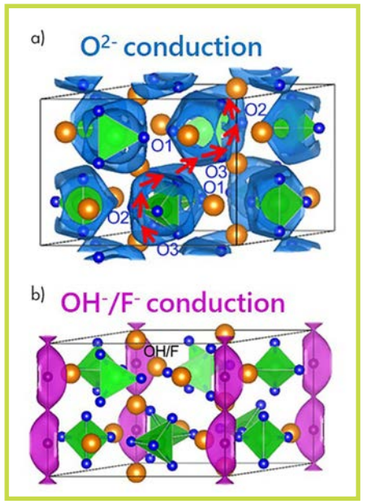

Figure 2

Anionic conduction paths deduced from BVEL calculations:
a) O^{2-} conduction paths are shown in blue leading to a conduction along [001] (red arrows);
b) OH^-/F^- conduction paths in the apatite channels running along [001] (purple). (Sr, Mn, OH/F and O atoms are orange, green, purple and blue, respectively.)

Sacha Fop. Italian
ISIS and University of Aberdeen (UK)
@sacha_fop

'I am an Instrument Scientist on the high-resolution powder diffractometer (HRPD) at ISIS and an Honorary Research Fellow at the University of Aberdeen. My research focuses on the discovery of novel solid-state ionic conductors for energy-related applications and on understanding their structure–property relationships using a combination of neutron diffraction and electrical characterisation methods.'

Hydration and ionic conduction mechanisms of hexagonal perovskite derivatives

High-resolution two-axis diffractometer D2B

Proton-conducting oxides are important materials, with applications in hydrogen-based energy conversion, storage and electrochemical solid-state technologies. Proton conduction in these materials is enabled by water absorption and the creation of mobile protonic defects. Understanding of the mechanisms of hydration and proton transport is essential for the sound design of novel materials with higher proton conductivity, a crucial requirement for the development of hydrogen technologies and devices with improved performance.

AUTHORS

S. Fop (ISIS and the University of Aberdeen, UK)
C. Ritter (ILL)
J.A. Dawson (Newcastle University, UK)
A.D. Fortes (ISIS, UK)
A.C. McLaughlin (University of Aberdeen, UK)

ARTICLE FROM

Chem. Mater. (2021)—doi:10.1021/acs.chemmater.1c01141

REFERENCES

[1] S. Fop, K.S. McCombie, E.J. Wildman, J.M.S. Skakle, J.T.S. Irvine, P.A. Connor, C. Savaniu, C. Ritter and A.C. Mclaughlin, Nat. Mater. 19 (2020) 752
[2] K.D. Kreuer, Annu. Rev. Mater. Res. 33 (2003) 333
[3] G. Kim, J.M. Griffin, F. Blanc, S.M. Haile and C.P. Grey, J. Am. Chem. Soc. 137 (2015) 3867

We recently discovered high proton conductivity in the cation-deficient hexagonal perovskite $Ba_7Nb_4MoO_{20}$ [1]. In dry conditions, the conductivity of $Ba_7Nb_4MoO_{20}$ is purely oxide ionic. Proton conduction is enabled under a humidified atmosphere, with a proton transport number (which is the ratio of proton conductivity to total conductivity) of ~ 0.8 at 500 °C. The proton conductivity is 4.0 x 10^{-3} S cm^{-1} at 500 °C, comparable to state-of-the-art doped barium cerate and zirconate cubic perovskite-type proton conductors. $Ba_7Nb_4MoO_{20}$ represents the first example of high proton conduction in a hexagonal perovskite derivative. The high proton conductivity is particularly surprising as normally proton mobilities are lower in perovskite oxide structures deviating from cubic symmetry [2]. To understand the origin of the high proton conduction in this hexagonal derivative, we used a combination of *in situ* neutron diffraction experiments under controlled dry/humidified air atmosphere and atomistic calculations in order to fully characterise the hydration and the proton transport mechanisms of $Ba_7Nb_4MoO_{20}$.

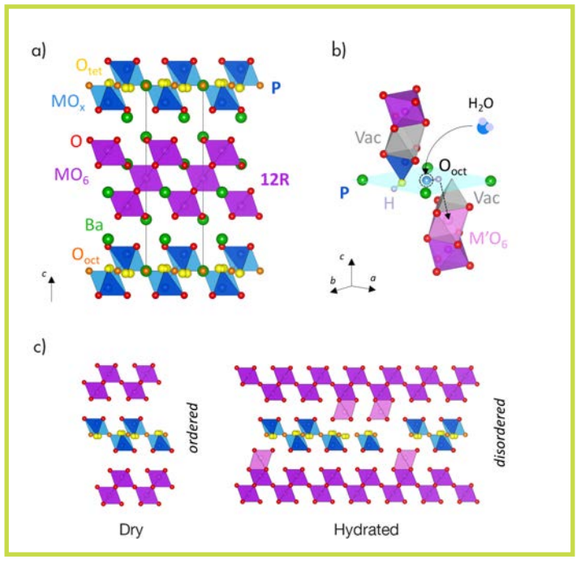

Figure 1

a) Structure of dry $Ba_7Nb_4MoO_{20}$, comprising an ordered intergrowth of palmierite-like layers (P) and 12R perovskite blocks.
b) Representation of the water absorption on a vacant O_{oct} site. Hydration forces the shift of a metal from a palmierite site to an adjacent vacant octahedral metal site (Vac), with the consequent formation of an MO_6 unit.
c) Representation of the ordered and disordered local metal-vacancy stacking configuration in dry and hydrated $Ba_7Nb_4MoO_{20}$.

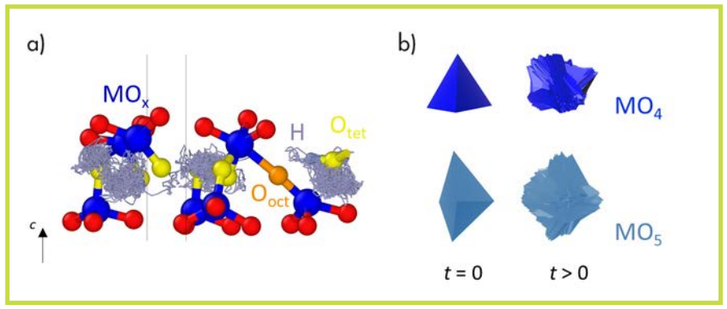

Figure 2

a) Proton trajectory plots for hydrated $Ba_7Nb_4MoO_{20}$ obtained by AIMD simulations. Proton migration occurs *via* rotation and hopping along the delocalised proton positions. **b)** Schematic showing the orientations of typical MO_x polyhedral units at the start ($t = 0$) and for every timestep ($t > 0$) of the AIMD simulations overlaid on each other. The MO_x polyhedra have high rotational mobility and flexibility.

In dry atmosphere, the typical structure of $Ba_7Nb_4MoO_{20}$ comprises an ordered intergrowth of 12R hexagonal perovskite blocks and oxygen-deficient ([BaO_2]) palmierite-like layers (**figure 1a**). The latter are formed by isolated MO_x polyhedral units with mixed local 4-, 5- and 6-fold co-ordination due to partial occupation of two mutually exclusive crystallographic tetrahedral and octahedral oxygen sites (O_{tet} and O_{oct}). Water absorption in proton-conducting oxides generally occurs *via* the hydration of extrinsic oxygen vacancies introduced by acceptor doping, resulting in the creation of protonic defects [2]. Neutron diffraction measurements under humidified atmosphere on the high-resolution powder diffractometer revealed that in $Ba_7Nb_4MoO_{20}$, water is absorbed in the intrinsic oxygen vacancies present on the palmierite-like layer and predominantly distributed on the O_{oct} sites. As demonstrated by maximum entropy (MEM) analysis and density functional theory (DFT) calculations, the water absorption leads to disordering of the metal-stacking vacancy distribution due to a shift of the cation in the palmierite-like layer towards an adjacent, mutually exclusive, vacant site (**figure 1b**). Partial occupation of the two metal sites results in the formation of disordered local stacking configurations, creating a complex disordered network of isolated, face-sharing and corner-sharing polyhedral units in the hydrated material (**figure 1c**). The significant structural flexibility of $Ba_7Nb_4MoO_{20}$ allows the accommodation of the local cation and anion disorder introduced by hydration and enables a high concentration of water uptake—≥ 0.8 molecules of H_2O per formula unit.

Low-temperature neutron diffraction measurements on D2B and DFT analysis on a hydrated $Ba_7Nb_4MoO_{20}$ sample demonstrated that protons are delocalised within the palmierite-like layers. The positional oxide-ion disorder generated by the proximity of available oxygen sites due to the particular topology of the palmierite-like layers leads to delocalisation of the protonic defects over a variety of low-energy configurations around their equilibrium site in the vicinity of the O_{tet} and O_{oct} sites. Delocalisation results in the creation of a two-dimensional low-energy transport pathway along the palmierite-like layers, where the proton defects can migrate *via* rotation and hopping motion as evidenced by *ab initio* molecular dynamics (AIMD) simulations (**figure 2a**). AIMD simulations also revealed high flexibility and rotational mobility of the isolated variable co-ordination MO_x units (**figure 2b**), which assists the proton motion [3]. The similar energies of the different proton configurations lead to a disordered proton sublattice, where frustration of the proton positions (and of the hydrogen-bond network) coupled with the dynamic flexibility of the metal units results in the high mobility of the protonic defects and the creation of low-energy transport pathways.

In conclusion, our findings demonstrate that water absorption is promoted in hexagonal $Ba_7Nb_4MoO_{20}$ thanks to the ability of the crystal lattice to accommodate anion and cation disordered environments, while frustration of the proton sublattice and the high dynamic flexibility of the variable co-ordination MO_x units enable fast proton transport. Our results provide innovative design rules for the development of novel proton-conducting oxides crystallising with disordered cation and anion sublattices.

Laura Paradis-Fortin. Canadian National Taiwan University, Taiwan

'I am an ambitious and highly motivated postdoctoral researcher working on the development of new thermoelectric materials. During my PhD in collaboration with CRISMAT (Caen) and ISCR (Rennes), I worked on the synthesis and processing of chalcogenide materials. During this period I got the chance to carry out a few experiments at the ILL—experiments that are among the work I am most proud of.'

Time-resolved *in situ* neutron diffraction study of the germanite $Cu_{22}Fe_8Ge_4S_{32}$: a guide to the synthesis of complex chalcogenides

High-intensity powder diffractometer D1B

Earth-abundant copper-based sulphides have been receiving considerable attention from scientists as the urgency to discover and improve the efficiency of sustainable materials for energy applications remains. Within just a few years, they have been promoted as cost-efficient and environmentally-friendly candidates for thermoelectric power generation [1, 2]. However, the development of new materials and an understanding of their structure–property relationships requires the preparation of high-purity samples, which can be very challenging in the case of complex, copper-based sulphides such as the germanite derivative $Cu_{22}Fe_8Ge_4S_{32}$ compound.

AUTHORS

L. Paradis-Fortin (Institut des Sciences Chimiques de Rennes and CRISMAT laboratory, Caen, France)
P. Lemoine, **C. Prestipino** and **S. Cordier** (Institut des Sciences Chimiques de Rennes, France)
E. Guilmeau, **V. Pavan Kumar** and **B. Raveau** (CRISMAT laboratory, Caen, France)
V. Nassif (Institut Néel, Grenoble, France)

ARTICLE FROM

Chem. Mater. (2020)—doi:10.1021/acs.chemmater.0c03219

REFERENCES

[1] P. Lemoine *et al.*, Angew. Chem. Int. Ed. 61 (2022) e202108686
[2] G. Guélou *et al.*, J. Mater. Chem. C 9 (2021) 773
[3] K. Simmance *et al.*, Phys. Chem. Chem. Phys. 12 (2010) 559
[4] T. Friščić *et al.*, Nat. Chem. 5 (2013) 66
[5] T.C Hansen and H. Kohlmann, Zeitschrift fur Anorg. und Allg. Chemie 640 (2014) 3044
[6] V. Pavan Kumar *et al.*, ACS Appl. Energy Mater. 2 (2019) 7679

Solid-state synthesis in a sealed tube is one of the fundamentals of inorganic material chemistry. However, in addition to being time-consuming, this method is unsuitable for detecting and determining quick reactions as well as short-lived or air-sensitive intermediates. Real-time, *in situ* reaction monitoring allows the development of rational synthesis schemes and a better understanding of the kinetic reactions and mechanisms that occur during crystallisation sequences [3,4]. Yet, such experiments remain limited to X-ray diffraction (XRD) analyses.

Thanks to the development of dedicated instruments on high-flux neutron sources enabling fast data acquisition [5], *in situ* neutron powder diffraction (NPD) has since been used to study the crystallisation of amorphous materials, cationic ordering, mechanical properties, solid–gas reactions and chemical processes in batteries. To date, *in situ* NPD studies of sulphide materials have been performed only on pre-reacted or already-formed sulphides, mainly to determine their temperature stability and decomposition mechanisms. Despite the clear advantages of neutrons over X-rays (*i.e.* high penetration depth suitable for bulk sample characterisation, scattering lengths of the same order of magnitude even for light elements and magnetic ordering detection), to the best of our knowledge *in situ* neutron diffraction has never been used to characterise the successive chemical reactions occurring during sealed-tube synthesis from elemental precursors in real time. In the case of certain complex compounds of the quaternary sulphide systems, such experiments are vital for determining the synthesis conditions.

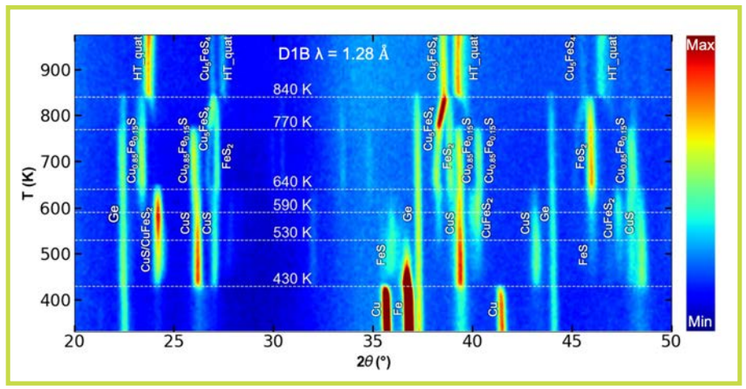

Figure 1

2D contour plot showing the NPD patterns of the *in situ* sealed-tube reaction during synthesis of the germanite $Cu_{22}Fe_8Ge_4S_{32}$ from elemental precursors (heating rate of 2 K min^{-1}, 2.5 min per pattern).

In this study we monitored, for the first time, the nature and crystal structure of the intermediate phases formed during the solid–liquid–gas reactions of the quaternary compound $Cu_{22}Fe_8Ge_4S_{32}$. Using time-resolved *in situ* NPD data, we analysed the successive chemical reactions as a function of temperature and determined the key conditions for producing high-purity samples.

First, we observed the successive formation of binary, ternary and quaternary compounds while heating from room temperature (RT) to 973 K, as shown on the 2D contour plot in **figure 1**. The first quaternary phase (HT_quat) appears above 840 K from the reaction of metallic Ge with the ternary Cu-Fe-S phases. Despite excellent qualitative results, one of the limitations of this *in situ* investigation is the inability to perform quantitative analyses by Rietveld refinement because of the noisy background caused by silica diffraction. To overcome this, we produced a sample that closely resembled the HT_quat intermediate in the laboratory by quenching a germanite synthesis at 973 K. The Rietveld refinement of the *ex situ* X-ray diffractogram revealed that the HT_quat phase is a mix of tetragonal and cubic phases, both highly disordered.

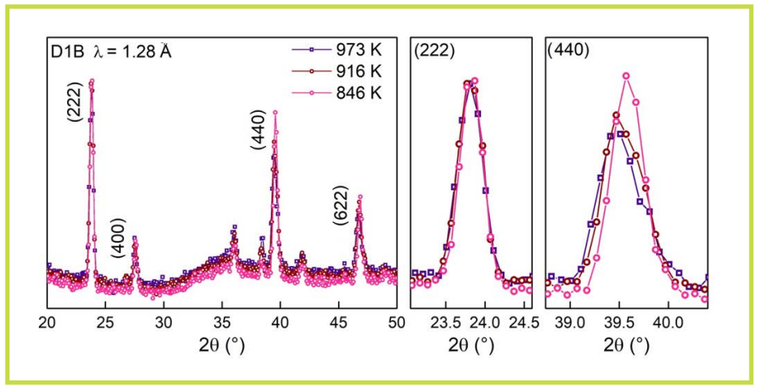

Figure 2

NPD patterns acquired during controlled cooling (2 K min^{-1}) at 973 K, 916 K and 846 K, showing the change from tetragonal to cubic structure during cooling.

Secondly, during controlled cooling the first change we observed was related to the profile of the peak detected at $2\theta = 39.5$ ° ($\lambda = 1.28$ Å), which evolves from a well-defined doublet at 973 K to a thinner single peak at 846 K, passing through a broad 'single' peak stage at 916 K (**figure 2**). This peak profile evolution suggests a structural change from tetragonal to cubic symmetry, as previously observed in the germanite-renierite series $Cu_{22-x}Zn_xFe_8Ge_4S_{32}$ [6]. The broadening of the 'single' peak at 916 K can be attributed to cationic disorder and/or the coexistence of both cubic and tetragonal phases. The second observable change was the emergence of a small peak at 25.9 ° in the temperature range 860 K to 820 K. This peak is attributed to the superstructure reflection (321) of germanite, referring to space group $P\bar{4}3n$, indicating that the cubic phase formed between 916 K and 846 K is germanite. Finally, the third observable change was the anomalous broadening of the main peak's base, observed while cooling the sample below 770 K and attributed to the appearance of a low crystallinity sphalerite-like derivative phase. The formation of this phase at 770 K hinders the synthesis of a pure germanite sample using slow cooling below this point and explains the need to quench the sample slightly above this temperature.

In conclusion, real-time investigation by *in situ* NPD allowed us to highlight the importance of the synthesis temperature and cooling method in the formation of a high-purity germanite $Cu_{22}Fe_8Ge_4S_{32}$ sample, a primordial step on the road to further characterisations (cationic distribution, magnetism…) of this exciting thermoelectric sulphide. In addition, this study is a proof of concept of the power of real-time investigation of chemical reactions in a silica sealed tube by *in situ* NPD that can easily be applied to the study of other ternary and quaternary chalcogenides and paves the way for the discovery of new materials.

Livia E. Bove. Italian
CNRS, Paris and Sapienza University, Rome

'I am currently a senior scientist at the Institut de Mineralogie, Physique des Materiaux et Cosmochimie (CNRS Paris) and an associate professor in the Physics Department at Sapienza University (Rome). Since my PhD in Physics and my postdoc at the ILL, I have been using neutron scattering to investigate the structure and dynamics of disordered systems. My recent research mainly focuses on water, methane, hydrogen and other simple molecular systems and their compounds under extreme conditions of pressure, temperature and confinement.'

About the formation of two distinct networks of water confined in hydrophilic zeolite nanopores at low temperatures

Disordered materials diffractometer D4 and spectrometer IN1-LAGRANGE

Whatever the nature of the surface of the porous matrix (hydrophilic or hydrophobic), restriction of the accessible space induced by nano-confinement has strong consequences on water behaviour. The adsorption of a strongly polar molecule like water gives rise to a rich and disparate phenomenology due to strong guest–guest interactions and tunable host–guest interactions, depending on the chemical nature of the nanopore's surface. We probed the structural and vibrational properties of water in the nanopores of hydrophilic $AlPO_4$-54•xH_2O zeolite by combining several experimental and simulation techniques, including neutron powder diffraction and incoherent inelastic scattering. Decreasing temperature down to 10 K we observed the progressive formation of two distinct water networks: an amorphous ice layer proximal to the pore walls having low density, a high degree of orientational order and low reactivity; and a denser, highly disordered and more mobile water network in the pore core.

Figure 1

Top: Experimental structure of $AlPO_4$-54•xH_2O at T = 135, 100 and 50 K, obtained from single-crystal XRD. The light blue and purple polyhedra are the AlO_4, AlO_5 and PO_4 units of $AlPO_4$ while the dark blue circles indicate the O atoms of water molecules (the O ADP are represented at 50 % probability). **Bottom**: Pair distribution functions PDF(r) of $AlPO_4$-54•xH_2O at T = 300, 173, 100 and 10 K, and for dehydrated $AlPO_4$-54 at T = 10 K as measured on D4.

AUTHORS

F.G. Alabarse (Elettra Synchrotron Trieste, Italy)
M. Jiménez Ruiz and **H.E. Fischer** (ILL)
B. Coasne (Grenoble Alpes University, CNRS, France)
J. Haines (University of Montpellier, France)
J.B. Brubach and **P. Roy** (Synchrotron Soleil, Saint Aubin, France)
S. Klotz and **L.E. Bove** (CNRS and Sorbonne University, Paris, France)

ARTICLE FROM

J. Phys. Chem. (2021)—doi: https://doi.org/10.1021/acs.jpcc.1c01254

REFERENCES

[1] J. Klein and E. Kumacheva, Science 269 (1995) 816; A.P. Deville *et al.*, Science 311 (2006) 515
[2] N. Giovambattista, P.J. Rossky and P.G. De Benedetti, J. Phys. Chem. 113 (2009) 13723; K. Koga, X.C. Zeng and H. Tanaka, Phys. Rev. Lett. 79 (1997) 5262
[3] K. Koga *et al.*, Nature 412 (2001) 802; S.D. Bernardina *et al.*, J. Am. Chem. Soc. 138 (2016) 10437
[4] F.G. Alabarse *et al.*, Phys. Rev. Lett. 109 (2012) 035701
[5] F.G. Alabarse *et al.*, J. Phys. Chem. C 125 (2021) 14378

The insertion and ordering of small molecules in one-dimensional arrays of channel-shaped cavities has been investigated largely because it is of great interest for various disparate applications, such as molecular sieves, phase separation, heterogeneous catalysts, nanotribology, fabrication of nanomaterials using simple molecules as a template, and even for the durability of concrete. As water is present in most molecular sieves, its order, structuring and reactivity as a function of temperature is of particular importance in several chemical–physical processes [1]. The versatility of the water network to re-adapt under different thermodynamic conditions gives rise to its incredibly rich phase diagram and is also responsible for the disparate behaviours observed for water confined in different environments.

Over the past decades, studies have been carried out on water confined in both crystalline and amorphous nanoporous materials. All have universally observed a lowering of the freezing point of confined water, but no general agreement has been reached on the conditions for suppression of crystallisation by confinement in terms of pore size, pore structure and the nature of the water–surface interaction. Some studies have shown that at temperatures below the bulk freezing point, water confined in hydrophobic nanopores crystallises [2]. This is also supported by the observation of the formation of ice nanotubes in carbon nanotubes [3]. A different scenario has been reported for the freezing of water in hydrophilic nanopores: here, the pore surface can induce order in the water that is in contact with its wall (*proximal water*) but crystallisation is suppressed because of the insufficient number of hydrogen bonds, while water in the pore centre (*inner water*) remains disordered [4].

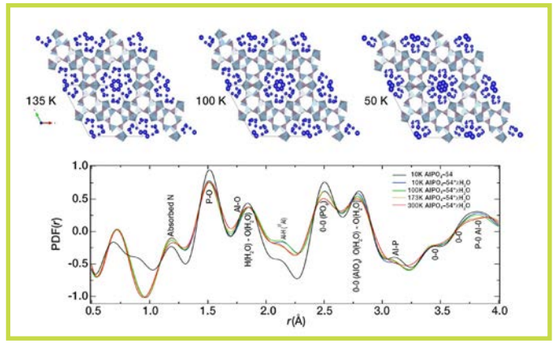

We performed a series of new experiments and simulations [5], combining single-crystal X-ray and powder neutron diffraction, incoherent inelastic neutron scattering (INS), far- and mid-infrared spectroscopy, *ab initio* molecular dynamics (AIMD) and grand canonical Monte Carlo simulations to unravel the structural and vibrational properties of water confined in the hydrophilic $AlPO_4$-54•xH_2O zeolite, from ambient temperature down to 10 K.

$AlPO_4$-54•xH_2O (hexagonal VFI structure, space group $P6_3$) exhibits highly hydrophilic 1D pores along the c direction with a diameter of 12.7 Å that are among the largest pores known for zeolites and aluminophosphates. Neutron diffraction data for pair distribution function (PDF) analysis were collected on both fully hydrated and dehydrated zeolite using the Disordered Materials diffractometer D4 at the ILL, as a function of temperature (cryofurnace), and over a large Q-range (Q_{range} = 0.5–23.5 $Å^{-1}$), using neutrons of 0.5 Å wavelength from the ILL's hot neutron source (**figure 1**). INS measurements of the generalised density of states of zeolitic-confined water were performed using the IN1-LAGRANGE spectrometer with the 2D-focusing Cu220 monochromator (**figure 2**).

The PDF(*r*) data provide information on both the local structure of nano-confined water and changes in the $AlPO_4$ structure as temperature decreases, while the INS data are highly sensitive to the number and strength of the hydrogen bonds formed by confined water molecules.

Upon cooling, there is a clear sharpening of several peaks in the PDF(*r*) and an increase in the number of O atoms bonded *via* H-bonds (HB) with a typical distance of 2.8 Å (**figure 1**). From the PDF(*r*) difference between hydrated and dehydrated phases [5] we observe that upon decreasing the temperature the HB peak (see before) (at around 1.82 Å) shifts towards lower values, which is consistent with a strengthening of the H-bond network. The shift, and a sharpening of the peak at 2.14 Å for temperatures lower than 173 K, indicates changes in the local structure of the octahedral environment of Al. With regard to the Al-H intra-octahedral distance (Al-O-H), the slight increase in the peak intensity and the shortening of the Al-H intra-octahedral distance (Al-O-H) suggest structural changes with T also in the Al-H environment.

Turning to the INS data, the librational band deriving from frustrated rotational oscillations of water molecules is clearly visible in the 300–1 200 cm^{-1} range, and indicates that the structural organisation of the nano-confined water molecules is the superposition of two distinct water networks—as also suggested by IR measurements of the OH-stretching and -bending bands. In particular, comparing the librational band of zeolitic-confined water with the ones measured for hexagonal (Ih), cubic (Ic), low- (LDA) and high- (HDA) density ices we observe that the former presents defined features arising from a lighter ordered local structure (such as Ic and/or LDA ices) superimposed on a broader band arising from a disordered and denser state (such as HDA). This band could only be probed by INS, as this region is typically dominated by the zeolite framework modes in Raman and IR spectra.

The body of our results confirms that water in the zeolite nanopores does not crystallise, even at the lowest temperature investigated, while an increasingly different structural and dynamical behaviour of proximal and inner water develops on cooling. From 250 K down to ~150 K we observe the orientational ordering of proximal water at the pore wall due to strong interactions with the pore surface, while inner water retains a disordered arrangement with glassy-like behaviour. From ~150 K down to ~10 K, a strengthening of the water–water interactions is observed. As a consequence, despite the strong hydrophilicity of the zeolite structure, proximal water shows a continuous increase in orientational order upon cooling while inner water becomes denser and more disordered. The simulations, far-IR and INS results suggest that inner water is even more distorted than HDA, but similarly denser. Since the framework is essentially rigid (XRD results show no variation in pore size) the overall density of water must be constant, therefore the density of proximal water must decrease to keep the overall density constant. This is essentially due to an excluded volume effect: the stacking up of water molecules at the pore wall is not 100 % efficient due to the wall constraint. This results in a lower density of proximal water with respect to the bulk.

In conclusion, the low T experiments suggest the presence of two distinct, unidirectional, arrangements of water molecules in the $AlPO_4$-54•xH_2O nano-channels, whose coexistence persists at the lowest T studied. Upon cooling, below 150 K a denser amorphous arrangement of water molecules with a disorder degree even greater than HDA develops and is embedded in a less dense and orientationally ordered local arrangement of water molecules closely linked to the pore surface. These two independent networks imply very diverse settings: one supporting mobile water with many free H-bonds located in the centre of the pores (inner water); the other, strongly bonded to both the interface and other water molecules (proximal water) and acting as a 2D ice layer with very low reactivity.

Figure 2

a) INS spectra of $AlPO_4$-54•xH_2O (coloured) at T = 10, 173, 235 and 293 K and dehydrated (black) $AlPO_4$-54 at T = 10 K. **Inset a)** Librational band for $AlPO_4$-54•xH_2O at T = 293 K, together with the deconvoluted Gaussian components (dashed lines) corresponding to the three librational modes around the three symmetry axes of water molecules (see **inset b**: H, white sphere; O, red sphere). **b)** INS spectra of $AlPO_4$-54•xH_2O at T = 10 K, together with the deconvoluted Gaussian components (dashed lines). **c)** Normalised INS spectra comparison between ice Ic (blue line) and high-density amorphous ice (HDA, red line).

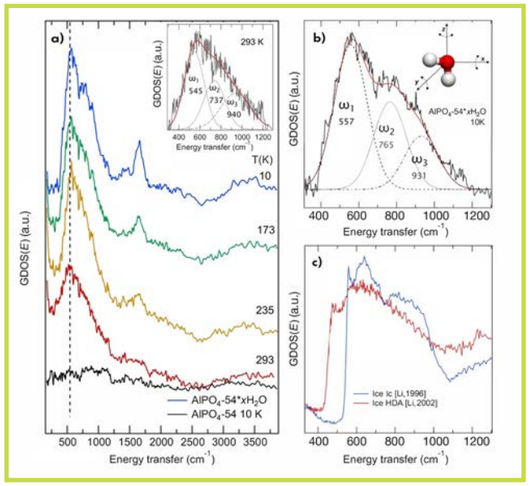

Philipp Gutfreund. German
ILL

'I am an instrument scientist at the ILL and responsible for the FIGARO reflectometer. My main research interest is devoted to the microscopic structure and dynamics of polymeric liquids in out-of-equilibrium or in confinement. I chiefly use neutron scattering techniques for my investigations, with an emphasis on the in situ combination of shear/rheology and neutron scattering. I am also working on the development of the reflectometry technique.'

The physics of art restoration: a neutron scattering study

Fluid Interfaces Grazing Angles ReflectOmeter FIGARO and Partnership for Soft Condensed Matter (PSCM)

AUTHORS
B. Cabane (ESPCI, Paris, France)
Y. Rharbi (Grenoble Alpes University (UGA), France)
Ph. Gutfreund (ILL)
A. Castel (ILL and Grenoble Alpes University (UGA), France)

ARTICLE FROM
Langmuir (2020)—doi:10.1021/acs.langmuir.0c02162

REFERENCES
[1] E. Caretti *et al.*, Acc. Chem. Res. 43 (2010) 751
[2] A. Castel *et al.*, Soft Matter 16 (2020) 1485
[3] A. Castel *et al.*, Langmuir 36 (2020) 12607

Artworks do not last forever. They are composed of changing materials that age with the passage of time. Indeed, varnish layers, there to protect easel paintings, lose their initial appearance with time and have to be replaced periodically. Typically, a painting from the 17th century may have been restored four times, and each restoration operation may have altered the composition and the cohesion of the underlying layers. It is often said that the 20th century was the century during which the largest number of paintings were damaged, not through war or natural calamity but through deliberate restoration operations. In this work, we used neutron reflectometry to investigate the physics of the dissolution process of varnish layers used on model substrates in art restoration. We focused on a particular way of removing the varnish, that entails using aqueous gels comprising only a small amount of good solvent to supposedly limit the impact of aggressive solvent on paintings. Neutron scattering was particularly useful in this case as we could follow the kinetics of solvent penetration of the varnish in real time, distinguishing between the good solvent and the water matrix by deliberately 'marking' the latter by deuteration. We found that although it is the solvent that first penetrates the layer, with sufficiently high concentrations of solvent and in the case of a polar solvent and a polar support it may also allow water to penetrate the layer. This leads to a dewetting of the entire varnish film from the support rather than the desired homogeneous dissolution, which obviously carries high risk for the underlying paint layers which in such cases are directly exposed to the water matrix.

Art plays a significant part in modern society, and the art of restoration is crucial to safeguarding our cultural heritage. However, through accidental damage or deterioration over time, much artwork has been lost. Art restorers and conservators work tirelessly to repair and preserve pieces of art against further damage and to bring them back to their original appearance.

This is particularly true for paintings. Varnishes on easel paintings lose their original appearance through dust and soot deposits in the air, oxidation and structural modification, *e.g.* the effect of free radicals. As a result, varnishes lose their transparency and turn yellow, thus preventing proper appreciation of the artwork. In order to reverse these processes, paintings are periodically restored and the old varnishes replaced. This major treatment requires the swelling and dissolution of the layer of polymeric varnish using solvents that can be penetrating and polar. These solvents can significantly alter the composition and cohesion of the original materials in the painting located under the varnish layers, as shown in **figure 1**.

It is therefore imperative to understand the processes used in restoration operations better, particularly when replacing varnishes. Conscious of this urgency, conservators and scientists have proposed the use of aqueous gels containing the solvents that allow only the quantity of solvent needed to dissolve the varnish to be transferred [1]. The macroscopic images obtained before and after application of these gels demonstrate the efficiency of this method. However, the physical and chemical processes involved are still poorly understood.

The aim of this work was to better understand the physics of the behaviour of varnish film when in contact with solvent/gel mixtures during processes similar to those used in the restoration of artworks. To study the physical processes, we used neutron reflectometry on FIGARO combined with optical microscopy and Atomic Force Microscopy (AFM) in the PSCM. The polymer resin chosen was Laropal®A81, which is mainly used as a modern varnish; for the solvent we used the common benzyl alcohol; and the hydrogel we used was Pemulen TR-2, which is widely used in many applications.

Figure 1
Schematic of the stratigraphy of a painting (not to scale) (ref from @Amélie Castel).

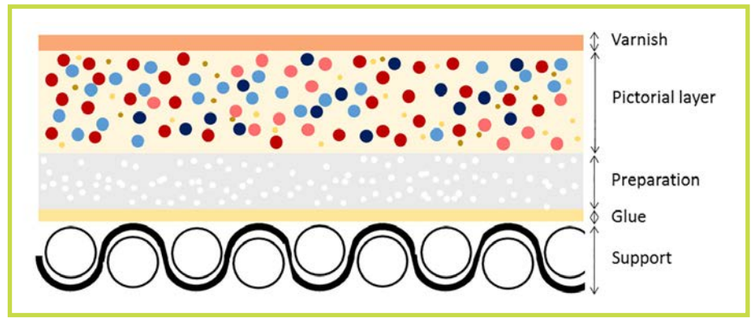

The use of neutron reflectometry in combination with heavy water allowed us to observe, *in situ*, the physical behaviour of ultra-thin polymer films deposited on silicon blocks in contact with the liquid phase. Thanks to the high scattering length density (SLD) contrast between heavy water and benzyl alcohol we could follow the kinetics of varnish swelling by the two liquids independently. Over time, the varnish is first homogeneously swollen almost exclusively by the good solvent (benzyl alcohol) and then penetrated by the bad solvent (D_2O), leading eventually to the dissolution and disappearance of the entire varnish film. As observed before in the case of pure water/solvent mixtures [2], the penetration of water happens not homogeneously, as is the case for the good solvent, but in the form of holes penetrating the entire varnish. These holes grow with time and finally lead to the coalescence of the entire varnish film into small droplets, a process known as dewetting, as shown in the series of optical micrographs in **figure 2** for an example varnish film exposed to a pure water/solvent mixture over different periods.

By investigating this dewetting process as a function of temperature [3] we observed that the speed of dewetting was not greatly affected by heating, even at temperatures elevated to the point of the varnish becoming liquid. An increase in the solvent fraction in the gel, on the other hand, accelerated the dewetting process considerably. This clearly shows that it is not the viscosity of the varnish that drives the dewetting but rather the reduced adhesion of the film to the substrate with the increased presence of the solvent. We argue that this is due to the polar nature of the solvent screening the stabilising polar interaction between varnish and substrate.

The findings of this study can contribute to safer restoration processes by encouraging a closer look at the polarity of the solvents (and non-solvents) used *vis-à-vis* the polar groups present in the protective layer of a painting and its support.

Figure 2
Optical microscopy images (scale bar is 20 µm) of an LA film immersed for different annealing periods in a 0.3 % benzyl alcohol aqueous solution. The annealing time increases from top to bottom.

Hani Cheikh Sleiman. Lebanese University Grenoble Alpes, France

'I have a PhD in Materials Science and Civil Engineering. My research focuses on the drying-driven thermo-hydro-mechanical behaviour of cement-based materials up to moderate temperature.'

Simultaneous X-ray and 4D neutron tomography study of the drying-driven thermo-hydro-mechanical behaviour of cement-based materials at moderate temperatures

Neutron and X-ray tomograph NeXT

The drying of cement-based materials is closely related to their durability, which has significant economic, social and environmental implications. This study explores the drying-driven thermo-hydro-mechanical (THM) processes in a cement paste sample using simultaneous *in situ* neutron tomography and X-ray computed tomography (CT). X-ray CT captures the initiation and propagation of cracks, while neutron CT captures the moisture migration in the heated sample. The combination of these complementary techniques allows the effect of cracks on the local evolution of water content to be quantified [1].

AUTHORS

H. Cheikh Sleiman, **M. Briffaut** and **S. Dal Pont** (University Grenoble Alpes (UGA), France)
A. Tengattini (ILL and University Grenoble Alpes (UGA), France)
B. Huet (LafargeHolcim Research Centre)

ARTICLE FROM

Cem. Concr. Res. (2021)—doi:10.1016/j.cemconres.2021.106503

REFERENCES

[1] H. Cheikh Sleiman, A. Tengattini, M. Briffaut, B. Huet and S. Dal Pont, Cem. Concr. Res. (2021)
[2] G. Viggiani and A. Tengattini. Proceedings of the XVII ECSMGE. (2019)
[3] A. Tengattini, N. Lenoir, E. Andò and G. Viggiani, Geomech. Energy Environ. (2020)

The durability of cement-based materials is a key focus in civil engineering, due to their significant economic, social and environmental implications. Drying plays a central role in this, given that changes in saturation of the pore network, together with the associated drying shrinkage, are the leading processes in cracking and the penetration of aggressive chemicals, both of which induce premature ageing.

Conventional experimental techniques for studying drying-driven processes, such as gravimetric and sensor-based measurements, provide only bulk-averaged or point-wise measurements which are insufficient to characterise these intrinsically heterogeneous processes. However, significant advances in full-field techniques allow unprecedented insight into these local processes [2]. Notably, X-ray and neutron tomography are highly complementary tools for studying the thermo-hydro-mechanical behaviour of cement-based materials [3]: on one hand, the high sensitivity to density variations of X-ray imaging provides insight into the development of fractures in 4D (3D + time); on the other, thanks to its high sensitivity to hydrogen and thus water, neutron tomography allows the evolution of the moisture field to be studied in 4D.

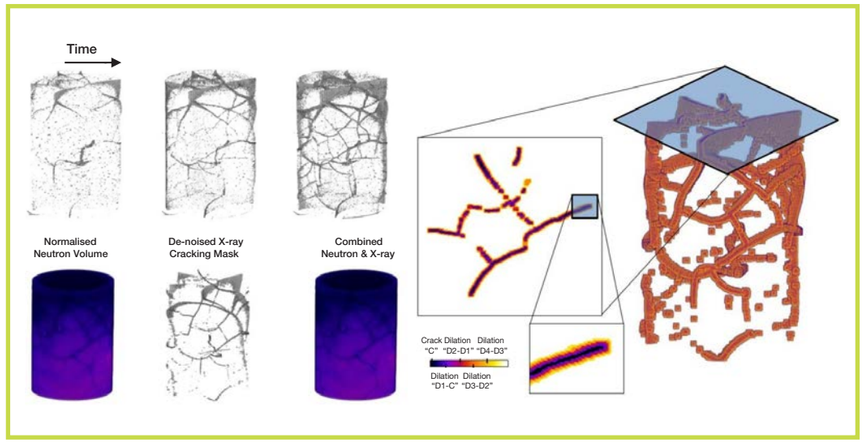

Figure 1

Top left) Initiation and propagation of cracks over time, extracted from selected X-ray tomography scans.

Bottom left) 3D visualisation of cracks and neutron images after multimodal registration: normalised neutron volume (**left**), 3D de-noised X-ray cracks (**middle**) and combined images (**right**).

Right) Crack dilation procedure.

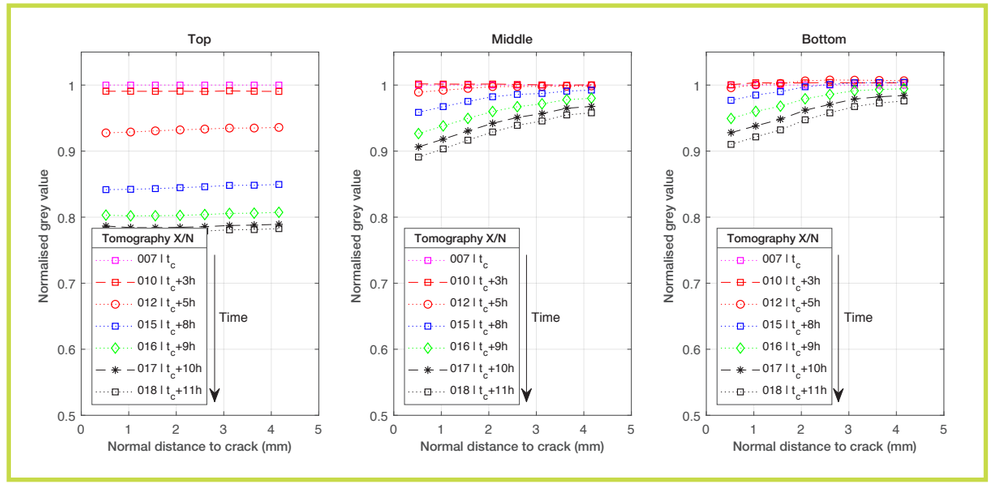

Figure 2

Evolution of the normalised cracking local effect on the water content, in the normal direction to the crack.

One of the experiments that we performed in [1] entailed heating a cement paste sample unidirectionally while simultaneously performing X-ray and neutron tomography scans. The cylindrical cement paste sample had a water-to-cement-ratio of 0.5. Just before the test, it was wrapped in layers of self-adhesive aluminium tape (aluminium being particularly neutron-transparent) to minimise moisture escape from the lateral surface. The sample was also equipped with type K thermocouples that were placed at the top of the sample to measure its surface temperature. X-ray and neutron tomography scans were obtained simultaneously every 30 minutes—a compromise between image quality and the expected speed of the processes.

Heating induces progressive drying and cracking in the sample. **Figure 1** highlights this cracking process in a few selected tomography scans isolated through image processing (**top left**). The crack network originates at the outer surface, predominantly in the warmer top section of the sample, and propagates inwards and downwards. Once this fracture network is isolated though data processing, it is possible to assess its effect on drying thanks to the complementary neutron dataset.

For this, a 5D volume registration (*i.e.* the alignment of the two 4D datasets) was pivotal to ensure that each voxel represents the same volume in space across time and modalities, as seen in **figure 1** (**bottom left**). Then, the effect of the cracks on water content was quantified by studying the acceleration of drying in the vicinity of the cracks, as deduced from the neutron dataset. From a technical standpoint it is possible to identify the areas neighbouring a fracture by dilating the binary image of the cracks, as shown in **figure 1** (**right**).

Figure 2 shows that no gradients were measured in the top part of the sample, due to the rapid occurrence of drying. However, in the middle and bottom the formation of hydric gradients can be observed near the fracture during the mid-to-late-drying stages (from a seemingly initial homogeneous state). **Figure 2** also shows that the hydric effect of the fracture can be as far as 4 mm away from its tip.

This is the first time that such an effect has been directly measured, a matter of key importance in identifying the hydro-mechanical coupling parameters in cement-based materials.

Mohamed Zbiri. French-Moroccan
ILL
@drmzbiri

'Using neutron spectroscopy techniques, underpinned as appropriate by numerical simulations, my research interests cover local and vibrational structural dynamics of functional materials with a potential practical impact.'

Neutron spectroscopy helps pave the way for greener hydrogen fuel production

Time-of-flight spectrometer IN5

Most hydrogen fuel is produced by splitting steam into hydrogen using natural gas, generating large quantities of carbon dioxide. However, if cleaner methods to produce hydrogen were to become technically efficient and economically viable, hydrogen fuel could contribute to a robust, carbon-free future. Using solar energy instead of natural gas to split water into hydrogen and oxygen could be key to achieving this goal. To do so requires suitable photocatalysts to drive the process and appropriate microscopic techniques to probe the behaviour of the host (photocatalysts)–guest (water) system.

AUTHORS
M. Zbiri (ILL)
C.M. Aitchison, R.S. Sprick and A.I. Cooper (University of Liverpool, UK)
A.Y. Guilbert (Imperial College London, UK)

ARTICLE FROM
Chem. Mater. (2021)—doi:10.1021/acs.chemmater.0c04425

REFERENCES

[1] Zhao *et al.*, Angew. Chem. 132 (2020) 9740
[2] Yu *et al.*, Appl. Catal. B 257 (2019) 117935
[3] Zbiri *et al.*, Chem. Mater. 33 (2021) 1363
[4] Guilbert *et al.*, ACS Appl. Polym. Mater. 3 (2021) 765

Hydrogen fuel generation can be achieved *via* the water-splitting process [1]. A cleaner way of splitting hydrogen from water uses the energy from sunlight rather than from fossil fuels. This cleaner method uses photocatalysts to speed up the reaction, the most common being inorganic semiconductors. Interestingly, targeted organic, porous, polymer photocatalysts offer a better alternative to their inorganic counterparts in terms of ease of synthesis, processability and cost. A chemistry-by-design strategy potentially leads to precise control over their chemical design and functionality.

Organic, porous, water-splitting materials can be seen as 'nano-reactors'. By accommodating water within their pores, ideally fuelled by solar energy, they trigger the process of splitting water molecules *via* oxidation and reduction reactions to release hydrogen (**figure 1**). The water-splitting mechanism depends strongly on the size and distribution of pores in these materials. Materials with higher porosity provide a larger surface area for the water-splitting process. Promoting a favourable environment in terms of intermolecular interactions and dynamics helps making this process faster and efficient. In this context, covalent triazine-based frameworks (CTFs) are potential target photocatalysts for water-splitting [2].

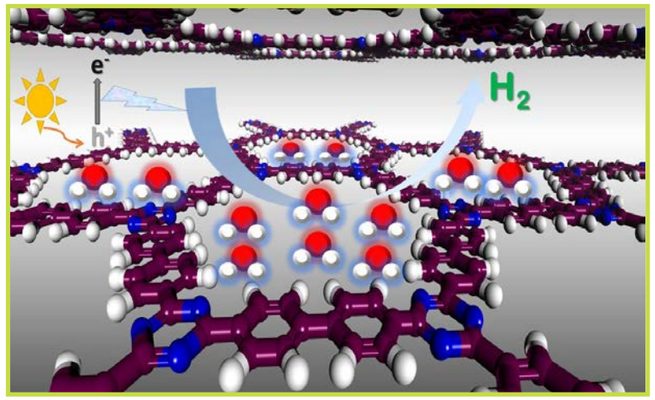

Figure 1

Organic, porous, water-splitting photocatalyst materials can be seen as 'nano-reactors'. They accommodate water within their pores and harness the sunlight energy to trigger the process of splitting water molecules, *via* oxidation and reduction reactions, to release both hydrogen and oxygen. The photocatalyst here is schematically illustrated in terms of the covalent triazine-based framework, CTF-2 (cf. also figure 2a).

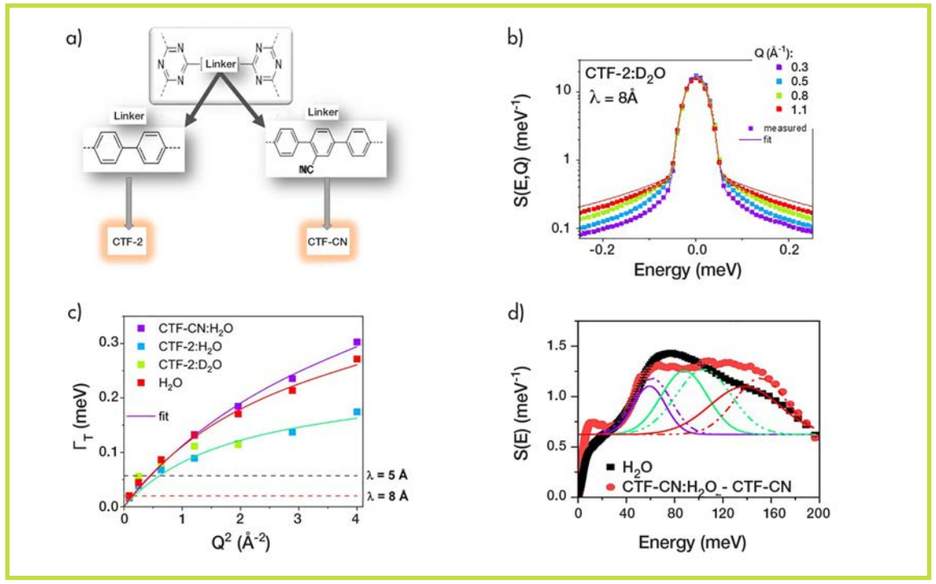

The selection of materials we studied was based mainly on their observed photocatalytic activities—*i.e.* how much water is taken up and how much hydrogen is subsequently produced. Thus, we studied the mass transfer of water in two porous CTFs, namely CTF-CN and CTF-2 (**figure 2a**), that differ in the polarity of their struts [3]. We then focused on the link between their chemical design, structure and water mass transfer. This link plays a key role in the water uptake process and the subsequent hydrogen generation.

By allowing us to probe time and length scales directly relevant to the water-splitting process in the CTFs, neutron scattering was instrumental in this work, as was the deuteration technique [3]. Neutrons are an excellent probe when studying organic materials made of light atoms, such as hydrogen. Hydrogen exhibits the strongest signal here, so the dynamics of water molecules could be clearly studied. The strong signal from hydrogen (H) forming the water can be tuned by using deuterium (D), an isotope of hydrogen but with a weaker neutron interaction, to probe the response of the photocatalysts to the introduction of water [3, 4]. The use of D_2O instead of H_2O allowed us to tune the contrast of the signal of the guest (water) and of the host (photocatalyst), as needed.

We used the IN5 spectrometer to perform quasi-elastic neutron scattering (QENS) and inelastic neutron scattering (INS) measurements of the CTFs (**figure 2a**). We investigated how the water (the 'guest') moved through and interacted with the photocatalysts (the 'host') on the picosecond time scale and nanometre space scale [3]. The QENS technique allowed us to examine the behaviour of the confined water within the pores, where most of the reaction is believed to take place (**figure 2b–c**).

Figure 2

a) Schematic illustration of the two covalent triazine-based frameworks studied, namely CTF-2 and CTF-CN, which differ in the polarity of their struts.

b) Example of QENS spectra highlighting the dynamics of CTF-2 in the presence of D_2O from measurements using IN5.

c) Associated data analysis of H_2O and the two CTFs hosting H_2O or D_2O, showing the impact of the host (CTFs) on the guest (water) dynamics [3].

d) Example of the INS spectra collected using IN5 and associated data analysis relating to the generalised density of states of free H_2O, and the H_2O spectral component of the guest–host system H_2O @ CTF-CN [3].

Our observations were further strengthened by INS, which allowed us to observe how the water molecules and photocatalysts interacted with each other (**figure 2d**).

Our microscopic probe of the local water environment and the related diffusion within the pores of the photocatalysts revealed the behaviour of water molecules in contact with the CTF photocatalysts. We found that water behaves differently in the presence of CTFs; furthermore, the polarity of the strut has an impact not only on the photocatalytic activity but also on how water molecules behave at the microscopic level.

This is the first validation by experiment that the underlying atomistic mode of interaction of water is important. These new studies have led to deeper and better insights into the behaviour of water and the response exhibited by photocatalysts [3, 4]. This work can be built upon by looking deeper into how the pore structures of materials affect their ability to split water into hydrogen fuel. The ultimate aim is to help provide improved chemical design rules for creating better photocatalysts with enhanced water-splitting ability, thereby leading to more efficient clean hydrogen fuel generation.

Adrian Sanchez-Fernandez. Spanish Pharmaceutical formulation group, Lund University, Sweden

'My research focuses on the supramolecular assembly of colloidal systems in exotic environments, specifically in deep eutectic solvents. The use of neutron scattering methods (e.g. small-angle neutron scattering, neutron spin-echo) allows us to determine the parameters that define the structure of self-assembled structures and colloidal interactions, thus providing the fundamental knowledge required to develop these sustainable solvents into technological applications.'

AUTHORS

A. **Sanchez-Fernandez** (Lund University, Sweden)
A.J. **Jackson** (European Spallation Source, Lund, Sweden)
S.F. **Prévost** (ILL)
J.J. **Doutch** (ISIS Neutron and Muon Source, Didcot, UK)
K.J. **Edler** (University of Bath, UK)

ARTICLE FROM

J. Am. Chem. Soc. (2021)—doi:10.1021/jacs.1c04781

REFERENCES

[1] Hansen *et al.*, Chem. Rev. 121 (2021) 1232
[2] Gebbie *et al.*, Chem. Commun. (Camb.) 53 (2017) 1214
[3] W. Kunz, Curr. Opin. Colloid Interface Sci. 15 (2010) 34

Long-range electrostatic colloidal interactions and specific ion effects in deep eutectic solvents

Small-angle neutron scattering instruments D11 (ILL) and SANS2d (ISIS)

Deep eutectic solvents (DES), novel mixtures that contain a salt paired with a neutral molecule to form room-temperature liquids, are viewed as sustainable and cheap alternatives to molecular solvents [1]. In these solvents, which are mainly composed of ions, it is naively expected that the high ionic strengths lead to extremely short Debye screening lengths and negligible long-range electrostatic interactions. However, considerable evidence points to the existence of electrostatic repulsion and specific ion effects in these liquids, and the origin of such effects in high-salt systems is cause for much debate. Here, we use small-angle scattering to probe the long-range electrostatic interactions, the specificity of ion–ion interactions and Hofmeister effects in DES.

We investigated the interactions between cationic surfactant micelles ($C_{12}TA^+X^-$) in 1:2 choline chloride:glycerol and 1:2 choline bromide:glycerol as a function of micelle volume fraction and surfactant counterion ($X^- = Cl^-$, Br^-, NO_3^- and SO_4^{2-}). SANS was used to study these systems as it constitutes one of the few techniques that allow us to directly probe interaction potentials within colloidal dispersions. The experiments were performed on the ILL instrument D22 and SANS2d (ISIS Neutron and Muon Source). From the SANS data, the effective structure factors, S'(q), which relate to the interparticle interactions, were extracted. These data were fitted using mathematical models that describe different interactions potentials: the rescaled mean spherical approximation (RMSA) for electrostatic repulsion, and hard sphere (HS) interactions for excluded volume effects.

Initially, the scattering from h-$C_{12}TA^+Cl^-$ micelles at different concentrations in 1:2 d-choline chloride:d-glycerol was measured (h- and d- refer to protiated and deuterated constituents, respectively). In these data we observe the characteristic interaction peak around 0.12 $Å^{-1}$ (**figure 1**). These results were then compared with those for D_2O and the predictions from hard sphere interactions. We found that excluded volume effects are not sufficient to account for the interaction between particles, and thus an excess interaction must exist in DES. This is also the case in D_2O, where the long-range interactions between charged particles are electrostatic in nature. The strength of such an interaction was parametrised by determining the Coulomb coupling constant, Γ_k. Our results show that the interactions between micelles in DES follow a similar pattern to those in D_2O, although the strength of these interactions is weaker in DES. Thus, we show that intermicellar repulsion prevails at unexpectedly long distances, countering the traditionally held understanding that the exceedingly high DES ion concentration (*ca.* 2.5 M) would completely screen long-range electrostatic interactions [2].

Figure 1

a) S'(q) data and best fits (HS model, dotted lines; RMSA model, solid lines) from different concentrations of h-$C_{12}TAC$ micelles in 1:2 d-choline chloride:d-glycerol.

b) Variation in osmotic compressibility: DES (yellow triangles), D_2O (red circles), and for hard sphere interactions (purple squares).

c) Variation in the Coulomb coupling constant: DES (yellow triangles) and D_2O (red circles).

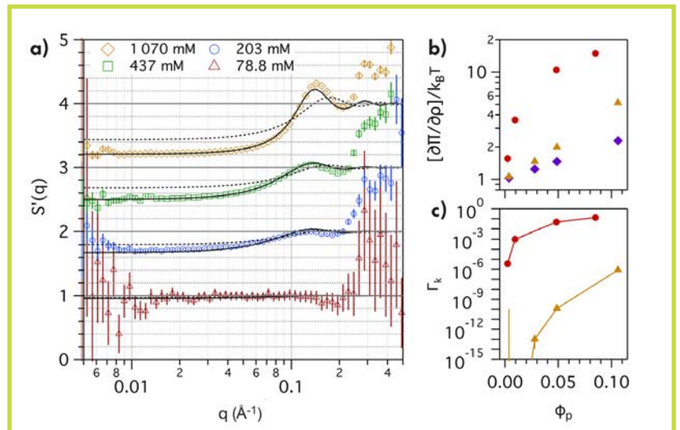

Figure 2

a) SANS data and best RMSA fits of counterion-exchanged 966 mM h-$C_{12}TA^+X^-$ micelles in 1:2 d-choline chloride:d-glycerol.

b) Variation in micelle structural parameters' equatorial radius, r_{eq}, and aspect ratio, AR.

c) Coulomb coupling constant as a function of micelle volume fraction for each counterion-exchanged surfactant in DES.

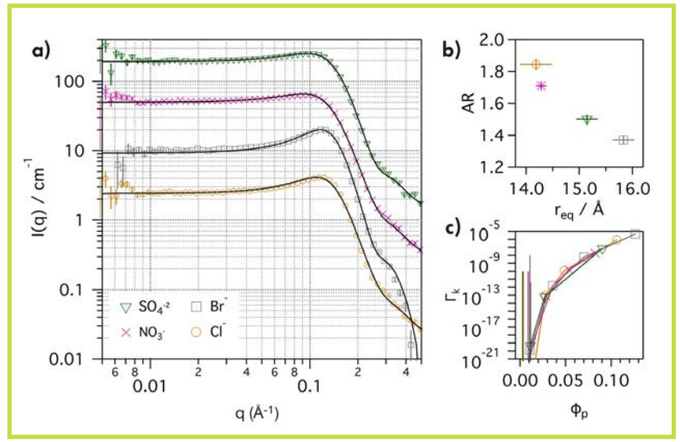

We continued by investigating specific ion effects in DES. The scattering from counterion-exchanged micelles was measured and analysed (**figure 2**). We found that the counterions have different effects on micelle morphology and interparticle interactions, potentially controlled by the condensation of the surfactant counterion, despite the high concentration of anions in the solvent. This modulation follows the Hofmeister series—the rule of thumb describing ion specificity in aqueous systems—from more solvated to more condensed counterions: $SO_4^{2-} > Cl^- > Br^- > NO_3^-$ [3].

The findings of this study demonstrate that electrostatic interactions prevail in DES, with certain similarities to those in aqueous solutions. These results will influence the development of new colloidal systems, the design of novel environments for the stabilisation and function of biomolecules, and the preparation of sustainable electrolytes using DES. They will also contribute to the development of a benchmark theory to describe electrostatic interactions in concentrated ionic environments.

Bruno Demé. French and German
ILL

'I am responsible for the D16 instrument. My research focuses on the molecular interactions that give rise to the structures found in self-assembled, biomimetic or biological lipid systems, in solution or solid-supported.'

High-temperature behaviour of early-life membrane models

High-resolution diffractometer with variable vertical focusing D16 and small-angle instrument D33

Origin of life scenarios [1, 2] assume that the onset of cell formation occurred in terrestrial hot springs or in the deep oceans close to hot vents, where energy is available for non-enzymatic reactions. The membranes of protocells therefore had to withstand extreme conditions, different from those experienced on the Earth's surface today. Simple models can answer fundamental questions, such as the stability of protomembranes at high temperatures required for a number of important reactions to take place.

AUTHORS

L. Misuraca, **I. Grillo** and **B. Demé** (ILL)
P. Oger (INSA Lyon, France)
J. Peters (ILL and Grenoble-Alpes University, France)

ARTICLE FROM

Langmuir (2020)—doi.10.1021/acs.langmuir.0c02258

REFERENCES

[1] D. Deamer, Life 7 (2017) 5
[2] I.A. Chen, K. Salehi-Ashtiani and J.W. Szostak, J. Am. Chem. Soc. 127 (2005) 13213
[3] J.-P. Douliez, B.H. Houssou, A.-L. Fameau, L. Navailles, F. Nallet, A. Grélard, E.J. Dufourc and C. Gaillard, Langmuir 32 (2016) 401
[4] S. Kapoor, M. Berghaus, S. Suladze, D. Prumbaum, S. Grobelny, P. Degen, S. Raunser and R. Winter, Angew. Chem. 126 (2014) 8537

This work presents a quantitative characterisation of two plausible protocell membrane models [3, 4] composed of short-chain fatty acids and alcohols forming vesicles: 1) pure capric acid (**figure 1a**); and 2) a capric acid:decanol 1:1 mixture (hereafter called the C10 mix, **figure 1b**). By tracking the properties and evolution of these vesicles (partitioning, size distribution, lamellarity, membrane thickness, coexistence with micelles), from below room temperature up to 80 °C, we show how simple models can answer fundamental questions—one of these being the stability of protomembranes at high temperatures required for a number of important non-enzymatic reactions to take place (*e.g.* DNA-strand separation and reannealing).

To investigate the ability of the vesicles to withstand the high temperatures expected at hydrothermal vents or hot springs, their stability was investigated by small-angle neutron scattering (SANS) on initially multilamellar vesicles (**figure 2**) and subsequently large, unilamellar vesicles (**figure 3**). Data were collected in the range 7–80 °C. The capric acid multilamellar vesicles (**figure 2, left**) present a broad correlation peak at $q = (1.8 \pm 0.1)$ nm^{-1} that corresponds to a d-spacing of (3.4 ± 0.1) nm. This correlation disappears at 16 °C and no other correlation is visible at higher temperatures. Remarkably, analysis of pure capric acid curves above 16 °C shows the need to consider a model of vesicles coexisting with micelles to properly reproduce the data (**figure 3**). For $T \leq 35$ °C, ~ 85 % of capric acid contributes to the vesicle signal, while ~10 % goes into micelles. When $T \geq 35$ °C, a steep decrease in the volume of vesicles is observed, followed by a concomitant increase in the micelle signal. The sum of the two components also goes down slightly with the temperature increase, due to the solubilisation of fatty acid.

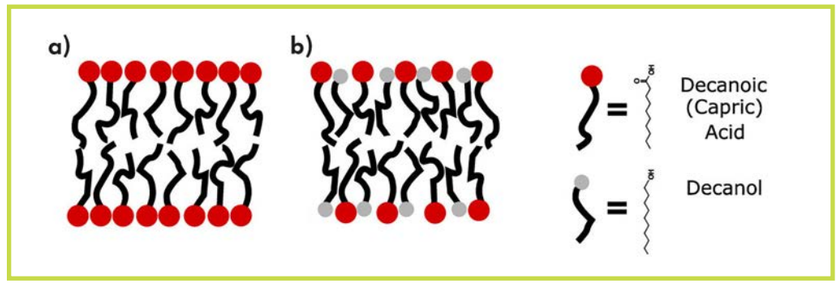

Figure 1
The protomembrane models:
a) bilayer made of capric acid;
b) bilayer made of a mixture of capric acid and decanol.

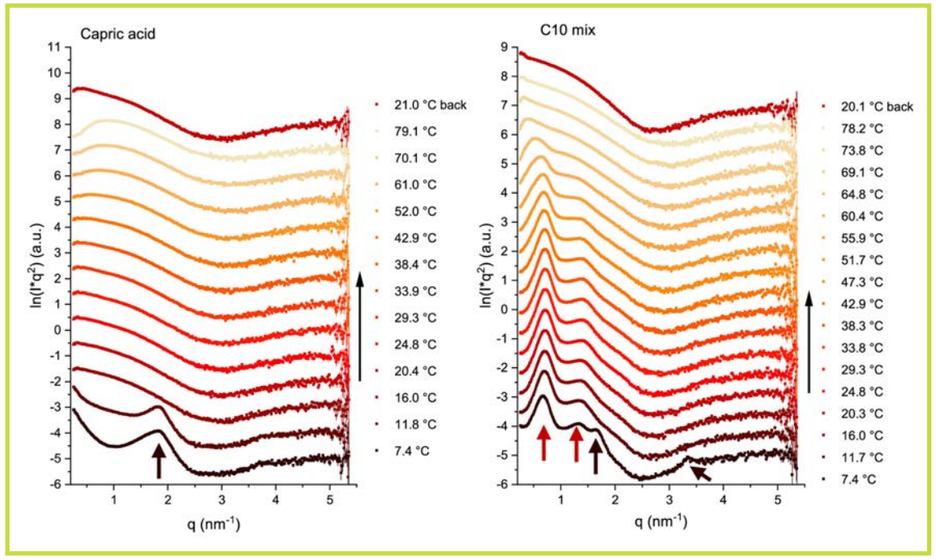

Figure 2
SANS curves collected on D16 at different temperatures:
Left) capric acid sample at 350 mM;
Right) C10 mix sample at 350 mM. Arrows show the first two orders of the observed lamellar phases structure factor S(q).

Conversely, the correlation peaks observed in the C10 mix (**figure 2, right**) show the coexistence of two lamellar phases at low temperature (7 °C): the first at $q = (0.7 \pm 0.1)$ nm-1 (d-spacing of (9.4 ± 0.1) nm), the second at $q = (1.70 \pm 0.1)$ nm-1 (d-spacing = (3.7 ± 0.1) nm). Above the gel–fluid phase transition of the C10 mix at 10 °C, only the swollen phase is still visible. Approaching the second phase transition (above 50–60 °C), the lamellar phase undergoes fast swelling (now due to the water entering between membranes), seen as a shift in the correlation towards lower q, until disappearing. This effect has been observed previously in the literature and is referred to as an unbinding transition. Both the C10 mix curves—the one at the highest temperature, T = 78 °C, and the one after cooling back to T = 20 °C—fit extremely well with a bilayer form factor, with $a \approx q^{-2}$ decay. These results indicate that the high-temperature structure of the C10 mixture is still a unilamellar membrane.

In summary, the insertion of alcohol into the mix leads to a number of substantial differences in the vesicles' behaviour: it leads to a much larger proportion of, and more stable, vesicles over micelles, a phenomenon essential for compartmentalising early forms of life; it protects vesicles from low-temperature vesicle disruption, maintaining multilamellar structures when present; and, it triggers an abrupt conformational change above 60 °C, leading to an unbinding transition from multilamellar to large unilamellar vesicles stable at high temperature.

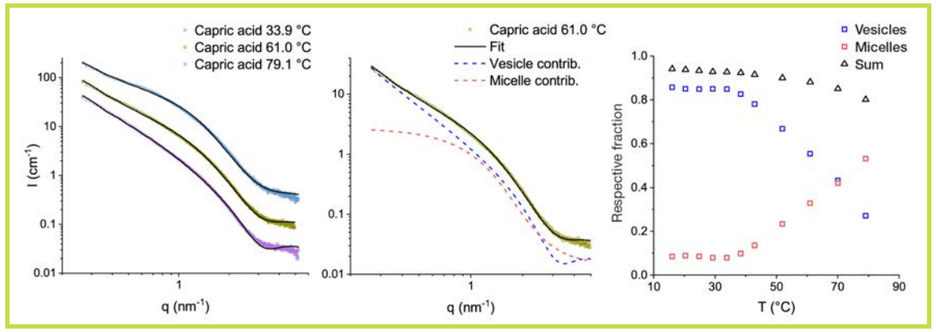

Figure 3
Left) Examples of fits to the D16 data of pure capric acid.
Middle) Vesicle and micelle contributions and their sum for T = 61 °C.
Right) Respective fraction of vesicles and micelles *vs* T.

Grégory F. Schneider. French
Leiden University, the Netherlands

'I am currently principal investigator and associate professor of chemical nanoscience at the Leiden Institute of Chemistry. I received an ERC starting grant and a Vidi grant from the NWO (Dutch Research Council) to carry out chemical research with graphene. My research interests include nanotechnology, bionanotechnology, surface and interfacial chemistry, physical and organic chemistry, materials science, biophysical chemistry, nanofluidics and self-assembly. More information can be found on my group website: https://schneider2dlab.com.'

AUTHORS

L. Lima, **H. Arjmandi**, **A. Kros** and **G.F. Schneider** (Leiden University, the Netherlands)
T. Charitat (CNRS Institut Charles Sadron, Strasbourg, France)
T. Mukhina and **G. Fragneto** (ILL)

REFERENCES

[1] H. Arjmandi-Tash, L.M.C. Lima, L.A. Belyaeva, T. Mukhina, G. Fragneto, A. Kros, T. Charitat and G.F. Schneider, Langmuir 36 (2020) 14478
[2] L.M.C. Lima, W. Fu, L. Jiang, A. Kros and G.F. Schneider, Nanoscale, 8 (2016) 18646

Encapsulation of graphene in the hydrophobic core of a lipid bilayer

Neutron reflectometer with horizontal scattering geometry D17 and Partnership for Soft Condensed Matter (PSCM)

Graphene is typically supported by—and sometimes sandwiched between—other two-dimensional materials to stimulate higher mobility and thus ensure the reproducibility of electrical performance and prevent environmental contamination. Frequently composed of inorganic, hard and crystalline materials, so-called Van der Waals heterostructures have emerged as a way of designing new and remarkably complex layer-by-layer films of 2D materials, including graphene. One challenge associated with 2D materials supporting and sandwiching layers is their limited chemical diversity, functions and inherent inorganic nature. The possibility of combining graphene with soft, dynamic and molecular self-assembled monolayers is therefore of considerable interest as an organic alternative to inorganic 2D materials, and could provide a versatile platform for applications such as biosensors, drug delivery systems and cellular devices [1].

Lipids are amphiphilic molecules that can self-assemble and form stable, quasi-two-dimensional fluidic membranes. Lipids can spread on graphene, but little is known about the formation, stability and molecular structure of the phospholipid molecules surrounding graphene. Studies in this area have mainly focused on graphene oxide (GO), as both lipid vesicles and GO form stable suspensions in aqueous environments. GO is an easily accessible form of graphene, suitable for studying the influence of oxidation states on the chemical characteristics of GO-lipid assemblies. Being negatively charged, GO has a particular affinity with positively charged lipid head groups, highlighting the importance of electrostatic interactions in the assembly process. Pristine graphene, however, does not contain charges on the basal plane, thus minimising electrostatic interactions and favouring hydrophobic interactions between lipid tails and graphene. To understand and quantify the interactions between lipid tails and graphene, we transferred graphene directly onto the lipid tails and analysed the molecular structure of the lipids by neutron reflectometry on D17.

Experimentally, the lipid–graphene–lipid structure was constructed in three steps: first, a DSPC monolayer was transferred onto a silicon wafer using the Langmuir–Blodgett technique; second, graphene was transferred onto the top of the DSPC monolayer by bringing a graphene monolayer floating in a copper etchant (ammonium persulfate solution) into contact with the silicon wafer coated with the DSPC monolayer; and third, a second DSPC monolayer was transferred onto the lipid–graphene heterostructure using the Langmuir–Schaefer technique (**figure 1**). After each fabrication step, the structure was characterised systematically using infrared reflection absorption spectroscopy (IRRAS) and ellipsometry, and the hybrid superstructure studied with Ångstrom resolution using neutron reflectometry.

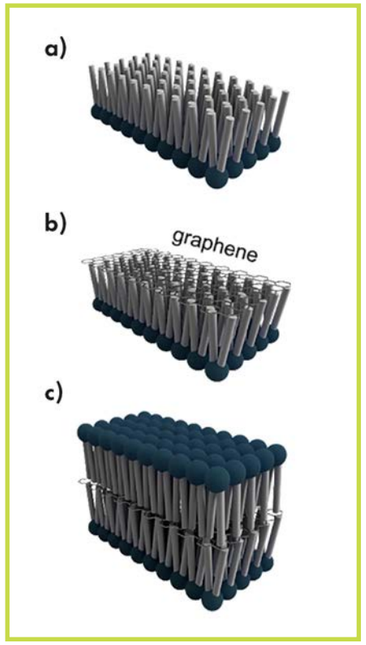

Figure 1
Schematic cartoon of:
a) lipid monolayer;
b) lipid monolayer with graphene on top; and
c) graphene encapsulated in the hydrophobic core of a lipid bilayer. For clarity, the solid substrate is not displayed.

The experiments at the ILL revealed the successful assembly of graphene within the hydrophobic core of a DSPC bilayer. The lipid layers below and above graphene arranged stably, with no significant graphene-related perturbation compared with a plain lipid bilayer. The results were in agreement with simulations (**figure 2**).

To understand how the second lipid monolayer structurally organises on top of graphene and whether or not graphene destabilises the two individual DSPC monolayers below and above, a DSPC lipid bilayer on the substrate without graphene was prepared as a control and compared with the DSPC–graphene–DSPC assembly (**figure 2**). The similarity of the IRRAS spectra implies that graphene does not significantly disturb the IRRAS fingerprint of the lipid bilayer, confirming a stable lipid–graphene–lipid structure (data not shown).

Finally, we studied the stability of the lipid–graphene superstructure when the bilayer was in the fluid phase (T = 55 °C). Our results show that compared with the gel phase, in this phase the superstructure remains stable with a more ordered structure of the outer leaflet of the bilayer due to the annealing of the sample. The confirmed possibility of inserting a graphene layer within the hydrophobic core of a lipid bilayer opens up a route for directly probing membrane-related processes *in situ* using graphene as an electrical sensor. Optimisation of the deposition process, leading to an improvement in the graphene coverage rate for large samples, could allow more accurate characterisation of the graphene layer in the lipid–graphene superstructure.

Figure 2
a) Neutron reflectivity profiles displayed as Rq^4 *vs* q (where R is the reflectivity and q is the wave vector transfer) from a DSPC bilayer at 25 °C (gel phase) in three contrasts: D_2O (red), silicon-matched water (SMW, green) and H_2O (blue). The solid lines correspond to the best fit.
b) The corresponding SLD profiles in three contrasts: D_2O (red), SMW (green) and H_2O (blue).
Reprinted from [1] (CC-BY-NC-ND license).

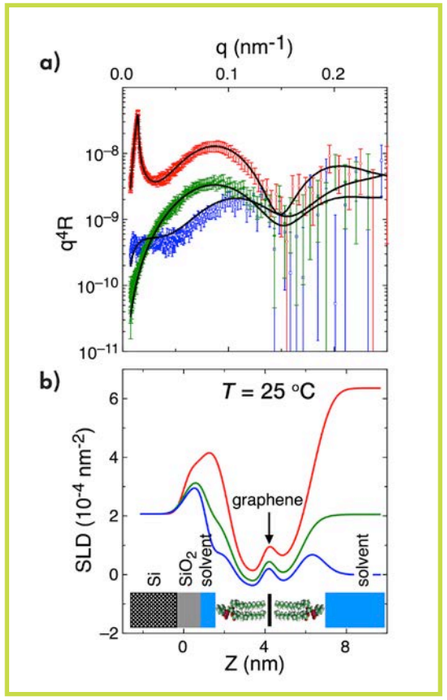

Olga Kuzminskaya. Azerbaijanian
Technische Universität Berlin, Germany

'I did my Master's thesis with TU Berlin and BASF Polyurethanes GmbH on the structure–property relationship in polyurethane elastomers. I am currently doing my PhD on the solubilisation and release of organic compounds of different polarity by interpolyelectrolyte complexes based on block copolymer micelles. My research interests are polymers and colloidal systems.'

AUTHORS

O. Kuzminskaya (Technische Universität Berlin, Germany)
I. Hoffmann (ILL)

ARTICLE FROM

Macromolecules (2021)—doi:10.1021/acs.macromol.1c00327

REFERENCES

[1] L. Chiappisi, I. Hoffmann and M. Gradzielski, Soft Matter 9 (2013) 3896
[2] E.D. Goddard and R.B. Hannan, J. Colloid Interface Sci. 55 (1976) 73

Mesoscopic origins of viscosity in polyelectrolyte surfactant solutions

Spin-echo spectrometer IN15

Some oppositely charged polyelectrolyte (PE) surfactant mixtures show a remarkable increase in viscosity near charge equilibrium, while other very similar systems do not show any appreciable effect. By comparing the mesoscopic structure and dynamics of two different systems, namely the highly viscous SDS/JR 400 and the low viscous SDS/PDADMAC, we shed light on the structural prerequisites for forming viscous PE/surfactant mixtures.

Some oppositely charged polyelectrolyte (PE) surfactant mixtures show a remarkable increase in viscosity near charge equilibrium with a slight excess of PE charges present, while other very similar systems show no appreciable effect [1]. The exact structural and dynamical prerequisites for achieving a significant increase in viscosity are still unclear.

We compared the structure and dynamics of polyelectrolyte surfactant complexes (PESCs) formed from anionic sodium dodecylsulfate (SDS) and the cationically modified hydroxyethyl cellulose JR 400, which enhance the viscosity near charge equilibrium enormously [2], with PESCs consisting of SDS and the cationic PE polydiallyldimethylammonium chloride (PDADMAC), which do not significantly increase the viscosity of solutions under similar conditions (**figure 1**).

Using small-angle neutron scattering (SANS), rheology, and neutron spin-echo spectroscopy (NSE), we gained insight into the system's mesoscopic structure and dynamics. PDADMAC differs from JR 400 in a number of aspects. For this study, we chose to keep the molecular weight (approximately 500 kg/mol) and the mass concentration (1 wt%) constant for the two different PEs. The sixfold higher charge density of PDADMAC makes it necessary to use a significantly larger amount of surfactant to come close

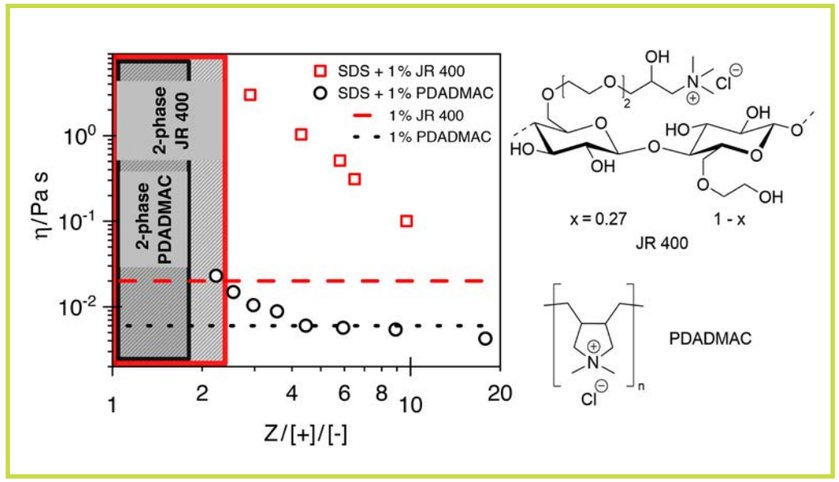

Figure 1

Left) Viscosity of SDS/JR 400 PESCS (red squares) and SDS/PDADMAC (black circles) as a function of charge ratio Z with 1 wt% PE. While SDS/JR 400 shows a remarkable increase in viscosity, SDS/PDADMAC barely increases.

Right) Molecular structure of JR 400 and PDADMAC. The charged group of JR 400 is located on a flexible spacer, while it is directly on the backbone for PDADMAC.

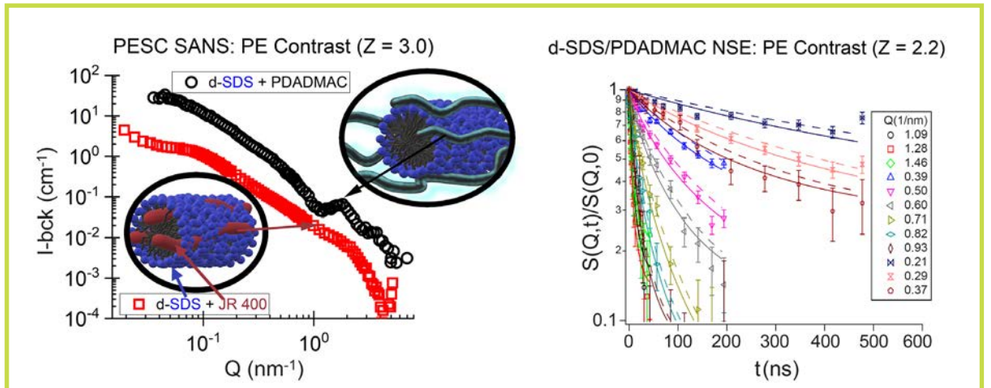

Figure 2

Left) SANS curves of dSDS/JR 400 (red squares, D11) and dSDS/PDADMAC (black circles, V16, HZB), both with 1 wt% PE, Z = 3; the minimum at 1 1/nm in SDS/PDADMAC indicates a core-shell structure of the aggregates, while the smooth curve of SDS/JR 400 indicates a homogeneous structure of the aggregates.

Right) NSE intermediate scattering functions of dSDS/PDADMAC at Z = 2.2. The full lines are best fits that take into account the extra dynamics of the loosely bound PDADMAC chains, while the dashed lines do not.

to reaching the same charge ratio Z = [PE charges]/[surfactant charges]. The charged group of JR 400 is located on a flexible side chain, on average 11 atoms away from the backbone, while in PDADMAC the charged group is part of the backbone. In addition, the cellulose-based JR 400 has an intrinsically stiff backbone.

We previously found that the increased viscosity in SDS/JR 400 PESCs is due to the formation of mixed, rodlike aggregates that interconnect three to four PE chains on average. SANS measurements on SDS/PDADMAC PESCs similarly show the formation of mixed aggregates that interconnect as many as five PE chains on average, and yet no significant increase in viscosity can be observed.

Through contrast matching, neutron scattering allows specific parts of a system to be highlighted simply by changing the isotopic composition of the sample; by using deuterated SDS (dSDS), D_2O and hydrogenated PE, it is possible to render the surfactant almost invisible and only highlight the structure of the PE in the aggregates. Comparing the scattering curves of dSDS/JR 400 and dSDS/PDADMAC, an additional minimum in the scattering curve of dSDS/PDADMAC becomes visible. This indicates a core-shell structure of the PESC, where the PESC is located on the outside of the aggregates around a surfactant core. For dSDS/JR 400, no additional feature can be seen in the scattering curve, which indicates a relatively homogeneous distribution of the PE through the cross section of the aggregates (**figure 2, left**).

These structural differences are also reflected in the mesoscopic dynamics, which was monitored by neutron spin-echo (NSE) on the instrument IN15 at the ILL. The dynamics observed in full contrast, where both PDADMAC and SDS are hydrogenated, can be described as a superposition of the fast dynamics of PDADMAC and the slower dynamics of the mixed aggregates. Performing NSE measurements on otherwise identical samples with deuterated SDS only, the observed dynamics is faster beyond the extent expected simply because of the decreased visibility of the aggregates (**figure 2, right**). While such a tendency is also observed in SDS/JR 400 it is significantly more pronounced in SDS/PDADMAC, indicating that the PE here is more loosely bound, which in turn is responsible for the lack of increase in viscosity in SDS/PDADMAC.

In summary, using SANS and NSE we were able to establish a link between the mesoscopic structure and dynamics of PESCS and their macroscopic flow behaviour. While SDS/JR 400 forms mixed PESCs where the PE is tightly integrated in the aggregates, SDS/PDADMAC forms aggregates where the PE is only loosely bound on the outside of the aggregates and possesses higher dynamics, which explains the much lower viscosity.

These differences in mesoscopic structure can be traced back to the different molecular architectures of the molecules. The charged group of JR 400 being located on a flexible spacer allows the backbone to be integrated into the mixed aggregate; conversely, the charge of PDADMAC being located directly on the backbone forces it to remain on the edge of the aggregate and form a core-shell structure.

Marie Lycksell. Swedish Department of Biochemistry and Biophysics, Stockholm University, Sweden

'I'm a PhD student in biophysics, and I am part of the Swedish research school for neutron sciences, SwedNess. My research focuses on combining experimental and computational methods in the study of pentameric ligand-gated ion channels, using small-angle scattering and molecular dynamics simulations as my main techniques.'

Probing the solution structure of the pentameric ligand-gated ion channel GLIC by small-angle neutron scattering

Small-angle scattering instrument D22

Pentameric ligand-gated ion channels are membrane proteins that open in response to a chemical signal to allow the passage of ions across cell membranes. These proteins are thus key for fast electrochemical signal transduction in many life forms. The prokaryotic channel GLIC has proven a valuable model system for membrane proteins, and using small-angle neutron scattering (SANS) we have been able to show how the crystal structures of GLIC compare with its solution structure.

AUTHORS

M. Lycksell, **U. Rovšnik**, **R.J. Howard** and **E. Lindahl** (Stockholm University, Sweden)
C. Bergh (Royal Institute of Technology KTH, Sweden)
N.T. Johansen and **L. Arleth** (University of Copenhagen, Denmark)
A. Martel and **L. Porcar** (ILL)

ARTICLE FROM

Proc. Natl. Acad. Sci. USA (2021)—doi:10.1073/pnas.2108006118

REFERENCES

[1] M. Lycksell *et al.*, Proc. Natl. Acad. Sci. USA 118 (2021) 37
[2] S.R. Midtgaard *et al.*, FEBS J. 285 (2018) 2
[3] N.T. Johansen *et al.*, Acta Crystallogr. D 74 (2018) 12
[4] C. Bergh *et al.*, eLife 10 (2021)

Knowing the structure of a protein helps us to understand its mechanism of function, which in turn can, for example, aid drug development. Structure determination methods are invaluable for obtaining atomistic models but often yield only a limited set of conformations. The crystal structure of GLIC has been determined with either closed or open pores. Still, our understanding of the gating landscape remains incomplete, with only limited knowledge about, *e.g.* the structural dynamics at room temperature and of intermediate states. With small-angle scattering it is possible to obtain low-resolution structural information on proteins in solution. Therefore, we set out to apply this technique to elucidate the solution structure of GLIC in conditions expected to yield open and closed channels, separately.

GLIC is a pH-sensitive protein that is expected to be in a resting state with the channel closed at neutral pH, and to adopt an active state in which the channel is open in response to a drop in pH. Therefore, we performed our measurements at neutral and acidic pH (pH values of 7 and 3, respectively). Furthermore, as GLIC is a membrane protein it can only be solubilised in the presence of a membrane mimetic around its transmembrane domain (**figure 1**). Neutrons are able, crucially, to distinguish between hydrogen and deuterium. Thus, selective deuteration of the solvent and/or the solute allows certain sample components to be rendered 'invisible' by matching the scattering length densities of the solvent and the solute. Here, this was achieved using a deuterated detergent that was developed to match the scattering length density of pure heavy water [2]. As the detergent micelles become 'invisible' to the neutrons, we were able to detect the scattering from GLIC rather than from the GLIC–detergent complex. This maximised the scattering contrast between the background and the sample, thereby improving the quality of our data. We performed the experiment using the size-exclusion chromatography set-up available at the small-angle scattering diffractometer D22 [3] to exclude as many protein aggregates in the measured sample as possible.

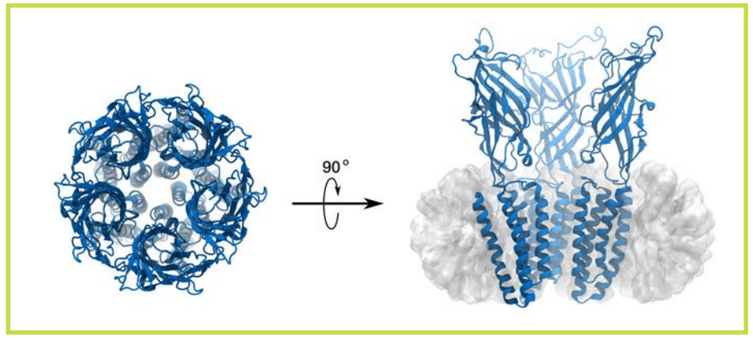

Figure 1

GLIC is a membrane protein composed of five subunits (**left**, view from the extracellular side), whose central channel opens wide enough for ions to pass through under activating conditions. SANS experiments were performed using a detergent-solubilised protein as well as a deuterated detergent developed to be indistinguishable from D_2O to the neutrons (**right**, showing three subunits and half the micelle).

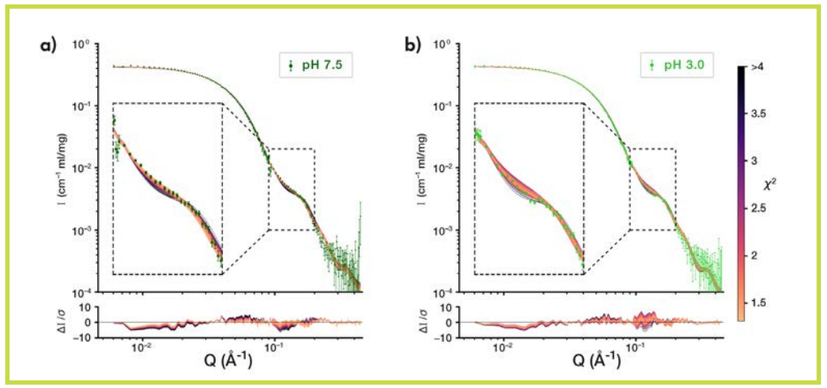

Figure 2

Fits of models from molecular dynamics simulations to scattering data from **a)** resting conditions, and **b)** activating conditions. Models coloured by goodness of fit. The lower panels show the error weighted residual between the models and the experimental data. Adapted from [1].

We found only small differences in the scattering profiles of GLIC under resting and activating conditions, both of which corresponded closely to a closed crystal structure. However, when fitting a linear combination of both the closed and the open structure it was clear that while including any amount of the open structure led to a worse fit with the resting state data, for scattering patterns obtained under activating conditions up to an 18 % contribution of the open structure could be included. This is in close agreement with the population of open-like GLIC channels observed in extensive molecular dynamics simulations of the protonated protein [4]. Since this protein family has previously been shown to have only a minority of channel populations adopting the conducting state under activating conditions, we find it likely that scattering under activating conditions reflects the average of several coexisting states rather than a majority population in an intermediate conformation.

Furthermore, because the scattering data represent a population- and time-averaged structure, we also used molecular dynamics simulations to sample conformations beyond those observed in static structures. We fitted models from unbiased simulations to our scattering data and were able to find models with improved fits to the scattering data from resting and activating conditions, separately (**figure 2**). Using these models we were able to identify the conformational features characteristic of the average solution structure of GLIC under each condition (**figure 3**): for resting conditions, the average solution structure is described well by a closed crystal structure with an expanded extracellular domain and a contracted pore; under activating conditions the average conformation differs from the crystal structure, featuring an intermediate expansion of the extracellular domain and a tolerance for both open-like and closed-like pore conformations.

With this work we have thus been able to describe condition-dependent conformational changes relevant to ion-channel gating, and to demonstrate the power of neutron scattering in combination with simulations to distinguish subtle shifts in membrane protein structure.

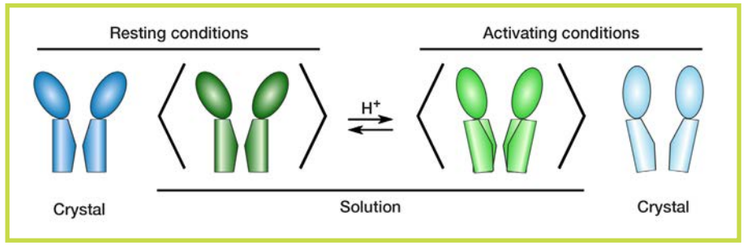

Figure 3

Comparison between the open and closed crystal structures of GLIC with the solution average conformation under resting and activating conditions. Reproduced from [1].

Nathan R. Zaccai. French
University of Cambridge, UK

'I am a structural biologist at the Cambridge Institute for Medical Research. My research has primarily focused on how unstructured, disordered proteins can modulate biological processes.'

Structures of a deAMPylation complex rationalise the switch between the AMPylation and deAMPylation activities of FICD

Small-angle instrument D11 and Deuteration Laboratory (D-lab)

BiP is the Hsp70 molecular chaperone of the endoplasmic reticulum (ER) and plays an essential role in facilitating protein folding in this compartment. Total BiP activity is tightly regulated to meet the protein-folding demands of the ER. A combined crystallographic and small-angle neutron scattering (SANS) study provides new insights into the mechanism of BiP's post-translational regulation by the enzyme FICD.

AUTHORS

N.R. Zaccai and **L.A. Perera** (University of Cambridge, UK)
S. Prévost, **J.M. Devos** and **M. Haertlein** (ILL)

ARTICLE FROM

Nat. Commun. (2021)—doi:10.1038/s41467-021-25076-7

REFERENCES

[1] P. Walter and D. Ron, Science 334 (2011) 1081
[2] K. Ibel and H.B.J. Stuhrmann, J. Mol. Biol. 93 (1975) 255
[3] S. Grudinin, M. Garkavenko and A. Kazennov, Acta Crystallogr. Sect. D Struct. Biol. 73 (2017) 449

The endoplasmic reticulum (ER) is responsible for the correct folding of about a third of all proteins synthesised in eukaryotic cells. The unfolded protein response (UPR) maintains a dynamic equilibrium between ER unfolded protein load and folding capacity [1]. In order to reduce the burden of unfolded proteins, the UPR lowers global protein expression and increases the number of ER chaperones able to facilitate protein folding. For example, a post-translational mechanism of the UPR involves the covalent addition of an adenosine monophosphate moiety onto the ER Hsp70 chaperone, BiP. BiP AMPylation and deAMPylation is catalysed by a single ER-localised enzyme, FICD. As the number of unfolded proteins declines, monomeric FICD rapidly AMPylates, and thereby deactivates, excess BiP. Conversely, as unfolded proteins accumulate, pre-existing AMPylated BiP (BiP-AMP) is rapidly deAMPylated by FICD, increasing the amount of unmodified active BiP within the ER.

We embarked on a structure-based approach to determine the nature of the FICD•BiP enzyme–substrate interaction and the mechanism of eukaryotic deAMPylation. High-resolution crystal structures of the complex (using monomerised FICD) demonstrated how AMPylated BiP engages FICD's active site. However, in order to assess the validity of these structural insights, the properties of the intact FICD•BiP-AMP complex in solution were studied by contrast variation, small-angle neutron scattering (SANS).

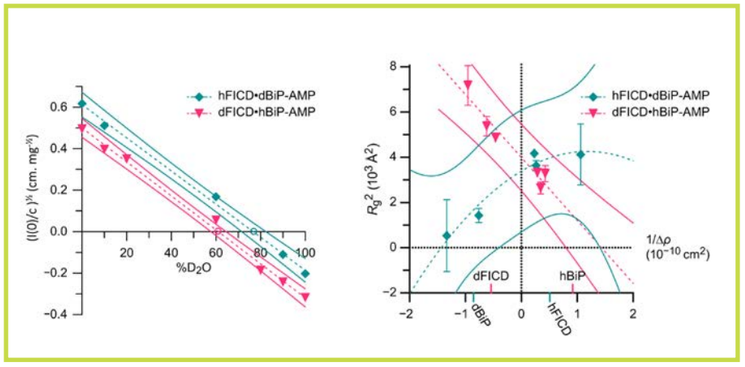

Figure 1

Left) Contrast variation plot of forward scattering I(0) over protein concentration c, as a function of solvent D_2O concentration. The zero average contrast (ZAC) is where I(0)/c = 0 (drawn as empty circles), while 95 % confidence bands are shown with colour-matched solid lines.

Right) Stuhrmann plots of the squared radii of gyration (R_g^2) against the reciprocal of contrast ($1/\Delta\rho$). Best fits are shown (dashed lines) with 95 % confidence bands (colour-matched solid lines). Contrast match points (CMP) of individual proteins are indicated on the *x*-axis.

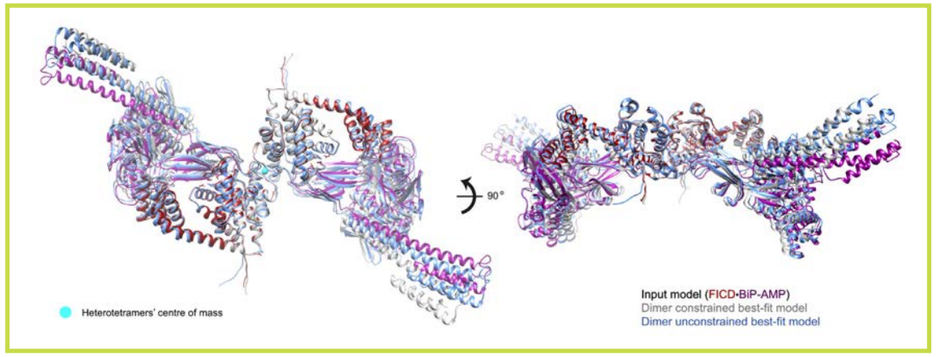

Figure 2

Protein dynamics captured by flex-fitting of contrast variation SANS data. The best fit structures are superimposed over the input deAMPylation complex model.

Unlike other biophysical or scattering techniques, contrast variation SANS analysis is able to ascertain stoichiometry, size and shape information as well as the internal organisation of a complex. As the ratio of H_2O to D_2O in the solvent is varied, the contrast of the complex, but also of each of its components, will change. Basically, at a specific D_2O concentration in the solvent (the contrast match point (CMP)), one component becomes essentially transparent while the other is still visible. The zero average contrast (ZAC) occurs when the whole complex is invisible. In the case of a selectively deuterated protein complex, the CMPs of the hydrogenated and matchout-deuterated molecules are very different (~40 % D_2O and ~100 % D_2O, respectively), with the resultant ZAC occurring somewhere between the two.

Matchout-deuterated FICD and BiP-AMP were therefore prepared and expressed at the ILL Deuteration Laboratory (D-Lab). After purification, they were mixed with their non-deuterated partner proteins and the resultant complexes isolated by gel filtration into buffers with different D_2O content. Small-angle scattering data were collected on the ILL instrument D11. Analysis of the low-*q* Guinier region provided information about the forward scattering intensity, I(0). This, along with the calculation of each complex's ZAC (**figure 1, left**), was in good agreement with FICD•BiP-AMP forming a 2:2 complex.

The radius of gyration, R_g, of each complex was also obtained by fitting the low-*q* region data with the Guinier approximation. The Stuhrmann plots (**figure 1, right**) are derived from the square of the R_g data against the reciprocal of the contrast [2]. This analysis provided information on the internal arrangement of the FICD•BiP-AMP heterotetramer, assigning FICD to the inside of the complex. The relatively linear Stuhrmann plot shape derived from the deAMPylation complex containing matchout-deuterated FICD suggests that this complex has a scattering length density (SLD) centre that is very close to the complex's centre of mass (COM). For the complex containing matchout-deuterated BiP-AMP, the plot reveals no overlap between the SLD centre and the COM. These findings are consistent with a heterotetramer whose centre of mass is closer to the centre of mass of the two FICD molecules than of the two BiP molecules.

A model of the heterotetramer in solution could consequently be constructed, based on this low-*q* Guinier analysis and the available crystal structures (**figure 2**). Across the entire scattering *q*-range and at all D_2O concentrations, the theoretical scattering profile of this model correlated well with the observed experimental scattering.

Finally, it was possible to capture some of the dynamics of the protein complex in solution with PEPSI-SANS [3]. Optimal *flex-fit structures* can be generated for each scattering dataset by allowing the structures to undergo normal mode flexing of their domains. The analysis indicated that most particles in solution have neutron scattering properties predicted by our model. The principal variation in the flex-fit structures relative to the input model was evident in the reorientation of BiP's lid domain, which does not come into direct contact with FICD (**figure 2**). This lid flexibility is consistent with previous experimental observations of other Hsp70 chaperones.

In conclusion, contrast variation SANS demonstrated that the monomeric FICD-containing deAMPylation complex crystal structure is indeed representative of the internal arrangement of dimeric FICD engaged with AMPylated BiP in solution. SANS also revealed the flexibility of more peripheral domains of the deAMPylation complex (information that could not be obtained by crystallography). Therefore, these neutron data contribute to a mechanistic understanding of post-translational regulation of protein folding activity within the ER.

Marité Cárdenas. Venezuelan/Swedish
Malmö University, Sweden and
Nanyang Technological University, Singapore

'I get the most enjoyment from finding new ways of applying neutron scattering to answer biological questions, which often entails making neutron scattering accessible to the wider scientific community.'

SARS-CoV-2 spike protein removes lipids from model membranes and interferes with the capacity of high-density lipoprotein to exchange lipids

Reflectometer with horizontal scattering geometry D17

The COVID-19 pandemic continues to have a worldwide impact. Understanding how the SARS-CoV-2 virus interacts with the body and why it has greater impact on some parts of the population than on others is of great importance. Early on, studies discovered the need for the presence of cholesterol for the interaction between the SARS-CoV-2 spike (S) protein and host cell membranes. Importantly, lower total plasma cholesterol, HDL and LDL levels, is correlated with increased risk for severe disease [1]. In this study we investigated the influence of the SARS-CoV-2 spike protein on model membranes and its interaction with HDL using neutron reflection, thereby offering insight into the role these components play in the COVID-19 disease.

AUTHORS

Y. Correa and **M. Cárdenas** (Biofilms and Department of Biomedical Science, Malmö University, Sweden)
S. Waldie (Partnership for Structural Biology (PSB), ILL; Biofilms and Department of Biomedical Science, Malmö University, Sweden)
M. Moulin and **M. Haertlein** (ILL and PSB, ILL)
T. Forsyth (PSB, ILL; and Keele University, UK)

ARTICLE FROM

J. Coll. Int. Sci (2021)—doi:10.1016/j.jcis.2021.06.056

REFERENCES

[1] A. Zinellu *et al.*, Front. Public Health 9 (2021) 1210
[2] C. Wei *et al.*, Nat. Metab. 2 (2020) 1391
[3] B. Plochberger *et al.*, Biochemistry 59 (2020) 4421
[4] S. Waldie *et al.*, Biochim. Biophys. Acta - Mol. Cell Biol. Lipids. 1865 (2020) 158769

Both cholesterol and HDL have been found to bind to the S protein [2]. One of the roles of HDL is to remove excess cholesterol from cell membranes for elimination in the liver, and these results together suggest that HDL functionality might be affected by interaction with the S protein.

Recently, HDL was shown to bind and deposit cargo at model membranes without receptors under physiological conditions using fluorescence microscopy [3], while only neutron reflection could determine the extent of cargo deposition and lipid removal by HDL [4]. Here, lipid deuteration was key, with the D-lab at the ILL providing both matchout-deuterated natural lipids and matchout-deuterated cholesterol. We then applied the same methodology to investigate the ability of the spike protein to modify lipid exchange by HDL. Experiments were carried out on the D17 instrument—a reflectometer perfectly suited to this type of experiment. Model membranes were prepared as supported lipid bilayers (SLBs) made of both saturated lipids and cholesterol. The membranes were characterised in three isotopic contrasts to compare membrane structure before and after incubation. This allowed us to determine the following different processes: lipid deposition, lipid removal and S protein and/or HDL adsorption (**figure 1**).

Three independent membranes were prepared. The first was incubated with the S protein, the second with HDL and the third with a mixture of HDL and the S protein. Neutron reflectometry data were collected at different time points during these incubations (**figure 2**). A progressive decrease in reflectivity in H_2O-based contrast over time indicates a reduction in the quantity of deuterated material adsorbed at the surface.

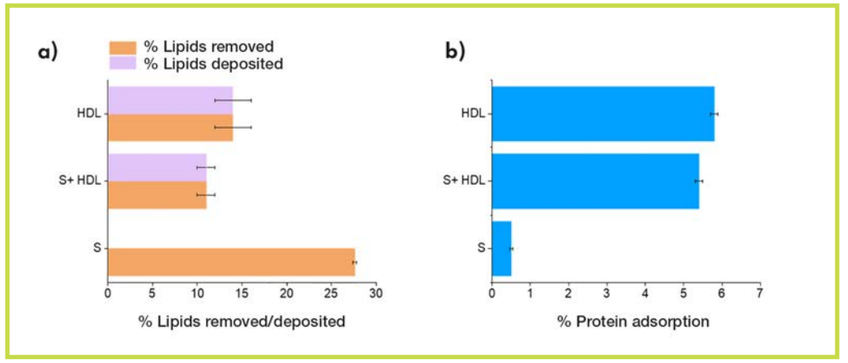

Figure 1

Quantities of lipids removed and deposited **a)** and protein adsorption **b)**, on the membrane surface during incubation with the S protein and/or HDL.

The S protein removed a portion of the membrane. However, the quantity of lipids removed by HDL in the presence of the S protein was only slightly lower than that for HDL alone, suggesting that the combined effect of S on lipid removal was not simply the additive effect of S plus HDL. This suggests that the S protein does indeed interact with HDL, which probably leads to the S protein being saturated with HDL lipids and might lead to HDL composition remodelling.

In summary, neutron reflectometry has proven to be an excellent tool for studying these systems. It has provided clear insight into how the S protein interacts with model membranes and how it affects HDL function by reducing the quantity of lipids removed and deposited from the membrane, probably by removing lipids from the HDL itself and remodelling its composition and structure. Further studies to map HDL functionality behaviour and HDL remodelling by the S protein could potentially lead to a better understanding of the COVID-19 disease.

Figure 2

Schematics of the spike protein and/or HDL incubation with model membranes, and corresponding graphs of lipid removal (red) and protein deposition (blue) over time. Incubations with **a)** the spike protein only; **b)** the spike protein with HDL; and **c)** HDL only.

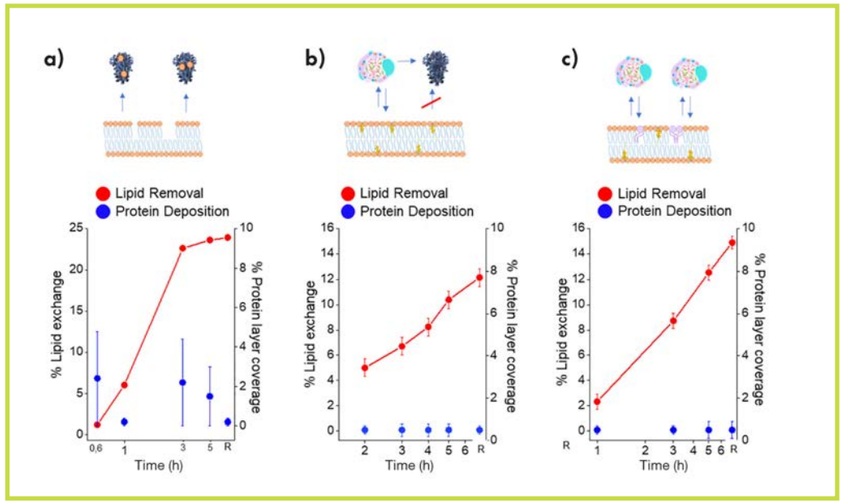

Alessandra Luchini. Italian
Paul Scherrer Institut, PSI, Switzerland
'I did my studies, including my PhD, in Physical Chemistry. My research is focused on lipid-based systems mimicking biological membranes and the characterisation of their interaction with membrane proteins.'

Samanha Micciulla. Italian
ILL
'I started my career as a polymer scientist working on multi-responsive polymer films. I then moved to biomimetic lipid assemblies mimicking bacterial surfaces and distance-dependent structural studies of interacting soft interfaces.'

Neutron reflectometry reveals membrane degradation induced by SARS-CoV-2 spike protein

Fluid Interfaces Grazing Angles ReflectOmeter FIGARO and reflectometer with horizontal scattering geometry D17

Spike proteins are located on the surface of the SARS-CoV-2 virus and enable the virus to enter a host cell and cause the infection. Understanding the mechanism through which the spike proteins interact with the host cell membrane can provide valuable information for developing new strategies to counteract the infection.

AUTHORS

S. Micciulla and **G. Fragneto** (ILL)
A. Luchini (Paul Scherrer Institut, PSI, Switzerland)

ARTICLE FROM

Sci. Rep. (2021)—doi.org/010.1038/s41598-021-93996-x

REFERENCES

[1] Y. Huang *et al.*, Acta Pharmacol. Sin. 41 (2020) 1141
[2] F.A. Rey *et al.*, Cell 172 (2018) 1319
[3] A. de Ghellinck *et al.*, PloS ONE 9 (2014) 1
[4] C. Toelzer *et al.*, Science 370 (2020) 725

Spike proteins are structural components of the SARS-CoV-2 viral envelope. They are known to bind to a protein receptor (angiotensin-converting enzyme 2, ACE2) located on the surface of mammalian cells [1]. The binding to ACE2 induces conformational changes in the spike protein, which promote fusion between the host cell membrane and the viral envelope. This membrane fusion event allows the viral RNA to be released into the host cell [2].

While the binding of the spike protein to ACE2 is well documented, there are fewer data on the interactions between the spike protein and surrounding membranes as well as on the consequences of such interactions for the membranes' structure and stability. Therefore, we decided to use supported lipid bilayers (SLBs) as models of the mammalian plasma membrane to investigate the impact of the extramembrane domain of the spike protein (sSpike) on the SLB structure in the presence and in the absence of the ACE2 receptor. Neutron reflectometry (NR) was our characterisation method of choice. Experiments were carried out on both FIGARO and D17.

Figure 1
Lipid surface coverage measured by neutron reflectometry.

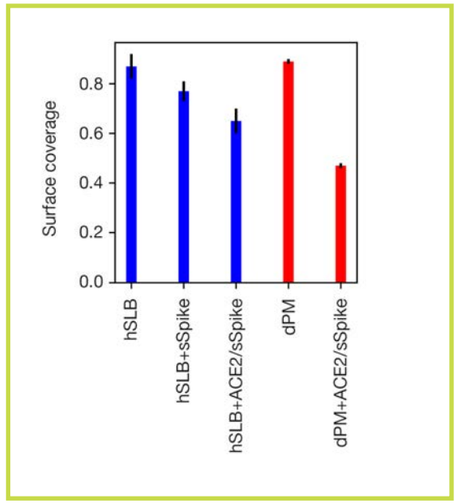

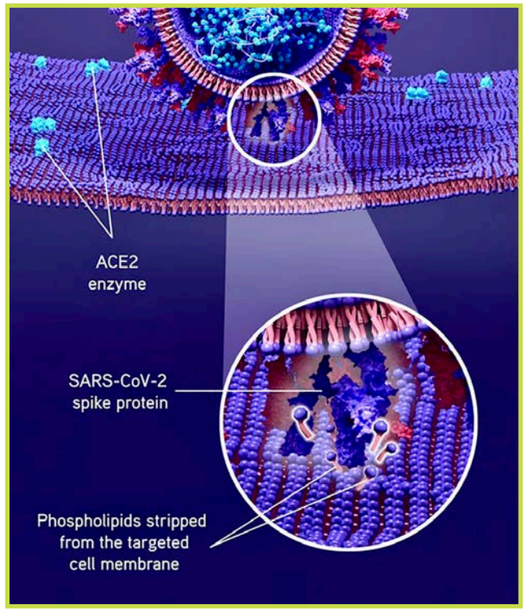

Figure 2
Schematic representation of the spike protein stripping lipids from the plasma membrane of the host cell.

We carefully selected the lipid composition of the SLBs used for this study. Specifically, we used as a reference a synthetic lipid mixture containing 70 mol % POPC (1-palmitoyl-2-oleoyl-sn-glycero-3-phosphocholine) and 30 mol % POPS (1-palmitoyl-2-oleoyl-sn-glycero-3-phospho-L-serine), since POPC and POPS are the most abundant phospholipids in the mammalian plasma membrane. The results collected for this synthetic lipid mixture were compared with those collected for a better mimic of the mammalian plasma membrane consisting of deuterated natural phospholipids extracted from the yeast *Pichia pastoris* [3] and mixed with 10 mol % deuterated cholesterol (hereafter called dPM). We produced the natural phospholipids in their deuterated versions at the L-Lab (www.ill.eu/L-Lab), to enhance the neutron contrast between the lipid membrane and the spike protein. The dPM mixture contained 59 mol % phosphatidylcholine, 20 mol % phosphatidylserine and 11 mol % phosphatidylethanolamine. These natural phospholipids feature a polydisperse acyl chain length (C16–18) and a level of unsaturation corresponding to zero to three double bonds.

We collected NR data after formation of the SLBs in the presence and in the absence of the soluble extramembrane domain of the ACE2 (called sACE2), and again upon injection of the sSpike solution and buffer rinsing to remove the protein molecules from the bulk solvent.

Our results suggested the successful formation of SLBs with high surface coverage in the case of both the hPOPC/hPOPS and dPM (**figure 1**). Using NR we were not able to directly detect the ACE2 because of its low concentration. Nevertheless, its presence on the SLBs was suggested by the various results collected upon the injection of sSpike. Exposure of the hPOPC/hPOPS SLB to the sSpike solution resulted in a remarkable reduction in the bilayer surface coverage of approx. 0.1 v/v. The reduction in bilayer surface coverage was even larger, approx. 0.23 v/v, when the SLBs were prepared with embedded sACE2. We trace these results back to the sSpike being strongly associated with the lipids within the SLB. Thus, during the buffer rinsing step used to remove the protein from the bulk solvent, the sSpike molecules are mostly removed from the SLBs and carry with them some of the lipids. This lipid-stripping effect is promoted by sACE2 as it most probably increases the number of sSpike molecules initially associated with the SLB.

Similar results were observed in the case of the dPM. In this case the resulting reduction in surface coverage was even larger, corresponding to approx. 0.42 v/v.

In conclusion, we found that the spike proteins not only interact with the ACE2 receptor but also show a strong association with host cell membrane lipids. This is consistent with the presence in the spike structure of lipid-binding pockets located very close to the unbound domain responsible for the interaction with ACE2 [4]. We hypothesise that such lipid-binding pockets are involved in the stripping of lipids from the host cell membrane. Such a process could indeed favour the conformation change of the spike protein required for fusion between the host cell membrane and the viral envelope.

Lukáš Gajdoš. Slovak
ILL

'This work formed the main part of my PhD thesis, which I completed in 2021 at the ILL and CERMAV. In my research, I am interested in understanding the molecular mechanisms of host–pathogen interactions at an atomic level. Currently I am working as a postdoctoral researcher at the ILL, combining neutron and X-ray crystallography to study the effects of radiation damage on protein crystals.'

Neutron crystallography provides insights into how bacterial lectins decipher the 'glycocode'

Quasi-Laue diffractometer LADI-III and D-Lab

Bacterial lectins recognise sugars present on the host cell surface, which they use to attach and initiate infection. Here, we used neutron crystallography to describe the interactions between a bacterial lectin and the monosaccharide fucose, both produced in perdeuterated forms, revealing unprecedented details of the hydrogen-bonding network. With antibiotic resistance a rapidly developing global threat, this new structural information can contribute to the design of novel, potent drugs for preventing bacterial infections.

AUTHORS

L. Gajdoš, M.P. Blakeley, M. Haertlein, V.T. Forsyth and J.M. Devos (ILL)
A. Imberty (CERMAV)

ARTICLE FROM

Glycobiology (2021)—doi:10.1093/glycob/cwaa059
Structure (2021)—doi:10.1016/j.str.2021.03.003

REFERENCES

[1] H. Lis and N. Sharon, Chem. Rev. 98 (1998) 637
[2] S. Cecioni, A. Imberty and S. Vidal, Chem. Rev. 115 (2015) 525
[3] M.P. Blakeley and A.D. Podjarny, Emerg. Top. Life Sci. 2 (2018) 39
[4] A. Kumar *et al.*, J. Biol. Chem. 291 (2016) 25032

Lectins are carbohydrate-binding proteins whose diverse functions participate in many physiological and pathological processes. Every human cell is covered with a thick layer of glycans in the form of glycoproteins and glycolipids, which presents the first layer of information to the outer cellular environment. Lectins read this complex 'glycocode' by specifically targeting different sugars and mediating molecular recognition [1].

Pathogenic bacteria produce lectins that can be directly involved in cell adhesion in the early stages of infection. Such infections are often treated by antibiotics, but increasing antibiotic resistance is a major health problem. An alternative approach that does not use antibiotics and hence does not promote antibiotic resistance entails preventing bacteria from binding to human cells, also known as anti-adhesive therapy. This can be done using novel glycomimetic compounds. Detailed knowledge about lectin–glycan interactions involved in host–pathogen associations is required for the design of novel, high-affinity glycomimetic compounds [2].

In collaboration with the Centre de Recherches sur les Macromolécules Végétales (CERMAV, CNRS) and the Central European Institute of Technology (CEITEC), we used neutron macromolecular crystallography (NMX) to gain novel insight into sugar recognition by lectins from pathogenic bacteria. Thanks to the sensitivity of neutrons to hydrogen, NMX can provide crucial details on the position of hydrogen atoms, the protonation states of amino acid residues and the directionality of water molecules that play a crucial role in sugar-binding by lectins [3]. The work presented here focused on a fucose-specific lectin from an insect pathogen named *Photorhabdus luminescens* that can also bind to human cells [4].

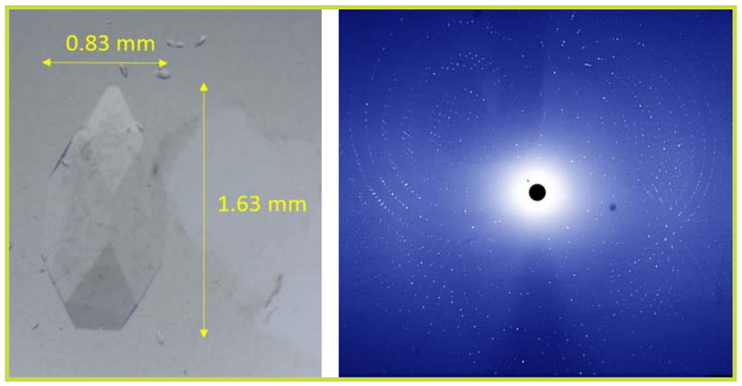

Figure 1
The 0.5 mm^3 crystal of the perdeuterated PLL/fucose complex that was used to collect data on LADI-III (**left**), with part of the diffraction pattern obtained from this crystal (**right**).

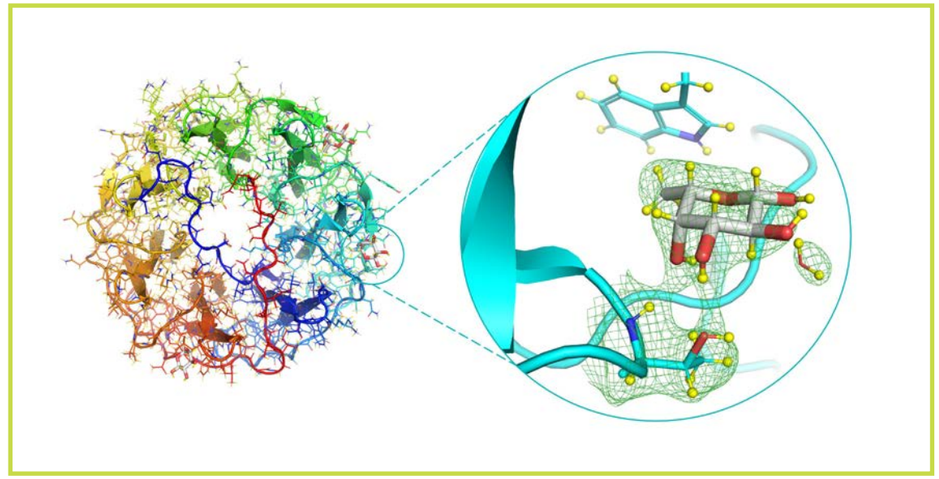

Figure 2
Neutron structure of the PLL/fucose complex, focusing on the fucose-binding site (**right**). The green mesh represents the neutron density.

Perdeuteration is a process that involves the complete replacement of all hydrogen atoms by deuterium atoms in a molecule. The scattering properties of deuterium atoms makes them easier than hydrogen atoms to visualise in the neutron scattering maps. Moreover, using perdeuterated molecules avoids the 'cancellation effects' around protein backbones and carbohydrate rings often observed in the neutron maps. While the perdeuteration of proteins is well established this is not the case for carbohydrate molecules. Here, we performed, for the first time, an *in vivo* perdeuteration of a monosaccharide, L-fucose, using a glyco-engineered strain of *Escherichia coli* that was designed by our collaborators at CERMAV. The production of both perdeuterated PLL protein and sugar was carried out in the Deuteration Laboratory (D-Lab) at the ILL. Perdeuterated fucose was co-crystallised with perdeuterated lectin, and room-temperature, single-crystal neutron diffraction data were collected on the LADI-III diffractometer at the ILL (**figure 1**). The X-ray data were collected from the same crystal to enable the joint X-ray/neutron structure analysis.

The neutron diffraction experiments yielded two structures: one in ligand-free form, and one in complex with the perdeuterated ligand. The results highlight the advantage of using perdeuterated molecules in NMX, as well as that of using ambient temperature during data collection to avoid artefacts arising during the cryo-protection and cryo-cooling of protein crystals. A complete hydrogen-bonding network between the lectin and L-fucose could be described, including details about hydrophobic contacts that could not have been obtained using X-ray diffraction experiments alone (**figure 2**). Our work can be applied to more complex systems, such as oligosaccharides present on human cells that are natural ligands of lectins. Providing details on the position of hydrogen atoms, as well as on the CH–π interactions commonly observed in lectin-carbohydrate binding, is necessary both for a better understanding of these complexes and for the structure-based drug design of glycomimetic compounds.

Erwin Jericha. Austrian
Atominstitut, Faculty of Physics, TU Wien, Austria

'I am an assistant professor working at the Vienna University of Technology. I have been a neutron physicist for three decades, interested in neutron-induced reactions, the development of new neutron techniques and relating neutron physics to fundamental questions about nature. My first visit brought me to the ILL in 1989, and I have been a regular and enthusiastic visiting scientist to various instruments ever since.'

MONOPOL: a neutron resonator that flexibly manipulates polarised neutron beams

Ultracold neutron facility PF2

Defining the characteristics of the incoming neutron beam is an essential procedure for each neutron experiment. Here, we present a concept for polarised neutron beams that allows for remarkable flexibility. By employing spatial magnetic spin resonance using a neutron resonator whose elements are controlled individually, we have overcome all known limitations associated with pulsed, polarised neutron beam tailoring. The very cold neutrons (VCN) of the PF2 instrument proved extremely valuable for testing this new, powerful variant of an already traditional technique.

AUTHORS

E. Jericha, **J. Bosina** and **G. Badurek** (Atominstitut, TU Wien, Austria)
P. Geltenbort (ILL)
M. Masahiro and **T. Odo** (Kyoto University, Japan)

ARTICLE FROM

Sci. Rep. (2020)—doi:10.1038/s41598-020-62612-9

REFERENCES

[1] M.M. Agamalyan, G.M. Drabkin and V.I. Sbitnev, Phys. Rep. 168 (1988) 265
[2] G. Badurek, A. Kollmar, A. Seeger and W. Schalt, Nucl. Instrum. Methods A 309 (1991) 275
[3] E. Krüger, W. Nistler and W. Weirauch, Metrologia 35 (1998) 203
[4] E. Jericha *et al.*, Sci. Rep. 10 (2020) 5815

Spatial magnetic spin resonance was discovered in Gatchina, near St. Petersburg, in the 1960s. Early work concerning this technique is discussed and summarised in [1]. The technique itself entails placing a neutron resonator in a polarised neutron beam. In order to retain the neutron polarisation, typically a magnetic guide field perpendicular to the neutron propagation accompanies the neutron beam throughout the experimental set-up. For magnetic spin resonance this field acts as a selector for the neutron resonance wavelength. The resonator itself is made up of a series of elements that generate a magnetic field perpendicular to the guide field with alternating directions in each adjacent element. This configuration flips the neutron spin for a given resonance wavelength and a specific wavelength band around it, upon a resonance and amplitude condition being fulfilled. Following the resonator, the neutrons pass a broadband spin flipper that inverts the polarisation of all neutrons in the beam. The beam is eventually analysed by a neutron polariser.

In the case of the resonator being switched off, in an ideal situation of perfect neutron polarisation no neutron may pass the analyser. Switching the resonator on leads to a spectrally defined neutron beam which is allowed

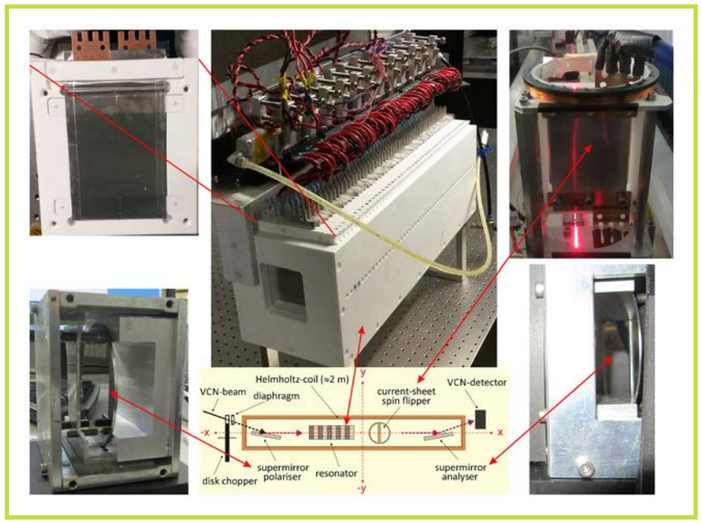

Figure 1

Essential components of the spatial magnetic spin resonance experiment. The neutron resonator (**top centre**) consists of 48 individual elements (**top left**) supplied by 48 current sources located on top of the resonator. A multilayer-coated mirror (**bottom left**) polarises the neutron beam that passes through the resonator, a broadband current-sheet spin flipper (**top right**), and is analysed by a second polariser mirror (**bottom right**). We put all these components into a large helium-filled box to reduce losses from VCN absorption in air.

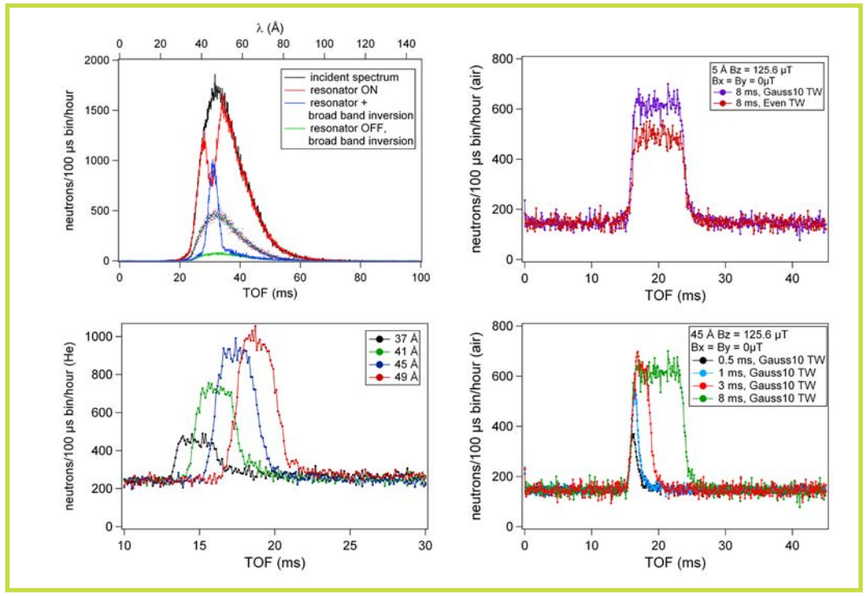

Figure 2

Time-of-flight spectra of the VCN beam, as measured by means of a mechanical single-disk chopper (**top left**) and by the resonator itself (**three other graphs**). The various spectra illustrate the high flexibility gained using this resonance technique.

to pass the analyser. Thus, the complete set-up acts as a neutron monochromator, with the magnetic field configuration defining the spectral shape of the resulting neutron beam.

Such monochromators were designed to replace analyser crystals in inverted geometry neutron spectrometers [2] or to precisely define the velocity of neutrons used to determine the fine structure constant by neutron resonance and perfect crystal reflection in a high-precision experiment [3]. Development of the new type of resonator was also motivated by high-precision studies, at that time investigating the beta decay of neutrons. In the traditional configuration [1], the resonator took the form of a single metal foil in meander shape, supplied by a common electrical current. To shape the corresponding magnetic field configuration it was necessary to tailor the resonator geometrically [1], which limited the neutron spectrum to a specific shape. In addition, the pulsing of this type of resonator relies on a timing that relates to the overall length of the resonator. In neutron instruments that rely on a sharp neutron pulse structure, the timing of a conventional resonator may be insufficient.

By creating a resonator with individually controllable elements, we have overcome all these limitations associated with pulsed, polarised neutron beam tailoring [4]. **Figure 1** shows the essential components of the experimental set-up that demonstrated this technique for the first time with a polychromatic white neutron beam. **Figure 2** displays a few aspects of the flexibility of this method. In the **top left** graph, we follow the action of the various components. A disk chopper offers appropriate timing for displaying the total incoming spectrum, the spectrum that misses the resonantly flipped neutrons, the spectrum of the resonantly flipped neutrons and the background as a result of non-perfect neutron polarisation. Also in **figure 2**, various neutron pulses obtained from different settings of the resonator can be seen. The **top right** plot compares different magnetic field distributions. The **bottom left** plot illustrates the importance of the selector field with respect to the resonance wavelength. The height of the pulses corresponds to the intensity of the incoming neutron spectrum. And finally, the **bottom right** plot shows estimates of the possible length of neutron pulses. For VCN, the minimum pulse lengths are of the order of 1 ms, from which we may extrapolate pulses in the order of 100 µs for cold neutrons and even shorter ones for thermal neutron beams. All this has been achieved simply by changing the currents in the individual resonator elements.

Corresponding developments may turn out to be attractive for polarised neutron diffractometers and spectrometers at the ILL, as well as for tailoring the long pulses at the European Spallation Source. A special place exists for the MEPHISTO beamline at the FRM II in Garching and its neutron decay facility PERC, which motivated this new development.

Matthieu Licciardi. French
Laboratoire de Physique Subatomique et Cosmologie, France

'My research activities focus on neutrino physics and statistical methods. I first studied neutrino–nucleus interactions on the GeV scale for my PhD on the T2K experiment. In 2019, I joined the STEREO collaboration as a postdoc to lead on the analysis of the reactor antineutrino spectrum.

A precision measurement of the ^{235}U antineutrino spectrum at the ILL

Search for sterile neutrino STEREO

Reactor cores are intense sources of electron antineutrinos ($\overline{\nu}_e$), used to study the fundamental physics of (anti) neutrinos. Flux predictions are key inputs to such studies but their modelling is very complex, leading to long-standing data-to-prediction discrepancies. Using the high-flux reactor (HFR) at the ILL, the STEREO experiment provides the community with a new experimental reference, free of detector effects, for the antineutrino spectrum from ^{235}U fissions.

AUTHORS

M. Licciardi (LPSC, Université Grenoble Alpes; CNRS; Grenoble INP, France)
R. Rogly (IRFU, CEA, Université Paris-Saclay, France)
on behalf of the STEREO collaboration.

ARTICLE FROM

J. Phys. G: Nucl. Part. Phys. (2021)—doi:10.1088/1361-6471/abd37a

REFERENCES

[1] K. Schreckenbach *et al.*, Phys. Lett. B 160 (1985) 325
[2] P. Huber, Phys. Rev. C 84 (2011) 024617
[3] M. Estienne *et al.*, Phys. Rev. Lett. 123 (2019) 022502
[4] F.P. An *et al.*, Chin. Phys. C 41 (2017) 013002
[5] H. Almazán *et al.*, arXiv:2107.03371 [nucl-ex]

In reactor cores, antineutrinos are produced by the β-decay of the fission products of fuel fissile isotopes, *e.g.* ^{235}U, ^{238}U, ^{239}Pu and ^{241}Pu. Accurate predictions of the antineutrino fluxes require detailed knowledge about the decay chain of all possible daughter nuclei, and are therefore difficult to obtain. As each antineutrino is emitted with an electron sharing the total energy of the transition, a workaround is to convert the total electron spectrum, *i.e.* the sum of the beta branches in all decay chains, into an antineutrino spectrum (conversion method). Historically, the first antineutrino-spectra predictions were derived in this way by Schreckenbach *et al.* [1], after measurements of the total electron spectra from all fissile isotopes performed at the ILL in the 1980s. This conversion method is still used to produce predictions today [2]. However, as nuclear databases are becoming more comprehensive, predictions based on the direct summation of antineutrino spectra from all possible branches in the decay chains (summation method) have become increasingly relevant [3].

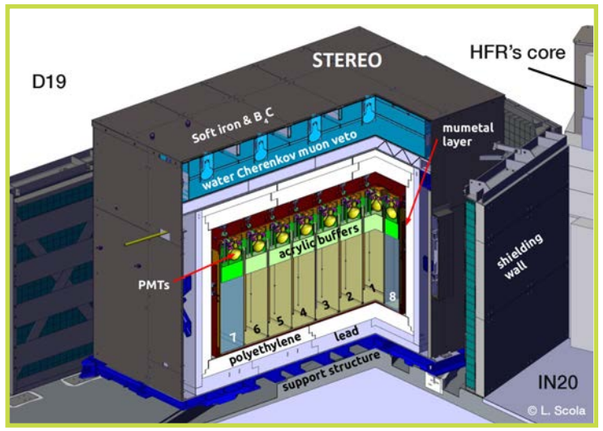

Figure 1
The STEREO detector at level C of the ILL's reactor hall. The target volume consists of cells 1–6 filled with Gd-loaded liquid scintillator; it is surrounded by Gamma-catcher cells filled with Gd-free liquid scintillator (7–8).

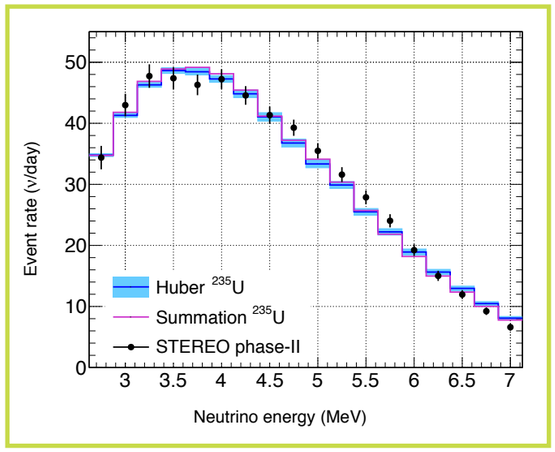

Figure 2
STEREO antineutrino spectrum from ^{235}U fissions, compared with normalised reference predictions (Huber Model [2] and Summation Model [3]). The measurement shows an excess of events in the 5-MeV region, reminiscent of the shape anomaly reported by experiments at commercial reactors.

Because of limitations with the conversion method or the incompleteness of nuclear databases, neither method perfectly succeeds in reproducing the measured antineutrino spectra, in terms of normalisation or spectrum shape. Several hypotheses have been put forward to explain the data-to-prediction discrepancies, one of which being oscillations involving a sterile neutrino. Initially designed to investigate this sterile neutrino hypothesis, the STEREO experiment also precisely measured the total antineutrino spectrum from ^{235}U fissions.

The STEREO detector operated (2016–2020) at about 10 m from the HFR's core in the ILL's reactor hall. In contrast to commercial reactors, where antineutrinos are produced from a time-evolving mixture of ^{235}U, ^{238}U, ^{239}Pu and ^{241}Pu fissions, more than 99 % of the antineutrinos from the HFR's core originate from ^{235}U fissions, allowing the direct study of this isotope. Antineutrinos are detected *via* the inverse β-decay process $\overline{\nu}_e + p \rightarrow e^+ + n$, producing a pair of signals with time and space correlation: an e^+e^- annihilation followed by a neutron capture. STEREO's 1.8 m^3 target volume is filled with liquid scintillator for particle detection, with the addition of Gd to enhance the neutron capture signal. Gamma-catcher cells filled with Gd-free liquid scintiallator surround the target volume to minimise energy losses. A thick shielding of lead and polyethylene mitigates the effect of neighbouring instruments and cosmic rays on the background, as does a water Cherenkov muon veto (see **figure 1**). The residual cosmic background is characterised when the reactor is turned off. Finally, the liquid scintillator provides particle identification based on the time-distribution of collected scintillation light (pulse shape discrimination), increasing the signal-to-background ratio to ~1. The results presented here use data recorded during 212 days of reactor-off and 118 days of reactor-on (phase-II of the STEREO experiment), representing 4.3 × 10^4 detected antineutrinos.

Thanks to regular monitoring of the detector's energy response with radioactive calibration sources, we achieved a percent-level accurate Monte Carlo simulation of the detector. This excellent control of the energy reconstruction allowed us to demonstrate both that all systematics remain small with respect to statistical uncertainties and that a precision measurement of the antineutrino spectrum is possible.

Given the discrepancies between previous measurements and the spectrum predictions, we took care to provide a measurement of the antineutrino spectrum corrected for all detector effects, so that it can be used as a reference in other experiments. Resolution effects specific to STEREO were therefore deconvoluted using the detector's response matrix. **Figure 2** displays the measured antineutrino spectrum from ^{235}U fissions along with two state-of-the-art predictions [2, 3], normalised to the same event rate. A significant spectral distortion with respect to these models is observed in the 5-MeV region. Our measurement indicates that this excess of events, first observed at commercial reactors with a combination of isotopes [4], is (at least partially) induced by ^{235}U fissions.

This measurement of the ^{235}U spectrum carried out by the STEREO experiment at the ILL facility is a milestone for the community in terms of describing reactor antineutrino spectra. As theoretical methods fail to predict these spectra, experimental measurements are becoming the reference in the field. We extracted the first ^{235}U spectrum free of detector effects, directly from a pure ^{235}U antineutrino flux. Ongoing analysis of the remaining sample from STEREO (more than 6.3 × 10^4 additional antineutrinos) and the combination of our dataset and those from other experiments using a pure ^{235}U flux [5] will increase the precision of this measurement to the benefit of all experiments using reactors as their antineutrino source.

Cristina Müller. Swiss Centre for Radiopharmaceutical Sciences, Paul Scherrer Institut, PSI, Switzerland

'I am a research group leader at the Centre for Radiopharmaceutical Sciences at the Paul Scherrer Institute and a private docent at the ETH Zürich, Switzerland. My research focuses on the development and preclinical application of novel radioligands for imaging and therapy for cancer. A particular interest of mine lies in the investigation of emerging radionuclides for radiotheragnostics.'

Terbium radionuclides for theragnostics: from bench to bedside

V4 high-flux position for neutron irradiation

Targeted radionuclide therapy (TRT) exploits biological vectors (*e.g.* peptides) to target tumour markers (*e.g.* peptide receptors) that are over-expressed on tumour cells but absent or rare on normal cells. These tumour-specific vectors can transport a radioactive payload to the tumour, *i.e.* radionuclides that emit diagnostic and/or therapeutic radiation. The concept of TRT is particularly suited to the treatment of disseminated disease that cannot be treated by surgery or external beam radiation therapy. For therapeutic purposes, short-range radiation such as alpha particles or low-energy electrons (beta, conversion electrons or Auger electrons) is preferred. Today, clinical applications mainly exploit the beta-emitter ^{177}Lu, although ^{161}Tb, another radiolanthanide with similar (bio-)chemical properties, is potentially superior because it emits about twice the number of electrons, short-range electrons in particular, per decay.

AUTHORS

C. Müller, **F. Borgna** and **N.P. van der Meulen** (Paul Scherrer Institute, PSI, Switzerland)
R.P. Baum (Curanosticum Wiesbaden-Frankfurt, Germany)
U. Köster (ILL)

ARTICLE FROM

J. Nucl. Med. (2021)—doi:10.2967/jnumed.120.258376, and Eur. J. Nucl. Med. Mol. Imaging (2021)—doi:10.1007/s00259-021-05564-0

REFERENCES

[1] C. Müller *et al.*, ILL Annual Report (2012) 80
[2] N. Gracheva *et al.*, EJNMMI Radiopharm. Chem. 4 (2019) 12
[3] R.P. Baum *et al.*, J. Nucl. Med. 61 (2021) 1391
[4] C. Müller *et al.*, Eur. J. Nucl. Med. Mol. Imaging 46 (2019) 1919
[5] F. Borgna *et al.*, Eur. J. Nucl. Med. Mol. Imaging (2021) https://doi.org/10.1007/s00259-021-05564-0
[6] J.P. Pouget *et al.*, Radiat. Res. 170 (2008) 192

A decade ago, we demonstrated the suitability of ^{161}Tb and its 'terbium sisters' (^{149}Tb, ^{152}Tb and ^{155}Tb) for nuclear medicine applications [1]. However, as is the case for any new medical product in this area, progress from initial preclinical studies using tumour cells, to small animal investigations and finally to clinical application in patients, has been long and laborious.

A necessary precondition for the human application of radiopharmaceuticals is their reproducible production under the highest quality standards. We demonstrated this in the production of so-called 'no-carrier-added' quality ^{161}Tb *via* repeated neutron irradiation of enriched ^{160}Gd targets at the V4 high-flux position of the ILL reactor and at other research reactors—thus producing ^{161}Tb by beta-decay of the intermediate radionuclide ^{161}Gd followed by radiochemical Tb/Gd separations [2].

The high chemical and radionuclidic purity of ^{161}Tb achieved in a separation process established at PSI opened the way to a first-in-human application. DOTATOC, a peptide known to target neuroendocrine tumours, was labelled with ^{161}Tb to obtain the radiopeptide ^{161}Tb-DOTATOC at the local radiopharmacy of Zentralklinik Bad Berka (Germany). Two patients with metastatic neuroendocrine tumours were administered with ^{161}Tb-DOTATOC at Zentralklinik Bad Berka (Germany). The biodistribution of ^{161}Tb-DOTATOC could be followed over time by SPECT/CT (single-photon emission computed tomography; see **figure 1**), thus providing the data necessary for quantitative dosimetry calculations. These data revealed the expected tissue distribution and showed that ^{161}Tb-DOTATOC was well tolerated and had no related adverse effects [3].

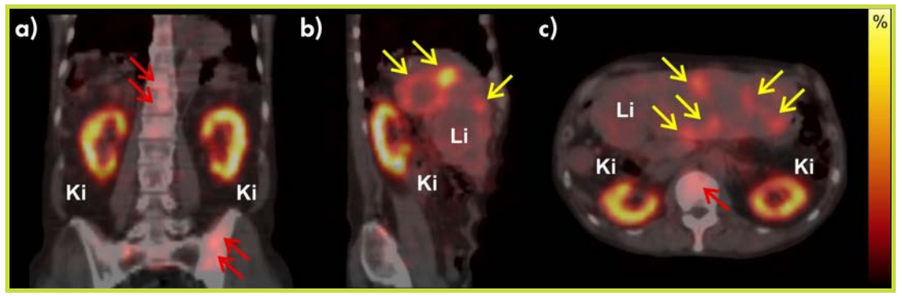

Figure 1

SPECT/CT images (**a**, coronal; **b**, sagittal; **c**, transverse section) obtained 19 hours after injection of ^{161}Tb-DOTATOC. Uptake of ^{161}Tb-DOTATOC is observed in liver (Li) metastases (yellow arrows), as well as in multiple skeletal metastases in the vertebral column and the pelvis (red arrows). Excess ^{161}Tb-DOTATOC is eliminated *via* the kidneys (Ki) and bladder. This figure was originally published in the J.Nucl. Med., in [3] © SNMMI.

In parallel with this first clinical achievement, we have been working on both broadening the applications of ^{161}Tb-based TRT to other tumour types and precisely quantifying its therapeutic superiority in dedicated experiments. We compared ^{161}Tb with ^{177}Lu after labelling the vector PSMA-617, which targets prostate cancer cells, with each radionuclide separately. The data showed that ^{161}Tb clearly outperformed ^{177}Lu, *in vitro* (*i.e.* in cell cultures) as well as *in vivo* [4]. This research project received the Marie Curie Award at the European Association of Nuclear Medicine (EANM) conference in 2019, while an associated article was awarded the Springer Best Paper Prize 2020, thereby putting ^{161}Tb at the centre of research and clinical interest.

To solve the question of where in a tumour cell ^{161}Tb can best deploy the action of its short-range Auger electron emission, three different peptides targeting neuroendocrine tumour cells were labelled with ^{161}Tb and ^{177}Lu: DOTATOC, which is known to accumulate chiefly in the cytoplasm; DOTATOC-NLS, which preferentially accumulates in the cellular nucleus; and DOTA-LM3, which accumulates at the cell membrane. ^{161}Tb outperformed ^{177}Lu in all cases (see **figure 2**); nevertheless, superior performance, in terms of the reduction in tumour cell viability at the lowest possible activity level, was most pronounced for DOTA-LM3. At first glance, this finding appeared surprising. However, it is actually in line with studies reported by Pouget *et al.*, who found a more pronounced effect of Auger electrons using ^{125}I-labelled antibodies that localised at the cellular membrane than with those that localised in the cytoplasm [6]. As a next step on the preclinical level, the data obtained with ^{161}Tb/^{177}Lu will be reproduced with other tumour cells and different vectors.

A clinical trial studying ^{161}Tb-DOTA-LM3 is planned to start in 2022 at Basel University Hospital. As part of the recently started European medical radionuclide programme PRISMAP [**https://prismap.eu**], both the ILL and the PSI will play a key role in supplying ^{161}Tb for further preclinical and clinical research.

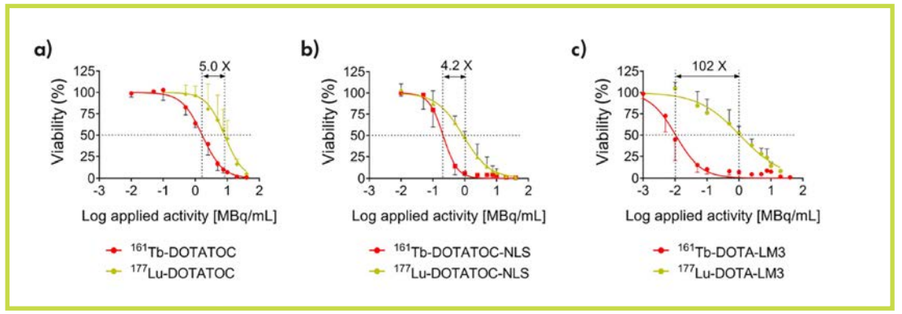

Figure 2

Results of the cell viability assessment of AR42J tumour cells after incubation with each radiopeptide: **a)** ^{161}Tb/^{177}Lu-DOTATOC; **b)** ^{161}Tb/^{177}Lu-DOTATOC-NLS; and **c)** ^{161}Tb/^{177}Lu-DOTA-LM3. The factor of the difference in efficacy between ^{161}Tb and ^{177}Lu when using the same peptide is indicated for 50 % cell viability. Figure adapted from [5], https://creativecommons.org/licenses/by/4.0/

Romane Schick. French and Swiss
ILL and Grenoble-Alpes University (UGA), France

'I am currently in the final stages of my PhD on theoretical physics at the ILL. My research focuses on frustrated magnetism. During my PhD, I used spin-wave theory to study order by disorder phenomena in frustrated antiferromagnets, and investigated related competition effects between quantum and thermal fluctuations.'

Quantum *versus* thermal fluctuations in the face-centered cubic antiferromagnet: alternative routes to 'order by disorder'

Competing forms of structural or magnetic order can lead to an infinite number of possible ground states. This macroscopic degeneracy can be lifted by either quantum mechanical zero-point motion or thermal fluctuations. Both are often assumed to act in a similar manner, but we have recently demonstrated a simply defined counter-example: the Heisenberg face-centred cubic (fcc) quantum antiferromagnet. Quantum effects select one symmetry while thermal fluctuations favour another, with the difference related to the topologies of soft modes in momentum space. For large values of spin, this implies a phase transition between the two states that is suppressed by stronger quantum effects at low spin.

AUTHORS

R. Schick (ILL and Grenoble-Alpes University, France)
T. Ziman (ILL)
M. Zhitomirsky (IRIG, CEA, Grenoble, France)

ARTICLE FROM

Phys. Rev. B (2020)—doi: 10.1103/PhysRevB.102.220405

REFERENCES

[1] P.W. Anderson, Phys. Rev. 79 (1950) 705
[2] J. Villain, R. Bidaux, J.-P. Carton and R. Conte, J. Phys. (Paris) 41 (1980) 1263
[3] R. Schick, T. Ziman and M.E. Zhitomirsky, Phys. Rev. B 102 (2020) 220405(R)
[4] R. Schick, O. Gotze, T. Ziman, R. Zinke, J. Richter and M.E. Zhitomirsky, Arxiv, to be submitted to Phys. Rev.

The quantum Heisenberg antiferromagnet on an fcc lattice is one of the oldest frustrated models. Analysis using linear spin-wave theory was recognised from the beginning of the 1950s [1] to be problematic and was thought not to give a clear result because of the infinite classical degeneracy, the difficulty of treating low-frequency modes and resulting ambiguity concerning the symmetry of the ground state. Theoretical difficulties led to a misleading phenomenological approach in which order observed in real physical systems was attributed to extra periods of anisotropy rather than to stabilisation by fluctuations.

The concept of 'order by disorder' [2] has now allowed a coherent picture to emerge. Here, we consider the Heisenberg model with spins of length S and begin with the simplest case with nearest-neighbour exchanges on a face-centred cubic lattice. Two criteria, *i.e.* a small zero-point energy and low free energy at low temperatures, lead to the dominant role of 'soft' magnons: those with vanishingly small energy. Note that the AF-I and AF-III structures both have, in linear order to 1/S and in addition to the zero-energy Goldstone modes corresponding to the broken rotational symmetry of the spin structure, extra lines of zero-modes reflecting the infinite degeneracies of the classical frustrated limit of infinite S. The topologies of these zero modes differ for the two competing states: in the quantum limit, AF-III turns out to have lower energy, whereas the different weighting of the soft modes in the free energy for finite temperatures favours AF-I. The difference is very small and at low temperatures the free energies of the two phases cross each other, giving a phase transition [3].

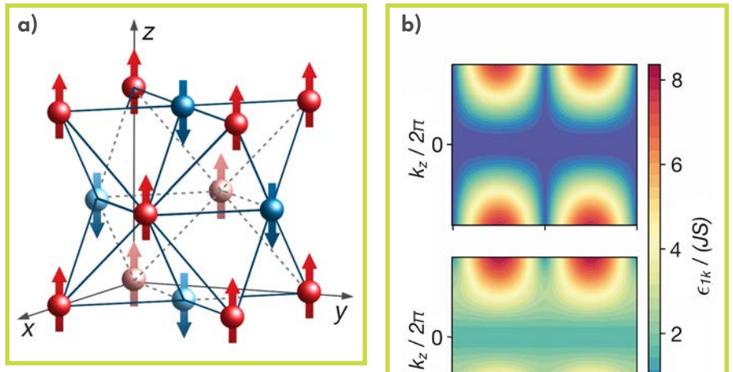

Figure 1
a) The antiferromagnetic type I structure in real space on the face-centered-cubic lattice.
b) Dispersion of magnon modes for the type I structure in reciprocal space, as calculated in linear spin wave theory (upper panel) and in anharmonic theory (lower panel).

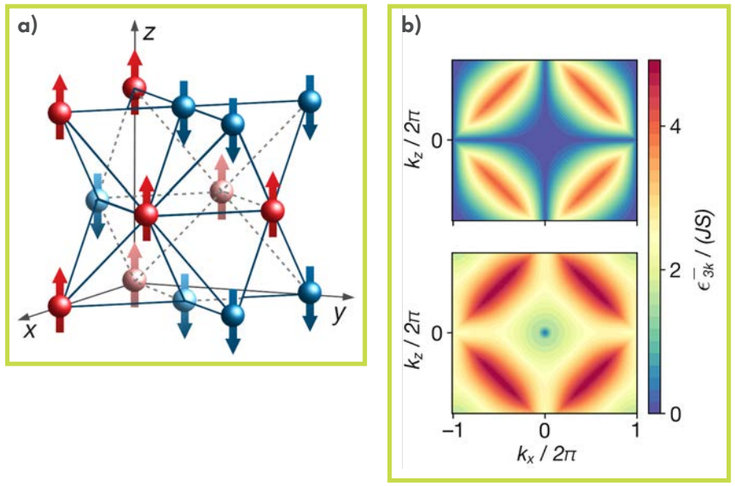

Figure 2
a) The antiferromagnetic type III structure in real space on the fcc lattice.
b) Dispersion of magnon modes for the type I structure in reciprocal space, as calculated in linear spin wave theory (upper panel) and in anharmonic theory (lower panel).

While this conclusion must be true for large quantum spin S, where harmonic spin-wave theory is accurate, what happens when S decreases down to spin ½ or 1 for example? We recently [4] answered this question by extending spin-wave theory to include magnon–magnon interactions in a self-consistent manner and comparing with numerically-intensive computations on finite clusters as an independent check on the accuracy. The two approaches concur, both finding that in fact the small gain of the AF-III is lost for all but the largest spins. Magnon–magnon coupling hardens the lines of soft magnons, leaving only the Goldstone modes guaranteed by symmetry. We can visualise the effects of magnon–magnon interactions by looking at the figures for the energies of spin-wave modes, as calculated for spin S = 1/2 in the k_x-k_z plane with fixed $k_y = 2\pi/a$ for the two different structures (with spins ordered in real space, as shown in **figures 1b** and **2b**), either harmonically (**upper panels**) or self-consistently including interactions (**lower panels**). The regions of soft modes are strongly reduced by quantum interactions, and the AF-I structure can occur even at ultra-low temperatures.

In conclusion, we have shown how quantum zero-point effects and classical fluctuations can lead to different results for order by disorder, with qualitatively different behaviour for large and small quantum spins. Similar phenomena will occur in other highly frustrated magnetic systems.

Evidence of an electromagnon in $GdMn_2O_5$: a multiferroic with huge electric polarisation

ILL Theory group, IN6-Sharp, THALES and IN12

The dynamical properties of $GdMn_2O_5$ are studied using inelastic neutron scattering and infrared spectroscopy, assisted by *ab initio* calculations. Our work sheds light on the electromagnon, a magnetic mode that can be excited by an electric field. Combining spin-wave measurements, simulations and *ab initio* calculations of single-ion anisotropies and super-exchange interactions, we describe in detail the magnetic contribution to this mode.

AUTHORS

M.-B. Lepetit (Institut Néel, CNRS, ILL, France)
P. Foury-Leylekian, **A. Vaunat** and **V. Balédent** (LPS, CNRS-U, Université Paris-Saclay, France)
S. Petit (LLB, CNRS-CEA, France)
P. Roy and **J.B. Brubach** (Soleil synchrotron, France)
G. Giri, **E. Rebolini** and **P. Steffens** (ILL)
S. Raymond (Université Grenoble Alpes, CEA, IRIG, France)
Q. Berrod (ILL, CNRS, CEA, IRIG, Université Grenoble Alpes, France)

ARTICLE FROM

Phys. Rev. B (2021)—doi:10.1103/PhysRevB.103.174434

REFERENCES

[1] G.A. Smolenskii and I.E. Chupis, Sov. Phys. Uspekhi 25 (1982) 415
[2] A. Cano, Phys. Rev. B 80 (2009) 012104
[3] H. Katsura, A.V. Balatsky and N. Nagaosa, Phys. Rev. Let. 98 (2007) 027203
[4] A.B. Sushkov *et al.*, J. Phys. Condens. Matter 20 (2008) 434210
[5] G. Yahia *et al.*, Phys. Rev. B 97 (2018) 085128
[6] S. Partzsch *et al.*, Phys. Rev. Let. 107 (2011) 057201

Magnetoelectric multiferroics, which simultaneously stabilise magnetic and polar static orders, have been predicted to present unusual dynamical magnetoelectric effects (ME) [1]. The relatively large magnitude of this dynamical ME response and its strong interaction with light [2] are extremely attractive for potential applications.

Using infra-red (IR) and inelastic neutron scattering (INS) experiments, carried out on the same crystal, we investigated the low-energy excitations in the model system $GdMn_2O_5$ and found evidence of the presence of an electroactive magnon. To describe this unusual property, various mechanisms have been proposed that rely on the very same microscopic mechanisms underlying static magnetoelectric properties. Lattice vibrations alter the exchange couplings or the anisotropies, which in turn affect the magnon spectrum. In helical magnetic systems where the multiferroicity originates from the Dzyaloshinskii–Moriya interaction (DMI), the same DMI has been proposed [3]. Other propositions are based on exchange-striction (ES), coupling a polar lattice mode to the magnon spectrum [4]. Completing our experimental work with spin-wave simulations and *ab initio* calculations, we show the absence of both lattice and crystal field modes in $GdMn_2O_5$, suggesting that another, purely electronic, mechanism is at work in this system.

IR measurements were carried out on the AILES beamline of the SOLEIL synchrotron. **Figures 1a** and **b** present the absorbance at 5 K for different (e,h) light polarisation configurations, calculated using the 40 K measurement as a reference. A very intense peak is visible in the configuration (e,h) = (b,a). In the configuration (e,h) = (c,a), where h remains along *a*, this mode disappears, proving its electroactivity for e//b, consistent with a polarisation direction along the *b*-axis. The disappearance of the peak for the (e,h) = (c,b) configuration confirms the electroactive nature of this excitation. **Figures 1c** and **d** display the temperature-dependence of the peaks. Both behave in a similar way: from 5 K up to 30 K, the energy decreases by 1 meV (8 cm^{-1}) while its width increases. No peak could be observed above the magnetic transition at T_c = 32 K.

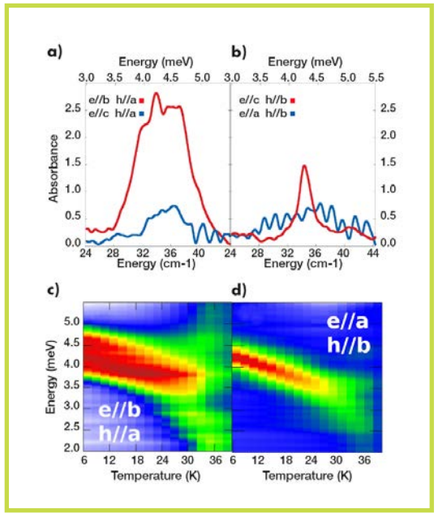

Figure 1

Absorbance at 5 K (with a reference at 40 K) in $GdMn_2O_5$. Red and blue curves correspond to different orientations of incident e and h (electric and magnetic field of the light).

We computed the phonon spectra in both the *Pbam* and *Pm* (AFM order, double-unit cell) space groups in order to check for a possible phonon origin to these modes. The calculations were carried out within the density functional (DFT-PBEsol) frame using the CRYSTAL code. The calculations are in good agreement with phonons measured above 13 meV (≈ 100 cm^{-1}); however, no phonon contribution is predicted below 9 meV (≈ 70 cm^{-1}). It thus seems that the detected electroactive, low-energy excitations are not related to a phonon, while their appearance at the magnetic transition points to an electromagnon.

Let us now investigate the low-energy spin dynamics. To avoid neutron absorption we used an 80 mg ^{160}Gd isotope-enriched single crystal. Magnon dispersion was measured along the H and L directions at 15 K. As can be seen from the colour maps in **figures 2a** and **b**, the magnetic spectral weight is at its maximum at the magnetic zone centre (1/200). It has an energy of 4.5 meV, which corresponds to the electroactive mode observed with IR spectroscopy (see **figure 1**). Unexpectedly, the minimum of the dispersion along L is not located at the magnetic zone centre (1.5 0 0) but is significantly shifted close to (1.5,0,0.4). This result is intriguing, as no elastic magnetic peak can be observed at this particular wave vector down to 5 K. To complete our magnetic study and put constraints on the spin dynamics simulations, the sub-meV dispersion was also measured along the L direction. As shown in **figure 2e** two modes arise, around 0.3 and 0.7 meV. To find evidence of any lattice contribution to the spectral weight at 4.5 meV, polarised INS was carried out at the magnetic zone centre. The result, shown in **figure 2h**, shows that the signal is purely magnetic, with no intensity observed in the non-spin-flip channel. The temperature-dependence of the energy of this mode, represented in **figure 2g**, is strikingly similar to the evolution of the IR mode (see **figures 1c** and **d**). The combined similitude in energy and temperature-dependence of the modes seen in IR and neutron scattering, leads us to conclude that it is one and the same mode.

To further understand the magnetic contribution of this electromagnon, linear spin-wave theory was employed to simulate the spin dynamics. The *Pbam* to *Pm* weak symmetry-breaking was ignored, as was the Gd anisotropy as our *ab initio* calculations had shown it to be negligible. The interactions between the rare earth and Mn atoms, as well as the Mn anisotropy terms were, however, necessary to describe the spin dynamics in the sub-meV range and the ferromagnetic arrangement along the *c*-axis. It is noticeable that the Mn^{3+}–Mn^{3+} interaction found from both the experimental fit and our *ab initio* calculations is very small, contrary to what is usually expected in the RMn_2O_5 family. The energy difference between the two low-energy modes is directly related to one of the *Gd–Mn* interactions. This could explain the different ordered moments measured for the two Gd sites in [5].

We should emphasise that this electromagnon electroactivity is not carried by any lattice mode or crystal field, as evidenced experimentally. This calls into question the very nature of this excitation. In the *Pm* space group, four different ferroelectric ground states are predicted in the magnetic phase, corresponding to the four sign combinations for the a and b components of the polarisation. In this picture, a change in magnetic structure modifies the electronic density. As a consequence, charge and spin degrees of freedom can no longer be treated independently. Thus the magnetic excitation described above as a spin wave actually dynamically modifies the orbital part of the wave function. This entanglement leads to a change in the polarisation amplitude visible *via* IR spectroscopy. This scenario is compatible with the IR polarisation selection rule, as both a and b electronic components exist in the actual *Pm* space group.

In conclusion, our complementary analysis of INS and IR results on $GdMn_2O_5$ highlights a relatively high-energy electromagnon bearing both magnetic and electroactive signatures. The magnetic contribution can be explained and modelled by standard linear spin-wave theory. However, the absence of any lattice or crystal field contribution on the one hand, and the unusual polarisation-dependence of the electroactivity on the other, call for new modelling. We therefore propose a purely electronic excitation, where orbital and spin degrees of freedom are no longer decoupled. This picture is strongly supported by the evidence, from soft X-ray resonant scattering at the oxygen K edge [6], to a coupling between the spin and orbital parts of the electronic wave function and a spin-polarisation of the oxygen atoms. It could certainly explain the exhaustive experimental results reported here. As such, this new framework could be relevant not only to the entire family of RMn_2O_5, but to many magneto-electric materials.

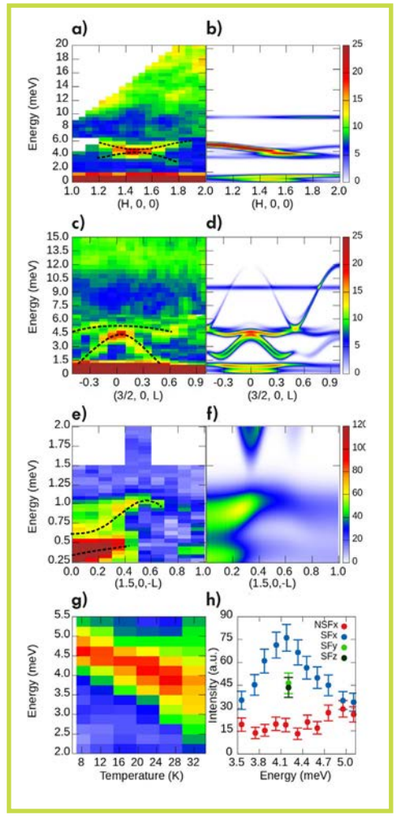

Figure 2

a), **c)** and **e)** Inelastic neutron scattering raw data recorded at 15 K along the (H,0,0), (3/2,0,L) directions. The measurements were performed on the 2T (E > 6.5 meV) and 4F2 (E < 6.5 meV) spectrometers for a) and c), and on IN12 for e).

b), **d)** and **f)** The numerical simulations associated with a), c) and e), respectively.

g) Evolution of the (3/2,0,L) energy scan as a function of temperature (to be compared with IR in figures 1c and d).

h) Inelastic polarised neutron scattering at Q = (3/2,0,0) and 15 K, performed on THALES. NSFx, SFx, SFy and SFz stand for non-spin-flip, and spin-flip with polarisation parallel to the *a*, *c* and *b* crystallographic axis, respectively.

MODERNISATION PROGRAMMES AND TECHNICAL DEVELOPMENTS

60 M€
ENDURANCE
8 YEARS (2016–2023)

D11 & D22 DETECTORS COMMISSIONED IN 2021

- MODERN MULTI-TUBE DETECTORS
- INCREASED AREA
- INCREASED EFFICIENCY
- HIGH COUNT-RATE
- EXTENDED DYNAMIC Q-RANGE
- MORE RAPID MEASUREMENTS
- REDUCED NUMBER OF INSTRUMENT CONFIGURATIONS

With the start of the long reactor shutdown on 13 October 2021, the execution phase of the H1–H2 long-shutdown projects—covering numerous instrument upgrades and the installation of two new advanced neutron guides—has begun. The following article highlights the achievements of the Endurance programme in 2021. In the meantime, we have now passed the 'point of maximum destruction' and work on installing the first new instruments and the renewed H24 guide is underway.

Several monochromators have been successfully assembled, including a double-focusing HOPG monochromator and an analyser for the upgrade of the IN20 thermal triple-axis spectrometer; an HOPG monochromator for the new XtremeD powder and single-crystal diffractometer; and a double-face Ge monochromator for the test instrument CT2. A new temperature gradient monochromator for the IN13 thermal backscattering neutron spectrometer is under construction and mosaic CaF_2 crystals have been produced. A new multilayer polarising analyser, consisting of a stack of 400 Fe/Si/Gd supermirrors coated on a sapphire substrate, represents a major upgrade for the D17 neutron reflectometer. The construction of the new ^{3}He filling station, known as 'Tyrex2', is on track and the station is currently being commissioned. Tyrex2 is due to deliver ^{3}He spin filter cells for ILL experiments using polarised neutrons during the first neutron cycle in 2023.

New position-sensitive detectors for XtremeD and D16 have been produced based on the novel trench-MWPC design. Preliminary results of the XtremeD detector with an AmBe source show excellent uniformity of response. The new detector on D16 is in the commissioning phase, while the project to equip D20 with a new detector based on this technology has been relaunched.

With continuing travel restrictions due to the pandemic in 2021, ILL's VISA software (Virtual Infrastructure for Scientific Analysis) proved to be a vital tool for ILL users. With its solutions for controlling instruments remotely via NOMAD, accessing instrument data and using ILL's data treatment software on a virtual machine, VISA—together with dedicated ILL staff on the instruments—was key to successful scientific operation during the three cycles in 2021. More information on VISA can be found in the article in this section by Jamie Hall.

Despite the complexity of the H1–H2 shutdown works, the tight schedule and interdependent sequencing—as well as the limitations imposed by the COVID pandemic, such as a reduced number of staff on-site—the H1–H2 project, including the rollout of Endurance instrumentation and infrastructure, is still on track. I am convinced that, thanks to the extraordinary team spirit at the ILL, we will master the challenges ahead and implement a full suite of new instruments by the end of 2022.

Andreas Meyer
Head of the Projects and Techniques Division

KEEP **UP-TO-DATE**:

facebook.com/ILLGrenoble
twitter.com/ILLGrenoble
linkedin.com/company/institut-laue-langevin

MODERNISATION PROGRAMME AND INSTRUMENT UPGRADES

Endurance: ‘On your marks, get set, go!’

AUTHORS
C. Dewhurst, B. Giroud and A. Meyer (ILL)

At the time of writing, January 2022, the ILL’s reactor building ILL5, main guide hall ILL7 and instrument suite are somewhere close to the point of ‘maximum destruction’! And there’s no going back. Don’t be alarmed, though. We’ve been waiting several years for this moment, which marks the way forward for the longevity of the ILL reactor and towards a fully modernised instrument suite under the **Endurance** programme. During the extended reactor outage between October 2021 and November 2022 we will replace the **H1–H2** beam tube and in-pile neutron guides that allow the extraction and transport of thermal and cold neutrons to instrumentation in the ILL7 guide hall. On the other side of the reactor wall, in the ILL7 guide hall, 10 of our user instruments have been disassembled and removed, making way for new and upgraded instrumentation on the renewed **H24** thermal- and **H15** cold-neutron guides.

3D model of instrumentation in ILL7 on the new **H24** and **H15** guides.

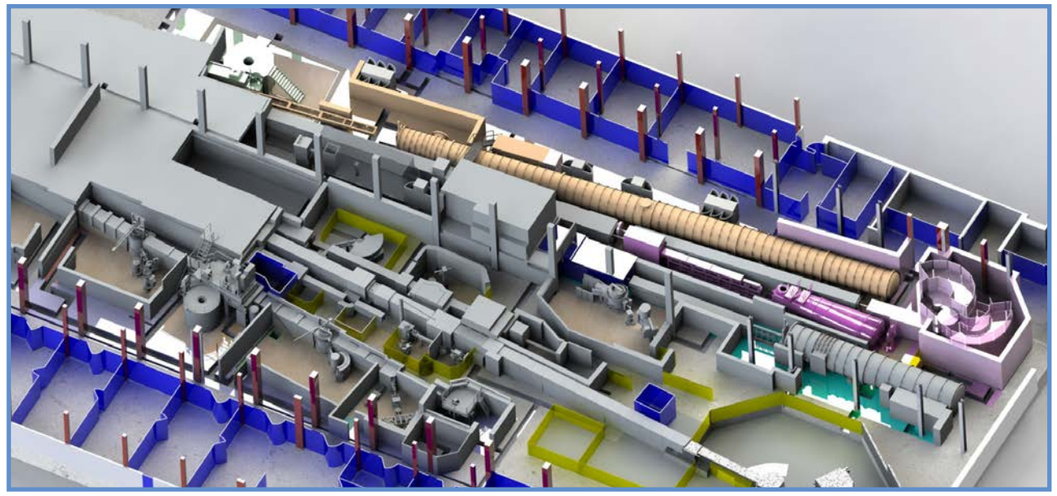

Endurance phases 1 & 2 encompass more than 30 new or upgraded instrument and infrastructure projects. Funded in phases, and with a financial envelope of nearly 60 M€, **Endurance** is being rolled out over eight years, between 2016 and 2023. It is a massive undertaking on the part of the ILL and the ILL’s Associates. Many new or upgraded instruments and infrastructure packages are already deployed and being used by users. The current **H1**–**H2** long reactor shutdown is now the ‘big push’ for **Endurance** to deliver a full suite of modernised instrumentation, which is critically dependent on the renewed in-pile beam extraction, **H1**–**H2** and the **H24** (thermal) and **H15** (cold) neutron guides. As the programme enters its final stages, it is useful to recap on some of our achievements. During 2021 we completed three more instrument upgrade projects: the **D3** Liquids project and the two new small-angle scattering detectors for **D22** and **D11**. Almost all our projects that are independent of the renewal of our **H24** and **H15** guide infrastructure have either been concluded or are in the final stages of construction and are described below.

Endurance 1 saw the completion of the installation and the commencement of user operation of the fission-fragment gamma ray spectrometer **FIPPS** (2016), establishing new capabilities for identifying prompt or short-lived fission products and entirely complementary to the existing Lohengrin mass spectrometer. In 2017, the **Rainbows** project was re-scoped and the **D17** reflectometer upgraded with a new focusing guide and chopper system to pursue an alternative high-flux mode of operation using the so-called ‘coherent summing’ method. The upgraded **IN5** (2019) cold time-of-flight

Dismounting of **IN3**, October 2021. (E. Villard, Ch. Mounier, P. Chevalier, F. Charpenay)

spectrometer and its new elliptically focusing **H16** neutron guide boasts huge gains in intensity, particularly at shorter wavelengths, while focusing on much smaller samples. Access to shorter wavelengths on **IN5** improves the overlap with the new thermal-neutron TOF spectrometer **PANTHER**, which entered the user programme early in 2021. A cascade of five background choppers is awaiting installation during the long shutdown to further improve the performance of **PANTHER**. The **D3** (2021) hot-neutron diffractometer is back in operation following its beam tube replacement and upgrade with a new position-sensitive area detector and polarisation components, allowing the efficient measurement of hydrogen-containing liquid samples through the precise discrimination of incoherent scattering. The new ultracold neutron (UCN) source **SuperSUN** remains in the commissioning phase following the successful construction and installation of the converter guide and the cool-down of the superfluid He converter volume. This long and complex project threw up a considerable number of technical and operational challenges along the way. However, when the reactor restarts, **SuperSUN** will begin to produce high densities of UCNs and allow science to begin on the PanEDM experiment. Upgrades to the **IN20** thermal triple-axis spectrometer (TAS) have begun with the receipt and installation of a velocity selector (2020) for wavelength filtering that will allow much greater flexibility in how the instrument is used and what energies are accessible; while a new Heusler monochromator is currently being manufactured to complement the new graphite monochromator and analysers, all of which will be available in 2023. Throughout the duration of **Endurance**, the service infrastructure projects **NESSE** and **BASTILLE** have continually delivered new and improved sample environment capabilities and modern data reduction and analysis software tools *via* the Mantid project.

Endurance 2: In a first round of funding for **Endurance 2** we were able to rapidly construct detectors for the SANS instruments **D22** and **D11**: **D22** received an additional high-angle detector, massively extending the instrument’s dynamic q-range and enabling more rapid measurements with fewer instrument configurations; while the new detector on **D11** replaces the ageing multi-detector with a modern, increased area, high efficiency and high count-rate detector. Both detectors were installed and commissioned during the winter shutdown of 2020–2021 and have been available to users since the first cycle of 2021. Noticeable gains in the speed at which experiments can be performed and the quality of data generated on the two instruments have been observed. During 2020 we were able to modify the **H141** guide and install a second protein crystallography instrument, **DALI**, in the previous IN11 position. **DALI** not only complements the existing LADI instrument but effectively doubles the capacity and throughput of protein crystallography measurements with an increased neutron flux and greater flexibility, thanks to the use of a velocity selector. **DALI** was commissioned with neutrons in autumn 2020 and welcomed its first users at the beginning of 2021. The **D16** cold-neutron diffractometer is undergoing renewal of its secondary spectrometer. This will include a new wide-angle detector bank with approximately four times the angular coverage of the previous detector, the addition of a low-background flight chamber between sample and detector, and various other upgrades. Work on **D16** is making good progress and will be completed before the reactor starts up again at the end of 2022. Finally, on the neutron imaging instrument **NeXT** we have begun a full re-build of the instrument’s backbone, which will allow for state-of-the-art imaging with advanced contrast techniques, high spatial resolution, intense neutron flux and combined X-ray imaging. **NeXT** will be available again to users in 2023.

MODERNISATION PROGRAMME AND INSTRUMENT UPGRADES

H24

The 'Big-Push': As well as witnessing a vast amount of maintenance and upgrade work to ensure the safety and longevity of the ILL reactor, the current **H1**–**H2** shutdown (October 2021 to November 2022) will see the installation of the new **H24** (thermal-) and **H15** (cold-) neutron guides and that of a large number of new and upgraded thermal- and cold-neutron instruments. The ILL7 guide hall is in the throes of a significant re-modelling of its instrumentation and infrastructure that also entails the creation of new instrument cabins providing comfortable workspaces for users.

The **H24** project will bring dedicated thermal neutron guides to the upgraded **D10**, **IN13** and the new **XtremeD** (CRG) powder and single-crystal diffractometer as well as providing neutrons to the test instrument **CT2** and **Cyclops**. As of January 2022, this work is progressing well and to schedule. The old **H24** guide and the instrumentation suite consisting of **IN3**, **IN13**, **D10**, **CT2**, **Cyclops** and **Orient Express** have been removed. Civil engineering works are now underway to prepare the new instrument zones and the foundations for the new **H24** guide(s). The indispensable sample alignment instrument **Orient Express** has been moved to the **H23** neutron guide, giving users uninterrupted access to sample alignment while work on **H24** goes on and freeing up an end-of-guide position for future instrumentation. The old **H24** guide was the original neutron guide installed in 1972 with the first suite of ILL instrumentation. Although advanced for its time, it was nevertheless a straightforward, nickel-coated (m = 1), single guide, and instrument performance was compromised by having the various instrument monochromators in series. The new **H24** guide has much higher critical-angle coating (m = 3). It also uses the rather elegant concept of a common-curved trumpet to exploit the two radii of curvature of the **H241** (R = 14 000 m) and **H242** (R = 8 000 m) sub-branches downstream to naturally divide and expand the guide over a distance of 22 m. **XtremeD** and **Cyclops** will have dedicated end-of-guide access to the lower and upper parts of the **H241** branch, while the upgraded **D10** and **IN13** will have dedicated end-of-guide access to the lower and upper parts of the **H242** branch. For the **H24** guide and instrument projects, essentially all the procurement, manufacturing and pre-assembly was completed before the long shutdown to enable the most seamless installation possible during 2022.


1.


2.


3.


4.

1. Dismounting of **IN13** (J. Rimez, C. Gomez, J. Laurent, L. Coustols, C. Clavel)
2. Dismounting **IN3**. (P. Chevalier, E. Villard)
3. Taking apart the **H24** instrument cabins. (V. Pichat, J. Blanc, A. Buriller)
4. B. Ouladdiaf recovering the **Cyclops** cameras.


5.


6.


7.


8.


9.

5/6. A. De Francesco, F. Natali & Ch. Mounier dismounting and sorting **IN13** for storage.
7. Clearing the **D10** instrument zone and the old **H24** guide. (S. Vial & P. Decarpentrie)
8. **H24** guide and instrument(s) zone during dismounting.
9. R. Gandelli setting up for the alignment of neutron guides.
10. New **D10+** will go here in the old **IN3** zone.


10.


11.


12.


13.


14.

11. Ground preparations for the new **H24** instruments.
12. Guide pass-thoughs from the reactor building to ILL7. (Ch. Monon)
13. Installation of the new twin neutrons guides of **H24**. (P. Lachaume, Ch. Monon)
14. Preparation of the new **D10+** zone.

MODERNISATION PROGRAMME AND INSTRUMENT UPGRADES

H15

The **H15** guide has a rather complex, opposing-curve, expanding section referred to as 'the trumpet' that serves two important purposes. The first is to spatially expand the neutron guide, thus converting the up-stream high divergence to lower divergence but extended over a greater area. This allows the guide to be split into multiple individual guide branches allowing dedicated end-of-guide beam positions for instrumentation. The second is that the opposing curve leaves a 'fingerprint' correlation between the divergence profile and the spatial position at the end of the trumpet. In other words, neutrons on the left of the guide have an average divergence distribution to the left, while neutrons on the right side of the guide have an average divergence distribution to the right. Importantly, this allows guide branches to be more widely separated in angle, thereby allowing space for substantially more instrumentation downstream. All the guide optics for **H15** have been ordered, while the instrument projects are at the end of their detailed design phase and are ready for tendering and manufacturing though 2022 for installation in 2023. **H15** will accommodate a substantially upgraded **D(00)7** instrument boasting more than x10 in neutron flux, making polarisation-analysis spectroscopic measurements a reality as well as achieving massive gains for the more usual diffuse scattering measurements. **D11** should receive an increase in neutron flux on the new **H15** guide and will be rebuilt and relocated with an optically cleaner collimation. The **T3** instrument used for characterising polarising supermirrors produced at the ILL will be rebuilt and upgraded. Two additional end-of-guide positions are available for new instrumentation: the **SHARP+** (CRG) cold TOF spectrometer, with an expected neutron flux more than x10 its predecessor **SHARP**/**IN6**; and a fourth short SANS instrument, **SAM** (CRG), with a MIEZE option.

As you can see from the photo montage presented here, the work has most definitely begun. We are on track to deliver an exciting new and upgraded instrument suite. The future looks intense!


1.


2.

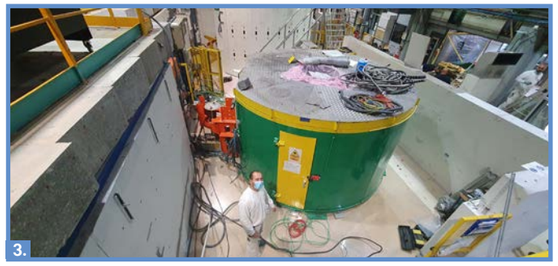
3.


4.


5.


6.


7.


8.


9.


10.


11.

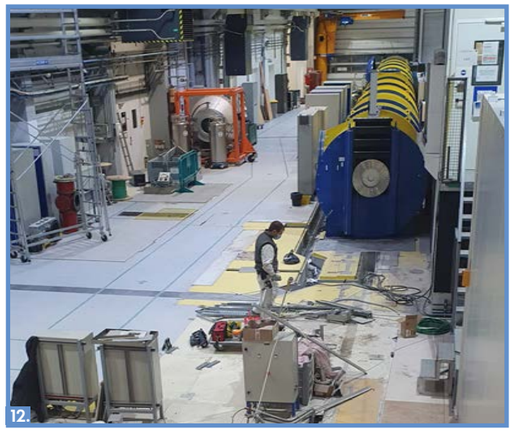
12.

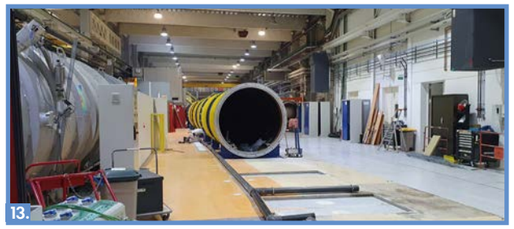
13.

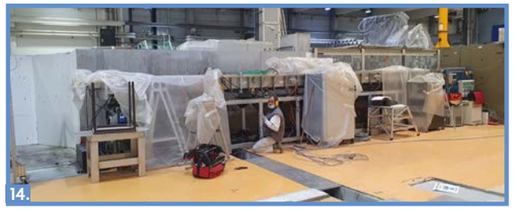
14.


15.

7. N. Roca de-cabling in the **D11** and **D33** zones.
8. Dismounting the common **H14** and **H15** casemat in ILL7.
9. The old **H15** guide removed leaving **H14**.
10. Breaking the concrete guide supports for the old **H15** guide.
11. Ground works in preparation for the multi-branch **H15** guide.
12. Just the **D11** detector tank to move now.
13. Taking apart the **D11** detector tank.
14. M. Vuillet partially de-cabling **D33** ready for …
15. …Preparation of the **D11**, **Sharp+** and **SAM** instrument zones. Please be careful so close to **D33**. (P. Cogo, P. Lacombe, K. Salem)

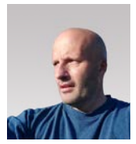

Jean-Marc Zanotti. French Laboratoire Léon Brillouin (LLB, CEA-CNRS), Saclay, France

'As an LLB scientist, my activity is twofold: instrument scientist on IN6-SHARP, and physicist developing personal scientific activity. My personal research focuses on the effects of interfacial and nanometric confinement on the dynamics of soft matter.'

AUTHORS

SHARP team:
S. Rodrigues, **P. Lavie**, **B. Homatter**, **P. Permingeat**, **F. Legendre**, **T. Robillard** and **J.M. Zanotti** (LLB)
Q. Berrod (CNRS, IRIG/SyMMES, Grenoble, France)
SHARP+ team:
G. Manzin, **S. Roux**, **G. Pastrello** and **M. Koza** (ILL)
J.M. Zanotti (LLB)

REFERENCE

[1] More details at https://www-llb.cea.fr/Phocea/Vie_des_labos/Ast/ast_visu.php?id_ast=2766

From IN6 to SHARP, and then SHARP+

Time-of-flight spectrometer SHARP

Within the framework of the construction of the European Spallation Source in Lund (ESS, Sweden), an agreement was reached to strengthen Franco–Swedish co-operation in the field of neutron scattering. The *Laboratoire Léon Brillouin* (LLB) subsequently became involved in the construction of an inelastic time-of-flight (ToF) spectrometer. When it was announced that the LLB's Orphée reactor would shut down in 2019, the construction project (originally planned for Saclay) was transferred to the ILL. Its resurrection took the form of a CRG-A contract, finalised in September 2017 between the *Direction de la Recherche Fondamentale* of the CEA, the *Institut National de Physique Nucléaire* of the CNRS and the ILL.

The SHARP project (Spectromètre Hybride Alpes Région Parisienne) [1] involved a complete rebuild of the IN6 secondary spectrometer. The construction process started at the end of the last 2020 cycle, in October, and ended on 21 March 2021 when neutrons first reached the brand-new instrument (**figure 1**). Thus, construction was completed in the remarkably short period of five months.

A key part of the work was the covering of the entire chamber with cadmium and the installation of 240 position-sensitive detectors (PSD) along with their collimators. The ILL technical teams worked with LLB personnel on the cabling, testing and integration of the detector electronics within the data-acquisition system, and a highly efficient pumping system was designed and installed by the ILL Vacuum Group. Coupled to the differential vacuum stage designed for the 25 m^3 ToF chamber, a primary vacuum can now be produced in 15 minutes and a pressure of 10^{-3} mbar maintained.

In addition to the factor four gain in solid-angle detection, these new detectors provide a spectacular gain in the definition and mapping of the (Q, ω) domains, thanks to the 240 PSDs under five bars of ^{3}He. This is critical, for example, in the study of single-crystal excitations in solid-state physics.

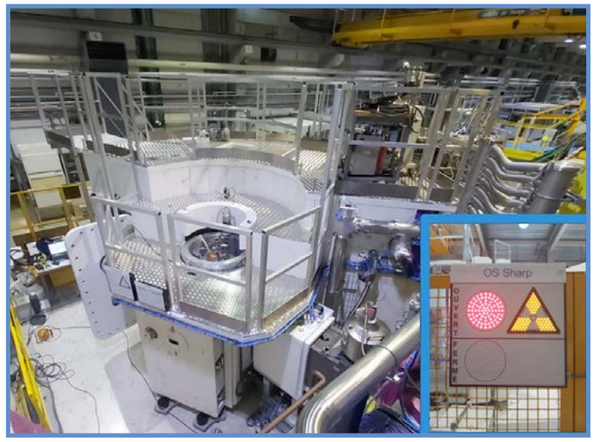

Figure 1
SHARP up and running with its first neutrons: 21 March, 2021.

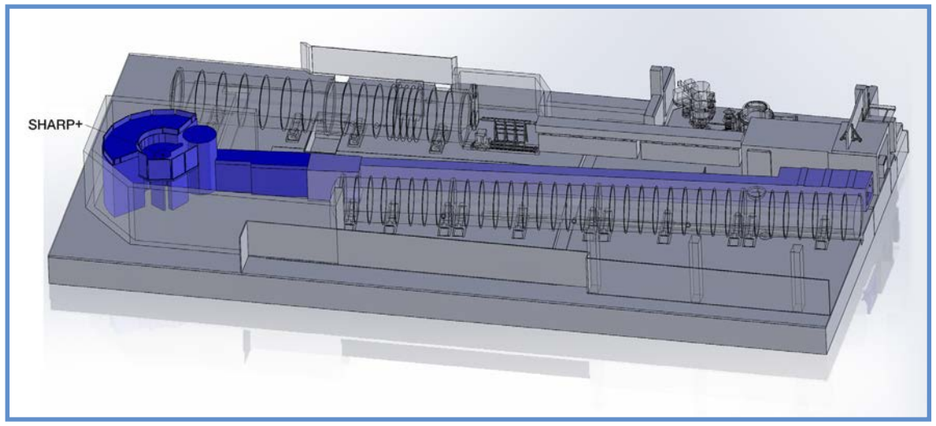

Figure 2
SHARP+, in blue, at the end of the new H15 guide, between D11 and D33.

In mid-2023, once the H15 guide has been rebuilt and extended, the *SHARP* secondary spectrometer will be transferred to the end of the guide hall between D11 and D33 (**figure 2**). The instrument will then become *SHARP+*.

SHARP+ will take advantage of this guide-end position with no direct sight and a 0.6 Å wavelength cut-off. The instrument will be equipped with a 20 * 30 cm^2, two-faced, horizontal and vertical focusing monochromator. Pyrolytic graphite will be used on one side, for incident wavelengths ranging from 2 to 6.2 Å. On the other side, fluorinated mica is being envisaged (currently under study) for wavelengths from 7 to 12 Å.

SHARP+ will combine two focusing modes: a time focusing (TF) mode, as on IN6, and an additional, so-called monochromatic focusing (MF) mode. The switch from MF to TF will be possible by retracting a 4.5-metre-long section at the end of the converging guide (turn-key system, *i.e.* no manpower required).

TF will primarily benefit quasi-elastic studies, in both soft matter and solid-state physics, where good resolution (few tens of μeV) is needed on a narrow energy-transfer range, in particular on the neutron energy-loss side. The MF mode is optimised for studies requiring the same kind of resolution but on a wide range of energy transfer on the neutron energy-gain side (this is critical for materials science).

Both modes will be enhanced by the three disk-choppers, used as anti-overlap and anti-harmonics filters, and a brand-new Fermi chopper (FC) with a maximum speed of 400 Hz. This will make it possible in the TF mode to perform inelastic TF (*i.e.* to minimise resolution on a narrow range of energy transfer) up to $\hbar\omega$ = 10 meV. In MF mode at long wavelengths, the full FC speed will be used to minimise resolution down to 25 μeV. Finally, compared with IN6, *SHARP+* will offer a factor 15 gain in counting rate with significantly reduced background.

The *SHARP* spectrometer offers significant potential while we await the delivery of *SHARP+* in April 2024. By this time, this very competitive, state-of-the-art instrument will be operating as a French CRG-A and will integrate nicely into the ILL's ToF instruments suite. It will be an asset for both the French and European neutron scattering communities in their endeavours to tackle the latest scientific and societal challenges.

Alexei Vorobiev. Russian and French
Uppsala University, Sweden
'I am responsible for the Swedish CRG reflectometer Super ADAM @ ILL. My main professional interest lies in surface science, related methods and instrumentation'.

Grazing-incidence small-angle neutron scattering (GISANS) studies using fan-shaped beams

SuperADAM reflectometer

Fan-shaped incident neutron beams allow significantly reduced counting times for measuring in-plane correlations. An increase in intensity of two orders of magnitude can be achieved on the SuperADAM reflectometer using this method. We extracted structure- and form-factors for monolayers of silica particles on silicon surfaces and iron inclusions in an aluminium oxide matrix. Here we describe the first successful grazing-incidence small-angle neutron scattering measurement (GISANS) on a liquid surface.

AUTHORS

A. Vorobiev and **M. Wolff** (Uppsala University, Sweden)
N. Paracini and **M. Cárdenas** (Malmö University, Sweden)

ARTICLE FROM

Sci. Rep. (2021)—doi:10.1038/s41598-021-97112-x

REFERENCES

[1] R.F. Egerton (ed.), Physical Principles of Electron Microscopy (2016) Springer, New York
[2] S. Hüfner (ed.), Photoelectron Spectroscopy (2003) Springer, New York
[3] P. Müller-Buschbaum, Polym. J. 45 (2013) 34

An understanding of the interfacial properties of materials, as well as that of interfacial processes in terms of structural, morphological and compositional changes, is of crucial importance in many scientific fields, including chemistry, physics, biology and engineering. Surface science has advanced enormously over the last decades, thanks to the development of a series of new, and already existing, experimental methods. Recent advances in atomic force and electron microscopy [1] and in photoelectron spectroscopy at modern synchrotron X-ray sources [2], for example, have opened up hitherto unknown territory.

Compared with electrons and photons, neutrons are more sensitive to light elements; they can penetrate deep into matter, and they provide a direct measure of magnetic induction in materials. Moreover, sensitivity to the nucleus enables contrast variation experiments by isotope substitution (hydrogen *versus* deuterium), a key element in soft matter research. The drawback of neutron scattering methods, however, is that the brilliance of neutron sources is limited. This is particularly relevant for small sample volumes or surface scattering studies.

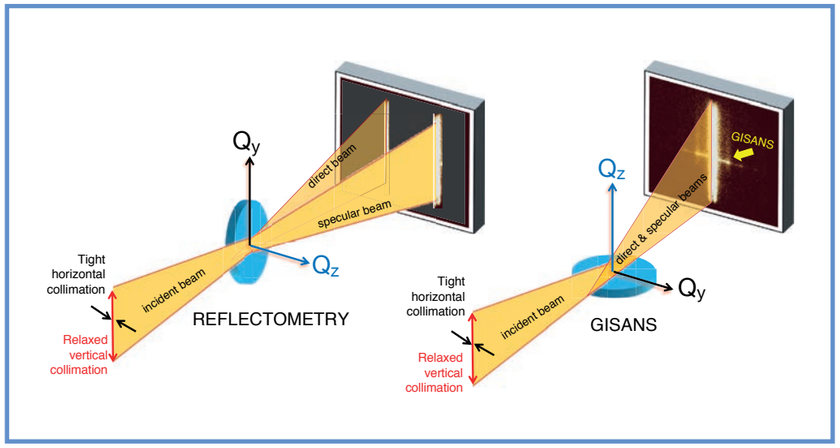

Figure 1

Sketch of the scattering geometry for neutron reflectometry (**left**) and one-dimensional GISANS (**right**). The sample and Q_y and Q_z axes are turned 90 ° for these two configurations.

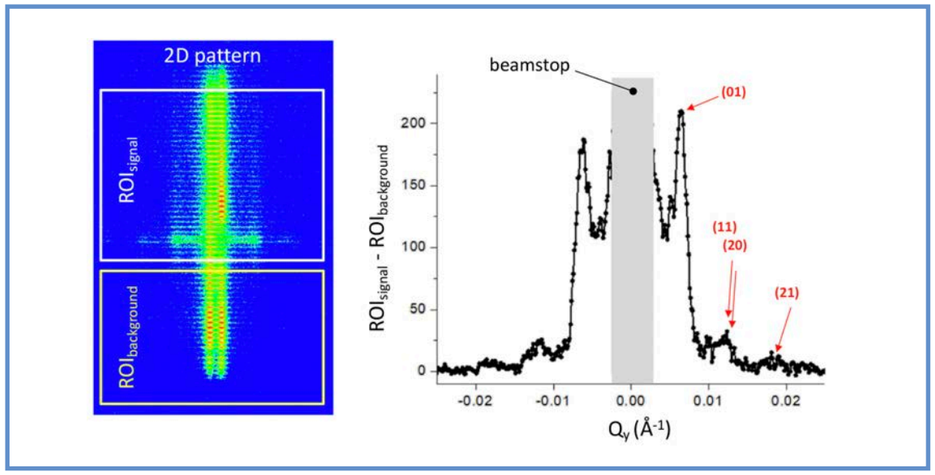

Figure 2

GISANS data recorded on SuperADAM for 100 nm silica particles, self-organised on a D_2O surface. **Left)** Raw detector image with the regions of interest for the signal (reflected) and background (transmitted) indicated. **Right)** GISANS signal (vertically integrated) minus background, plotted against Q_y on a linear scale.

To increase the incident neutron flux, different focusing elements can be used. On the SuperADAM reflectometer, the monochromator consists of seven highly ordered pyrolytic graphite (HOPG) crystals focusing the beam in the vertical plane. For standard reflectivity measurements the neutron beam is reflected off a vertically mounted sample surface, allowing us to extract neutrons from the full height of the H53 guide. However, this is at the expense of a relaxed vertical resolution. Along the horizontal direction, high collimation allows excellent Q_z resolution and neutron reflectivity (NR) measurements (**figure 1**, left panel).

Recently, we have shown that the same instrument configuration may be used for GISANS studies of the lateral structure of surfaces and interfaces [3]. To switch from NR to GISANS, we change the sample geometry from vertical, as used for NR, to horizontal (**figure 1**). In this configuration, the in-plane resolution is high whilst sacrificing resolution along the normal surface. Consequently, we are able to collect high-quality, one-dimensional GISANS data across the Q_y direction much faster, but we gain only very limited information about the depth profile across an interface. For the study of single thin films and interfaces this drawback is often acceptable; it can be overcome by complementing the GISANS data with reflectometry measurements in the vertical geometry.

In addition, by switching the sample geometry on SuperADAM to horizontal we are also able to perform GISANS studies on liquid surfaces! **Figure 2** shows data taken with silica particles of size 100 nm, self-assembled on a D_2O surface. Measurements were performed using a water basin consisting of a silica frame glued onto a silicon block and mounted on an active anti-vibration device. The volume of nanoparticles was calculated such that the total projected area of the spheres was equal to that of the water surface, to form a densely packed layer. After integration along Q_z and subtraction of the background, several Bragg reflections were resolved and could be indexed by assuming a hexagonal, densely packed monolayer of 100 nm silica particles.

The scattering geometry used in our experiment can be applied to other instruments, allowing one-dimensional GISANS data to be captured about 100 times faster. GISANS could thus become a standard method in neutron scattering as well as enabling the performance of kinetic studies.

Adrien Perrichon. French
ISIS Neutron and Muon Source, UK

'I work as an instrument scientist at the ISIS Facility on the development of instrumentation and methods for neutron spectroscopy (INS, QENS) and other techniques. My research focuses on energy materials and non-stoichiometric oxides.'

Resonant enhancement of grazing-incidence neutron scattering for the characterisation of thin films

SuperADAM reflectometer

We have demonstrated proof of concept of signal enhancement for the characterisation of thin films using neutron reflectometry, based on resonant enhancement in a quantum resonator. Combined with consistent data analysis of the attenuation cross section, we quantify off-specular and small-angle scattering. Our method has the potential to both speed up parametric experiments and facilitate grazing-incidence small-angle neutron scattering experiments.

AUTHORS

A. Perrichon (ISIS and Uppsala University (UU), Sweden)
A. Devishvili and **A. Vorobiev** (ILL and UU)
K. Komander, **G.K. Pálsson** and **M. Wolff** (UU)
R. Lavén and **M. Karlsson** (Chalmers, Sweden)

ARTICLE FROM

Phys. Rev. B (2021)—doi:10.1103/PhysRevB.103.235423

REFERENCES

[1] M. Wolff *et al.*, Phys. Rev. Lett. 123 (2019) 016101
[2] H. Schober, Hydrogen Metal Systems 49 (1996) 357
[3] V.F. Sears, Physica B+C 151 (1988) 156
[4] A. Miksovsky, Phys. Stat. Sol. (a) 130 (1992) 365

A quantum resonator can be formed by intercalating a layer of low scattering length density (SLD) between two thin layers with high SLD. Here we use a vanadium hydride layer intercalated between two Fe layers (**figure 1**) [1]. Similar resonators may be formed, for instance from a lipid membrane confined between a sapphire substrate and heavy water.

While incident neutrons with grazing angle α_i are totally externally reflected below a critical value, the presence of quantum resonances (marked m = 1–3 in **figure 1**) may create 'dips' in the total reflection region (**figure 2c**). The positions of the dips or resonances depend on the SLD and the thickness of the resonator layer. The 'missing intensities' from the specular line are connected to the attenuation (incoherent scattering and absorption) and, if present, off-specular and small-angle scattering of the evanescent wave field.

Figure 1

Scheme of the vanadium hydride resonator thin film and the first three resonances.

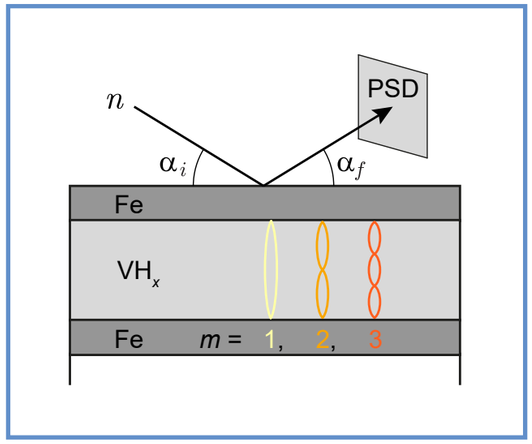

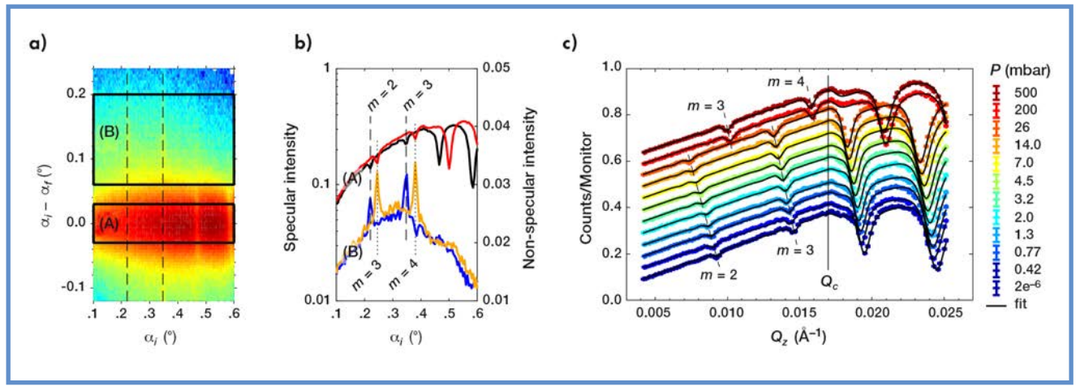

Figure 2

a) Colour map of the spin-up intensity measured on the PSD. The regions of integration of interest are marked by black rectangles: (A) specular, (B) non-specular.

b) Integrated spin-up intensities: black/blue lines specular/non-specular for lowest-pressure data; red/orange lines specular/non-specular for high-pressure data. The positions and order of the resonances are indicated.

c) Specular spin-up intensity as a function of hydrogen gas pressure. Data are vertically offset for clarity.

This effect is prominent for the (mainly) incoherent scatterer VH_x. At the resonances' positions we observe a dip in specular reflectivity and a peak in non-specular intensity (**figure 2b**), indicating the resonant enhancement of incoherent scattering from V and H. The sample is kept in a gas-loading system, and by varying the hydrogen gas pressure in the sample chamber the hydrogen concentration in the VH_x layer changes. This results in changes in SLDs and the thickness of the layer, and thus in a shift in the positions of the resonances, as shown in **figure 2c**. It turns out that we can track the changes in the thickness and the SLDs of the VH_x layer by monitoring only the resonances in the region of total external reflection. This is very efficient, as it effectively involves direct beam measurement rather than requiring full reflectivity profiles to be taken at each pressure. The parameters obtained from the fit of the total external reflection region only and from the fit of the fringe region are identical in the statistics; this demonstrates proof of concept. The pressure–concentration isotherm and expansion co-efficients of the VH_x layer derived from this method are in good agreement with the literature [2].

Our approach also offers opportunities for exploiting the information from the attenuation cross section, which is often ignored. The excellent statistics of the dips in the total external reflection region allow the attenuation cross sections to be extracted reliably. The attenuation cross section generally depends on the incoherent and absorption cross sections [3], which are tabulated.

We show that consistent results are obtained from analysis of the SLD and from the attenuation cross section. Moreover, analysis of the attenuation cross section allows any scattering that may not be captured by the detector, or is too smeared to be identified, to be detected and quantified. This scattering is quantified by the remaining apparent absorption cross section after taking into account the known contributions of incoherent and absorption effects. For instance, for VH_x we distinguish concentration-dependent low-Q scattering (small-angle scattering from hydride precipitates [4]) from other concentration-independent contributions.

The combination of resonant enhancement with analysis of the attenuation cross section is a very powerful tool, speeding up parametric measurements, increasing the consistency of data analysis and enriching the output of the experiment. The approach is widely applicable, as resonators can be constructed for many different systems.

Nebil A. Katcho. Spanish
ILL

'Before joining the ILL, my research focused on the properties of condensed matter using atomistic simulation techniques. Since 2018 I have been a member of the ILL's Diffraction Group, developing crystallography and data-analysis software for single-crystal neutron diffraction. In 2020 I was appointed instrument scientist for D9.'

Int3D: data reduction software for single-crystal neutron diffraction

D9 and D19

The neutron community has not seen the development of robust and easily adaptable software for performing data reduction in single-crystal diffraction experiments on the various instruments worldwide. The Int3D package should help close that gap. It relies on a graphical user interface providing tools to visualise, interact with and process data in a way that makes data reduction accessible to a wide range of users.

AUTHORS

N.A. Katcho, L. Cañadillas-Delgado, O. Fabelo, M.T. Fernández-Díaz and J Rodríguez (ILL)

ARTICLE FROM

Crystals 11 (2021) 897—doi:10.3390/cryst11080897

REFERENCES

[1] M.S. Lehmann and F.K. Larsen, Acta Cryst. A 30 (1974) 580
[2] C. Wilkinson, H.W. Khamis, R.F.D. Stansfield and G.J. McIntyre, J. Appl. Cryst. 21 (1988) 471

The conclusions drawn from single-crystal diffraction experiments ultimately depend on the accuracy of the integrated intensities of the diffracted beams. These intensities are obtained from the detector records by a process called data reduction. In contrast to commercial X-rays, the neutron community has not produced software that provides user-friendly access to data reduction. The ILL's in-house software was developed a long time ago; it requires considerable expertise and does not always handle complex problems easily.

The ILL Diffraction Group therefore decided to develop data reduction software for single-crystal diffractometers with area detectors. Int3D relies on a powerful graphical environment that allows easy validation of the various steps in the data reduction process, making it accessible to a wide range of users. The most delicate step, the integration of Bragg reflections, follows the extension to three dimensions of the Lehmann and Larsen integration method [1, 2].

The graphical tools built into Int3D can display data in either direct (2D detector + scan angle) or reciprocal space. Integration is performed in direct space; it assumes that the shape of the reflections can be modelled by ellipsoids. **Figure 1** shows the results of such an integration. The user can readily check whether the integration boxes are large enough, whether neighbouring reflections are well masked and whether the ellipsoids are well centred and enclose the intensity of the reflections.

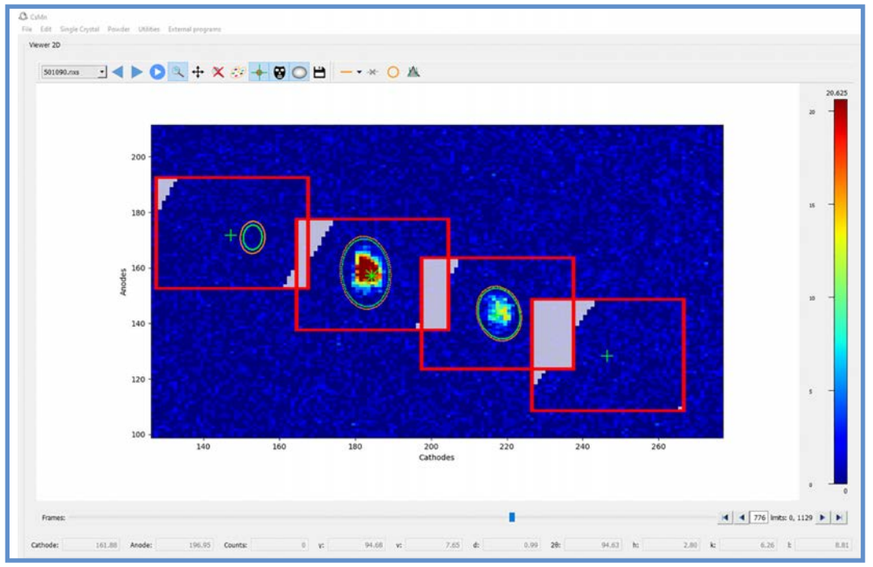

Figure 1

Integration of collected data at D19. The position of the Bragg peaks predicted by the orientation matrix is represented by plus symbols. The green ellipsoids represent the volume used to integrate the intensity of the Bragg peaks, the orange ones are used to compute the background. Grey pixels correspond to the masking of neighbouring reflections. Red lines represent the integration boxes around each Bragg peak.

In reciprocal space, the user can display either the raw data or just the centres of the Bragg peaks, as well as the reciprocal lattice. The peaks can be classified in different sets by selecting them graphically; this is particularly helpful when orienting complex crystals as twins or incommensurate structures. **Figure 2** shows the raw data, the set of nuclear Bragg peaks and the reciprocal lattice for a $TbMnO_3$ crystal. The raw data exhibit a very strong magnetic scattering, with two incommensurate propagation vectors due to Tb and Mn magnetic ordering. The high degree of peak overlapping prevents the integration of Bragg peaks using the direct space approach based on ellipsoids. Int3D's reciprocal space tools allow intensity profiles to be created along a given direction of reciprocal space, as illustrated in the **figure 2 inset**. The profiles thus obtained can be integrated in a similar way to that of powder data, where overlapping is not a limitation. This allows problems to be tackled that are usually considered intractable.

Int3D is packaged with all the required libraries and executables so that the user can run the application without needing to install a Python interpreter or other external module. It is currently used on the D19 and D9 diffractometers. It could easily be extended to D10 and the ILL's new instrument XtremeD. Its extension to other instruments, such as Wombat (ANSTO, Australia) and Zebra (PSI, Switzerland), is underway.

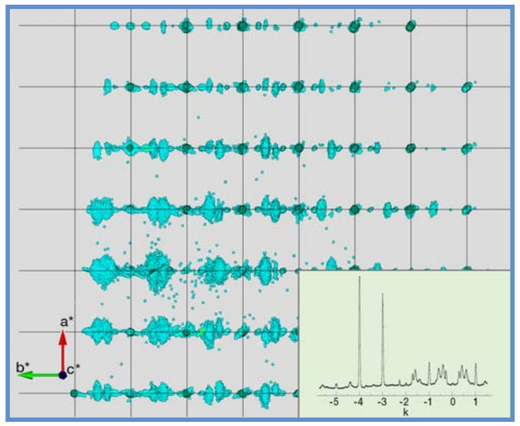

Figure 2

$TbMnO_3$ data collected at D19, displayed in the reciprocal space. Raw data is represented in blue, clearly showing incommensurate magnetic scattering along b*. The green spheres represent the centres of the nuclear Bragg peaks. Black lines correspond to the reciprocal lattice. The inset shows the intensity profile obtained by projecting the data along the *b**-axis for h = 2, l = 3.

Jamie Hall, British
ILL
'I am a senior full-stack developer working in the ILL's IT Services. I develop tools and services to support the scientific activities at the organisation.'

AUTHORS
J. Hall (ILL)

VISA – data analysis in the cloud

With the introduction of VISA (Virtual Infrastructure for Scientific Analysis) in June 2020, there has been a significant change in how scientists analyse experimental data and perform experiments at the ILL. Since the beginning of the COVID-19 pandemic VISA has played an essential role in the success of the ILL's user programme, allowing researchers to perform remote experiments and data analysis despite travel restrictions and national lockdowns.

Before performing data analysis, scientists spend a considerable amount of time configuring their analysis environment. The process of identifying, downloading and installing the relevant analysis software, obtaining access to the experimental data and pursuing the multiple email exchanges between researchers and local contacts can be time-consuming.

Thanks to VISA, researchers can now create and configure their own virtual machine and enter a secure, high-performance data-analysis environment in a couple of minutes with a simple web browser. There, they have all the scientific software they need and direct access to experimental data. The VISA team ensures that the analysis environment is constantly upgraded with the latest software and tools and regularly adds new features to the platform.

But VISA does far more: it also provides an ideal platform for remote experimentation. It is accessible from anywhere in the world with an internet connection, and scientists are therefore free to pilot an experiment remotely, using the instrument control software from any location and any computer.

Last but not least, because data analysis is often performed as a team, VISA has been designed with real-time collaboration at its core. The platform makes it easy to share analysis environments between proposal team members, ILL scientists and computing experts. In this way, it can also be used for training new users.

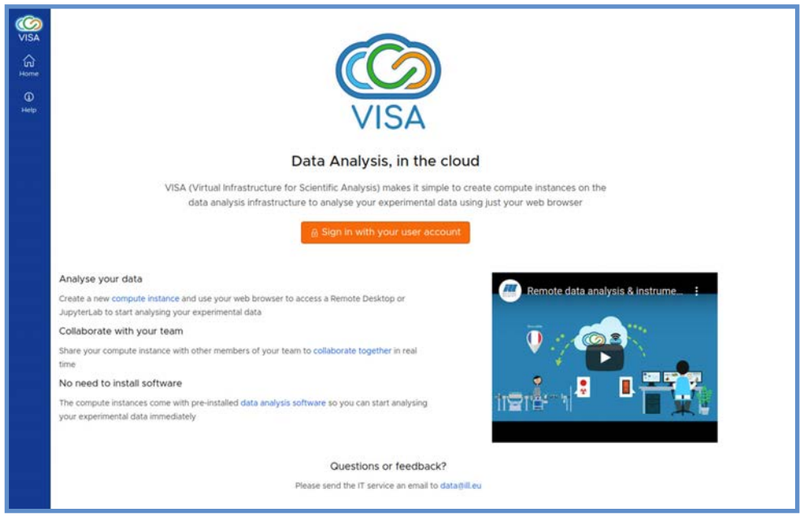

Figure 1
The VISA homepage.

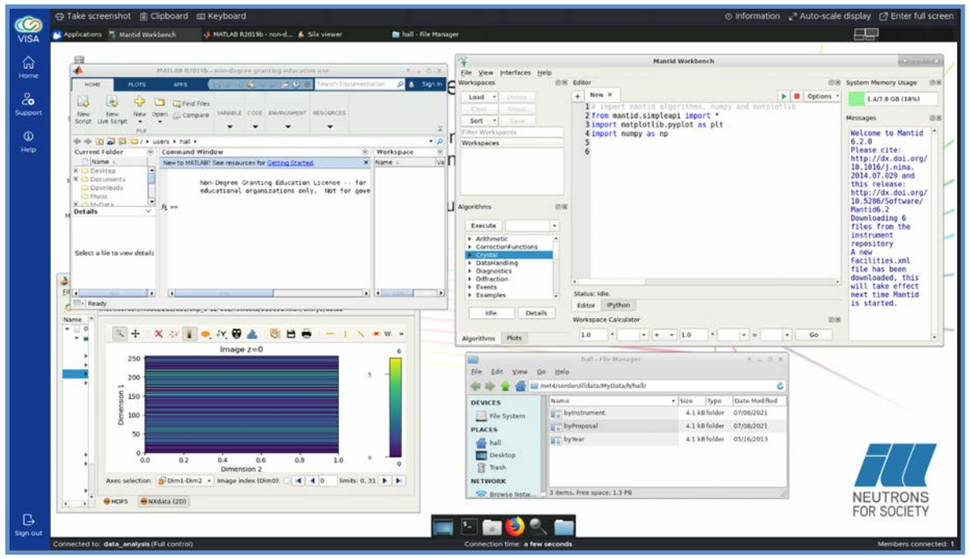

Figure 2
Data analysis software running inside a VISA analysis environment.

How does it work?

Users log into the platform (*visa.ill.fr*) using a web browser and their ILL User Club account. Once logged in, they create a new virtual machine on the ILL's cloud infrastructure that comes pre-configured with a fine-tuned Ubuntu data-analysis environment—it is as if the user was sitting directly in front of a data-analysis workstation at the ILL. VISA takes care of the creation and lifecycle of the virtual machines, and resources are allocated depending on the type of experiment. Fission experiments, for example, which produce a huge amount of data, require access to a machine with sufficient memory to produce multi-dimensional histograms.

The virtual machine has direct access to experimental data stored by the ILL, analysis procedures and scientific software (*i.e.* MANTID, MatLab, FullProf, LAMP, *etc.*). Users can use Nomad Remote (the software used to control ILL instruments) to pilot their experiment remotely. There is also the option of accessing a full Remote Desktop or launching a JupyterLab notebook environment for performing data analysis, alone or with the support of the ILL experts. Jupyter is an interactive, web-based, online Python environment that allows for reproducible data analysis and the sharing of analysis routines. ILL users can set up two simultaneous data-analysis environments at any time on the platform and start collaborating in real time with their colleagues. In the near future we will be opening up the platform to allow any user to use VISA to analyse open data.

A fruitful collaboration

VISA was developed as part of the PaNOSC (Photon and Neutron Open Science Cloud) project financed by the European Commission. All six of the large-scale photon and neutron facilities involved in this project (ILL, ESRF, ESS, ELI, XFEL, CERIC-ERIC) are in the process of deploying the platform at their facilities. The VISA team is currently providing support and assistance to get VISA ready for production at their facilities.

A flagship product for remote experiments

The benefits of VISA have been widely acknowledged since its creation, and the product is seen as a flagship tool for performing remote data analysis. The platform has also been very well received by our users, with more than 1,000 scientists using it. All the feedback we receive is very positive and is helping us to continuously improve the tool.

VISA played an essential role in the success of the ILL's 2020 user programme, allowing researchers to perform remote experiments and data analysis despite pandemic-induced travel restrictions and national lockdowns. But VISA is not limited to photon and neutron facilities: it can also be used in other research domains. To contribute to a larger, worldwide scientific community, all the VISA source code has been open-sourced and the ILL is currently working to help other interested institutes deploy the platform.

If your facility is interested in VISA and would like more information, please get in touch with the VISA Team, at **visa@ill.fr**

INDUSTRIAL ACTIVITIES

The ILL provides industrial users with access to state-of-the-art neutron instrumentation and the expertise of its scientific and technical staff. The Industry Liaison Unit (ILU) is the focal point of industrial activities at the ILL. The objective of the Unit is to bridge the gap between the ILL as a facility largely oriented towards academic research, and industry as an actor in projects that benefit from neutron techniques, often on subjects with high societal impact.

Contact: industry@ill.eu

KEEP **UP-TO-DATE**:

- facebook.com/ILLGrenoble
- twitter.com/ILLGrenoble
- linkedin.com/company/institut-laue-langevin

106 COMPANIES SINCE 2011

26 MEASUREMENT PERIODS

REVENUE: 506 k€

14 UNIQUE CUSTOMERS

The ILL's unique suite of advanced instruments and scientific expertise attract industrial clients from all over Europe and in many domains important to our modern society: from nano-technologies and next generation energy devices to aerospace applications and advanced chemicals. The Industrial Liaison Unit (ILU) is the single entry point to matching client's needs with the appropriate neutron-based characterisation techniques. Furthermore, the ILU is the driver behind several important local and European projects in which the ILL actively participates. In this way it increases the visibility of neutron applications and solutions to a wide range of potential users while also providing a modest additional income to the ILL's finances.

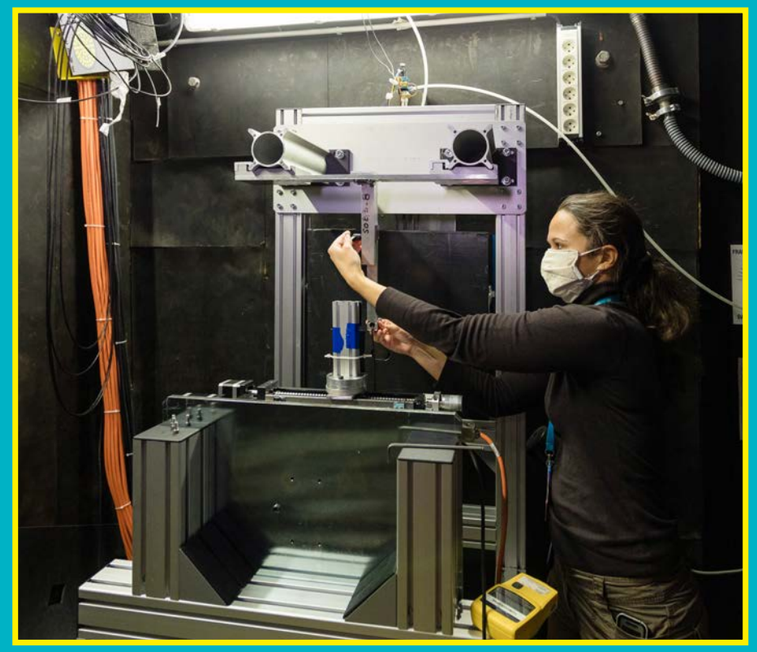

Sample positioning at the TENIS irradiation station.

The year 2021 was an exciting one for the ILU, with 26 industrial measurements being carried out for 14 customers despite the constraints imposed by the prevailing health crisis. For instance, a major collaboration with an aerospace company that we hope to build on in future years was initiated, making use of the cutting-edge performance of the NeXT imaging instrument. As with the majority of industrial beamtime, tests were performed in remote mode, resulting in the increased implication of beamline scientists and ILU staff to perform industrial measurements. Small-angle neutron scattering (SANS) is a technique that remains popular in various industrial sectors, from the investigation of fuel-cells to the study of alloy ageing and chemistry applications (*e.g.* for the cosmetic industry and other advanced materials). Several well-known companies, including L'Oréal, Infineum and Toyota, have made use of the three SANS instruments at the ILL. And last but not least, the capabilities of the strain-mapping instrument SALSA were successfully applied for the first time by the CNES and the ITER organisation this year.

As mentioned above, the ILU is involved in several European projects. In the case of energy storage, and in particular electrochemical battery systems, the ILL is an active partner in the ambitious Horizon 2020 Battery 2030+ BIG-MAP collaboration (**https://www.big-map.eu**). This unique project aims to combine characterisation techniques, artificial intelligence (AI) and machine learning (ML), along with numerical modelling to provide integrated, autonomous development tools to accelerate the design of new generations of batteries and to place European industry at the forefront of this vital domain. One of the main pillars of this project is compliant with the EU's Green Deal to decrease the emission of greenhouse gases, using renewable and recyclable materials that are readily available and minimising negative environmental/societal impact. Initially planned to run from 2019 to 2023, this project will, we hope, be extended for at least a three to four years in order to bring the revolutionary methods proposed to a stage of maturity.

Regarding the implementation of advanced stress measurement techniques using neutron or synchrotron X-ray diffraction, the EASI-STRESS project began early in 2021 and several important measurements have already been carried out on SALSA. In addition, the Neutron Quality Label NQL, developed through Brightness2, is now a trademark accompanied by a charter of use. The label will be applied for assessing whether specified operating procedures are being utilised across research infrastructures. This is expected to pave the way for a common international standard for strain-scanning (being considered under the work package WP6 of EASI-STRESS).

Elsewhere, the InnovaXN doctoral programme, in co-operation with the ESRF, saw the arrival of the second wave of PhD students (see InnovaXN section, p. 110).

The ILU also represents the ILL in the French project Institut de Recherche Technologique (IRT) Nanoelec. This focuses on R&D in the micro-/nano-electronics industry in the Grenoble area, which is recognised as one of the five international hubs for microelectronics. A new phase of the programme started in 2021 in which the ILL, along with its partners in the consortium and in particular IROC-Technologies, is focusing on developing irradiation methodologies. The irradiation station TENIS became operational in the first quarter of 2021, providing a high flux of thermal neutrons within a controlled energy spectrum. About a dozen academic and industrial users have already used the TENIS instrument to investigate the effects of thermal neutrons on electronics.

This summary underscores the diversity of the ILU's activities, including attracting funding, improving ILL's visibility in many industry sectors and aiding European companies to tackle key technological challenges leading to societal improvements.

ENGAGING MORE CLOSELY WITH INDUSTRIAL R&D

The ILL's know-how and industrial applications

A neutron detector on board

Airbus Avionics is running a project to manage the risks associated with neutron particles for avionics programmes. Qualification for components to be used in aircraft equipment relies partially on the characterisation of cross sections, *i.e.* the probability of interaction with materials, for high-energy neutrons (already well known) and thermal neutrons. The only way to estimate the real thermal neutron fluxes inside an aircraft is to perform direct measurements during flights at cruising altitude.

In 2021, the ILL provided thermal neutron detectors for on-board use in commercial flights, whilst also sharing its technical expertise in this area. The design, development and implementation of highly advanced neutron detectors is at the heart of the ILL's activity, as all forty of its scientific instruments require detectors with unique technical specifications.

This collaboration is one in a series of experiments carried out over several years by experts at the ILL or the Laboratoire de Physique Subatomique et de Cosmologie (LPSC-CNRS) where neutron irradiation stations have been made available through the IRT Nanoelec at Grenoble [1]. The ILL's instruments were first used by Airbus to predict thermal neutron risk on state-of-the art semiconductor technologies [2]. It was these initial measurements that first brought the Airbus Group into contact with the ILL's experts in neutron science and technology, since which Airbus has gained a better understanding of the ILL's skills and services in the field of thermal neutrons.

REFERENCES

[1] https://irtnanoelec.fr/programme-de-caracterisation-par-les-grands-instruments/

[2] Contribution of Thermal Neutrons to Soft Error Rate, Weulersse *et al.*, IEEE Transaction on Nuclear Sciences, 2017, Volume 65, Issue 8, DOI10.1109/TNS.2018.2813367

High-energy X-ray diffraction

The hard X-ray diffractometer developed by the Neutron Optics group at the ILL is dedicated to the characterisation of large mosaic crystals manufactured on site for neutron monochromators. This facility delivers high-energy X-ray radiations of up to 450 keV, allowing fine analyses of structural defects in the volume of large monocrystalline samples that cannot be penetrated by regular X-rays (because of highly absorbing elements, for example). This equipment may also be accessed by private companies for specific investigations. For instance, the set-up provides unique data to the company SAFRAN on specific crystals to be qualified as components in space technologies. This facility has proven to be a powerful tool for non-destructive testing, providing essential information on the presence of crystal defects that may lead to in-flight failure of critical components.

An ILL detector is currently being used by Airbus to measure the flow of cosmic neutrons at different altitudes of flight.

European Data Relay System (EDRS).

X-ray diffraction bench (IRT-Nanoelec).

Launch of the Grenoble Battery Hub

REFERENCE

[1] D. Atkins *et al.*, Adv. Energy Mat. (2021) 2102694

On 24 November 2021, the ESRF, the European Synchrotron, the ILL and the French Alternative Energies and Atomic Energy Commission (CEA) signed a memorandum of understanding (MOU) to create the 'Grenoble Battery Hub' for research on sustainable electrical energy storage, based on the use of cutting-edge neutron and X-ray techniques and instruments. The aim of this partnership is to accelerate research and innovation so that next-generation batteries are more efficient, safer, cheaper and more sustainable.

At the ILL, various techniques (*e.g.* powder diffraction, SANS, radiography/tomography, QUENS and reflectometry) are available to the research community through the scientific proposal system.Long-term projects requiring access to several instruments over a two- or three-year period are also possible, as is direct proprietary access for industrial clients. Around 50 scientists, PhDs, Postdocs and engineers from CEA, ESRF and ILL are already working on a range of strategic R&D battery-related projects:

- Studies of the ageing and degradation of battery components in order to understand the internal processes in batteries during charge, discharge and failure.
- Studies of electrochemical performance and the conditions of battery cycling to improve the capacity, efficiency, cycling stability, lifetime and recycling of batteries.
- Studies of thermal runaway in batteries to improve their safety.
- The investigation of promising components that could overcome the obstacles of lithium-ion batteries.

The Grenoble Battery Hub is linked to the European initiatives 'BIGMAP', co-funded by the European Union's H2020 programme, and BATTERY 2030+. The next step for the Hub is to open up to the European battery R&D community to advance research in support of the European Green Deal, the UN Sustainable Development Goals and the European Action Plan on Batteries.

'*Developing new generations of efficient, sustainable and affordable electrochemical batteries is an integral stepping-stone on the path to carbon-free energies. In order to fully understand the complex interactions involved in batteries and to obtain insights permitting new breakthroughs, the most powerful and well adapted experimental methods must be deployed to assist researchers. By combining the unrivalled complementary neutron and X-ray techniques available at the ILL and the ESRF with the outstanding scientific know-how of the CEA, a major step has been taken to provide Europe's scientific and industrial battery R&D community with the tools necessary to meet this common objective*', says Jacques Jestin, Director of Science at the ILL.

EXPERIMENTAL AND USER PROGRAMME

The **User Guide** contains all the practical information required to prepare a visit
https://www.ill.eu/users/user-guide/

Detailed information on the experimental programme can be found at
https://www.ill.eu/users

KEEP **UP-TO-DATE**:

facebook.com/ILLGrenoble
twitter.com/ILLGrenoble
linkedin.com/company/institut-laue-langevin

1 435
ILL and **CRG** EXPERIMENTS
including **56 DDT**, **294 EASY** and **53 internal** research experiments

176 DAYS OF NEUTRONS
5 506 DAYS FOR SCIENCE

920
DISTINCT USERS

1 413
USER VISITS
FROM **27** COUNTRIES

USER SATISFACTION
ABOVE
95 %*

* feedback participation rate 70 %

User programme

PROPOSAL SUBMISSION FOR ACADEMIC RESEARCH

Neutrons beams and instrument facilities are free of charge for academic users of accepted proposals. There are various ways of submitting a proposal to the ILL, as summarised in the following table.

Detailed information can be found at
https://www.ill.eu/users/applying-for-beamtime/

INDUSTRY-SPONSORED ACADEMIC RESEARCH AND INDUSTRIAL USERS

Neutrons have significant, specific applications for industry. Beamtime can be sold directly for proprietary research, in which case the experimental data are not made publicly available. The Industry Liaison Unit (ILU) is the single point of contact for industry looking to use the ILL's facilities (see p. 88). However, around 25 % of industry's use of the ILL is made *via* academia. The data from these experiments are publicly available and the results may be published. The ILL is now measuring the number and nature of industry-*via*-academia experiments more accurately, with a view to promoting this use of neutrons and potentially enhancing it in the future. In 2021, **26 measurements were sponsored by industry**.

Table 1

Mechanisms for submitting a proposal to the ILL. All type of access (except DDT) are reserved for users from ILL member countries or for collaboration between non-member and member teams. The stopwatch symbol indicates quick access. Most types of proposals are submitted *via* the User Club interface at **https://userclub.ill.eu/userclub/**

TYPE	APPLIES TO	WHEN	WHO FOR	RESPONSE TIME
External peer review				
Standard	All experiments, all instruments, all conditions	Deadlines twice a year, spring and autumn	All users from member countries (and non-members *via* 2/3 rule)	4 to 8 months after deadline
BAGs	College 8 proposals on D22	Deadlines twice a year, spring and autumn	All users from member countries (and non-members *via* 2/3 rule)	4 to 8 months after deadline
CRG	All experiments, CRG instruments, all conditions	Depends on CRG policy	All users from CRG collaboration	Depends on CRG policy
D-Lab	Access to the ILL sample deuteration lab	All year	All users from member countries	
Internal peer review				
DDT	Urgent experiments, hot topics, excellent science from non-member countries, all instruments, all conditions	All year	All users	ASAP
EASY	A small amount of beamtime, not a full experiment (must be very simple measurements), all instruments, limited number of configurations	All year	All users from member countries	From one to a few weeks
LTP	All instruments, for projects over several cycles if it can be demonstrated that they bring extra resources or capabilities that are of benefit to all users	Once a year, autumn round	All users from member countries	4 to 8 months after deadline
No peer review				
TEST	Test of sample, equipment, instrument configuration, all instruments	All year	All users from member countries	Usually on same day
INDU	Proprietary beamtime	All year	Contact the Industrial Liaison Office	ASAP

USER AND BEAMTIME STATISTICS

USER AND BEAMTIME STATISTICS

Figure 1

National affiliation of ILL users in 2021.

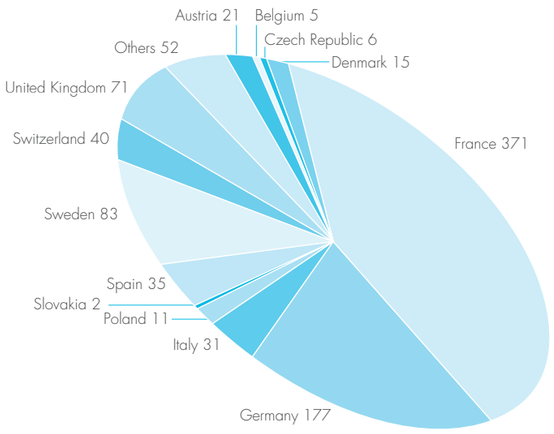

The ILL welcomed 920 visitors in 2021, including 371 from France, 177 from Germany and 71 from the UK. Many of our visitors were received more than once (giving a total of 1 413 visits).

PUMA is new ILL software developed in the FILL2030 project. It combines the ILL's databases for proposals and publications with Web of Science, in order to develop a comprehensive understanding of beamtime use based on a wide range of analyses. It should also allow us to identify laboratories and countries that might be interested in working with us at the ILL in the future. One feature of PUMA is its ability to match proposals with publications, thereby tracking the scientific process from idea to experiment to outcome.

Overall, the panel meetings in the November 2020 and April 2021 rounds examined 1 264 proposals requesting 6 122 days. Of these, 507 proposals received beamtime, requiring the allocation of 1 880 days of beamtime on the various instruments and corresponding to 550 experiments. These experiments were performed in 2021.

Figure 2

Chart—obtained using the PUMA software—showing the origin of the authors of ILL publications in Europe (taken from the addresses of their associated institutes). Authors associated with the ILL have been removed from the figures.

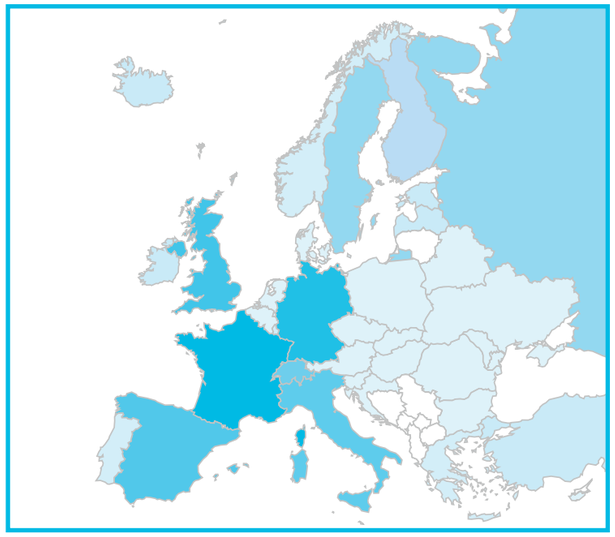

Figure 3

Proposals are divided amongst the various colleges. The figure shows how the accepted proposals were distributed amongst them.

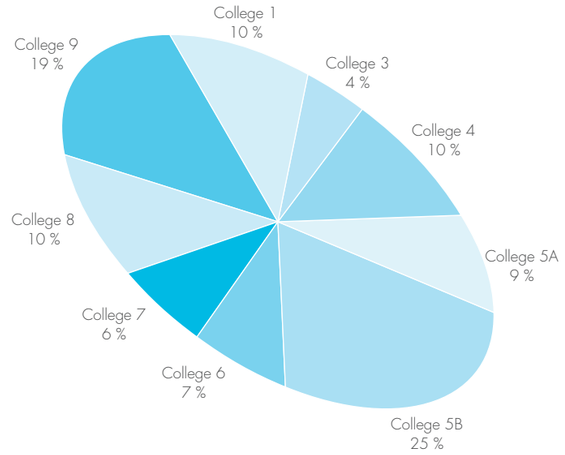

Table 1

Distribution amongst the ILL member countries of beamtime requests and allocation in the November 2020 and April 2021 panel meetings. Proposals from purely non-member countries do not appear in this Table, and therefore the total request and allocation is different in Table 2.

	Request days	Request %	Allocation days	Allocation %	Allocation days	Allocation %
	Without non-member countries and ILL and EU facilities redistributed				After national balance	
AT	146.17	2.39	62.95	3.17	63.27	3.36
BE	15.42	0.25	6.92	0.35	5.55	0.30
CH	384.72	6.28	167.00	8.42	67.44	3.59
CZ	28.18	0.46	7.36	0.37	7.38	0.39
DE	1 540.34	25.16	488.22	24.62	508.10	27.02
DK	112.40	1.84	38.92	1.96	33.98	1.81
ES	382.44	6.25	118.84	5.99	99.86	5.31
FR	1 470.76	24.03	466.06	23.50	480.83	25.57
GB	1 302.85	21.28	411.48	20.75	455.69	24.24
IT	184.88	3.02	54.07	2.73	24.14	1.28
PL	94.21	1.54	23.61	1.19	12.47	0.66
SE	407.18	6.65	116.75	5.89	102.66	5.46
SI	24.88	0.41	16.92	0.85	14.93	0.79
SK	27.34	0.45	3.95	0.20	3.97	0.21
Total	**6 121.77**	**100.00**	**1 983.05**	**100.00**	**1 880.27**	**100.00**

In calculating the **statistics for beamtime per country** shown in **Table 1**, attribution is based on the location of the laboratory of the proposers, not their individual nationality. For a proposal involving laboratories from more than one member country, the total number of days is divided amongst the collaborating countries and weighted by the number of people from each. Local contacts are not counted as proposers. The beamtime requested by and allocated to scientists from the ILL is allocated to the member countries according to a weighting system based on the fractional membership of the country of the institute concerned. When a proposal involves collaboration with a non-member country, the allocated time is attributed entirely to the collaborating member countries. Proposals in which all proposers are from non-member countries therefore do not appear in this Table.

USER AND BEAMTIME STATISTICS

Table 2 gives a summary of **instrument performance** for 2021. Around 5 213 days were made available to our users in 2021 on ILL and CRG instruments (*via* standard request or the EASY and DDT routes), representing about 80 % of the beamtime available; a total of 293 days were used by ILL scientists to carry out their own scientific research; and about 10 % of the total beamtime available on the ILL instruments was allowed for tests, calibrations, scheduling flexibility, recuperation from minor breakdowns and student training. In all, 377 days were lost as a result of various malfunctions, accounting for less than 6 % of the total available beamtime.

In 2021 the reactor operated for three cycles, representing 176 days of neutrons. During this time, **a total of 1 435 ILL and CRG experiments were performed** (including 56 DDT, 294 EASY and 53 internal research experiments). **Beam days given to science (used for users, EASY, DDT and internal research) in 2021 amounted to 5 506 (84 % of the total available).**

Figure 4
Use of ILL beamtime.

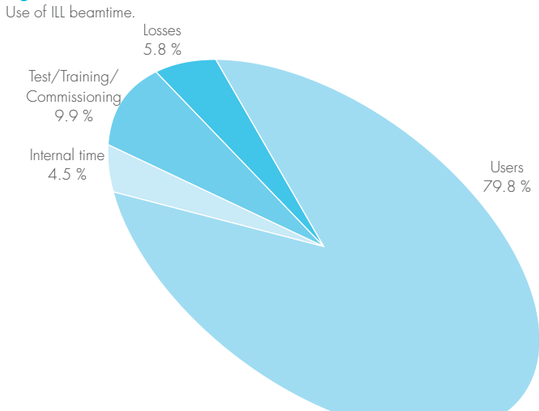

Science in the time of pandemic.

Table 2
Beamtime request/allocation (*via* standard subcommittees and Director Discretion Time (DDT) combined) by instrument and instrument performance. CRG instruments are in blue.

* 'days allocated' refers to only those days reviewed by the subcommittees (*i.e.* excluding CRG days and DDT)

** 'days available' are the days of reactor operation

*** 'days used'refers to the total number of days given to users (*i.e.* including CRG days for CRGs and DDT)

PF2 consists of different set-ups where several experiments are running simultaneously. The values given are averages for these positions (and normalised by a factor of 5).

D4 and IN1 share the same beam port and cannot be run simultaneously.

SHARP operated only during the third cycle in 2021.

Instrument	Days requested	Days allocated *	Number of accepted experiments	Available days **	Days used for users ***	Days lost	Days for test/ commissioning /training	Days for internal research	Days for EASY/ DDT
D10	251	62	11	176	142.5	2.5	5.0	0.0	26.0
D11	248	51	38	146	119.0	2.6	14.4	3.0	7.0
D16	192	78	16	176	147.5	6.5	16.0	6.0	0.0
D17	161	61	23	176	140.5	4.5	15.0	6.0	10.0
D19	96	65	12	176	138.0	2.0	7.0	3.0	26.0
D1B	127	38	27	176	148.7	5.0	8.0	0.0	14.3
D20	267	68	34	176	140.0	6.5	6.0	10.6	12.9
D22	153	54	29	176	125.0	2.0	27.3	4.0	17.7
D23	113	27	6	176	159.0	0.0	13.0	4.0	0.0
D2B	161	70	40	176	128.0	1.5	1.5	8.0	37.0
D33	254	64	25	176	146.0	6.1	10.9	8.0	5.0
D3	280	68	13	176	123.0	10.0	32.0	0.0	11.0
D4	128	33	10	106	65.0	16.3	8.8	6.0	10.0
D7	203	80	16	176	141.0	1.5	26.5	0.0	7.0
D9	185	60	14	176	95.2	2.8	3.0	0.0	75.0
DALI	23	18	2	176	26.0	0.0	120.0	16.0	14.0
FIGARO	202	50	19	176	128.3	7.3	5.0	28.5	7.0
FIPPS	24	18	3	176	124.0	32.0	20.0	0.0	0.0
IN12	101	17	4	176	131.0	4.0	12.0	29.0	0.0
IN13	37	20	2	176	149.0	10.0	6.0	11.0	0.0
IN15	140	35	9	176	119.0	0.0	43.0	10.0	4.0
IN16B	306	72	24	176	121.0	2.7	23.0	16.9	12.4
IN1	82	13	6	70	55.0	1.0	6.0	0.0	8.0
IN20	97	41	6	176	35.0	120.8	10.3	9.0	1.0
IN22	101	22	3	176	152.0	4.5	19.5	0.0	0.0
IN5	378	70	23	176	158.5	2.5	3.0	1.0	11.0
IN8	119	54	10	176	140.0	2.5	14.5	8.0	11.0
LADI	157	35	8	176	156.0	0.0	6.0	2.0	12.0
NEXT	289	54	19	176	145.0	2.0	11.0	12.0	6.0
PANTHER	197	75	26	176	106.5	9.5	32.0	7.0	21.0
PF1B	115	67	4	176	134.0	18.0	14.0	10.0	0.0
PF2*	105	73	13	176	104.0	31.6	18.6	16.2	5.6
PN1	209	49	5	176	152.0	24.0	0.0	0.0	0.0
S18	21	0	0	176	168.0	5.0	3.0	0.0	0.0
SALSA	189	62	17	176	114.0	13.8	17.2	31.0	0.0
SHARP	29	0	0	50	38.0	2.0	10.0	0.0	0.0
SUPERADAM	53	32	7	176	141.0	1.0	16.0	18.0	0.0
THALES	242	80	15	176	159.5	6.0	6.5	2.0	2.0
WASP	119	50	11	176	120.0	7.0	38.0	7.0	4.0
Total	**6 154**	**1 886**	**550**	**6 532**	**4 835**	**377**	**649**	**293**	**378**
Percentage					74 %	5.7 %	10 %	4.5 %	5.8 %
						Days for science	5 506	78 %	
						4 835 + 293 + 378			

INSTRUMENT LIST

INSTRUMENT LIST – DECEMBER 2021

ILL INSTRUMENTS		
D2B	powder diffractometer	operational
D3	single crystal diffractometer	operational
D4 (50 % with IN1-LAGRANGE)	liquids diffractometer	operational
D7	diffuse-scattering spectrometer	operational
D9	single crystal diffractometer	operational
D10	single crystal diffractometer	operational
D11	small-angle scattering diffractometer	operational
D16	small momentum-transfer diffractometer	operational
D17	vertical reflectometer	operational
D19	single crystal diffractometer	operational
D20	powder diffractometer	operational
D22	small-angle scattering diffractometer	operational
D33	small-angle scattering diffractometer	operational
DALI	quasi-laue diffractometer for biological macromolecules	operational
FIGARO	horizontal reflectometer	operational
FIPPS	fission product prompt gamma-ray spectrometer	operational
LAGRANGE (50 % with D4)	neutron vibrational spectrometer	operational
IN5	time-of-flight spectrometer	operational
IN8	three-axis spectrometer	operational
IN16B	backscattering spectrometer	operational
IN20	three-axis spectrometer	operational
LADI	Laue diffractometer	operational
PANTHER	time-of-flight spectrometer	operational
PF1B	neutron beam for fundamental physics	operational
PF2	ultracold neutron source for fundamental physics	operational
PN1	fission product mass-spectrometer	operational
SALSA	strain analyser for engineering application	operational
SuperSUN	ultracold neutron source for fundamental physics	commissioning
ThALES	three-axis spectrometer	operational
WASP	wide-angle spin-echo spectrometer	operational

CRG INSTRUMENTS		
D1B	powder diffractometer	CRG-A operational
D23	single crystal diffractometer	CRG-B operational
IN12	three-axis spectrometer	CRG-B operational
IN13	backscattering spectrometer	CRG-A operational
IN22	three-axis spectrometer	CRG-B operational
SHARP	time-of-flight spectrometer	commissioning
SuperADAM	reflectometer	CRG-B operational
S18	interferometer	CRG-B operational

JOINTLY FUNDED INSTRUMENTS		
IN15	spin-echo spectrometer	operated with FZ Jülich
NeXT (75 %)	imaging instrument	operated with Ni-Matters composed of HZB, UGA and ILL

TEST AND CHARACTERISATION BEAMS	
CT1, CT2	detector test facilities
CYCLOPS	Laue diffractometer
OrientExpress	Laue diffractometer
TENIS	neutron irradiation position
T3	neutron optics test facility
T13A, C	monochromator test facility

Details of the instruments can be found at **https://www.ill.eu/users/instruments/instruments-list**

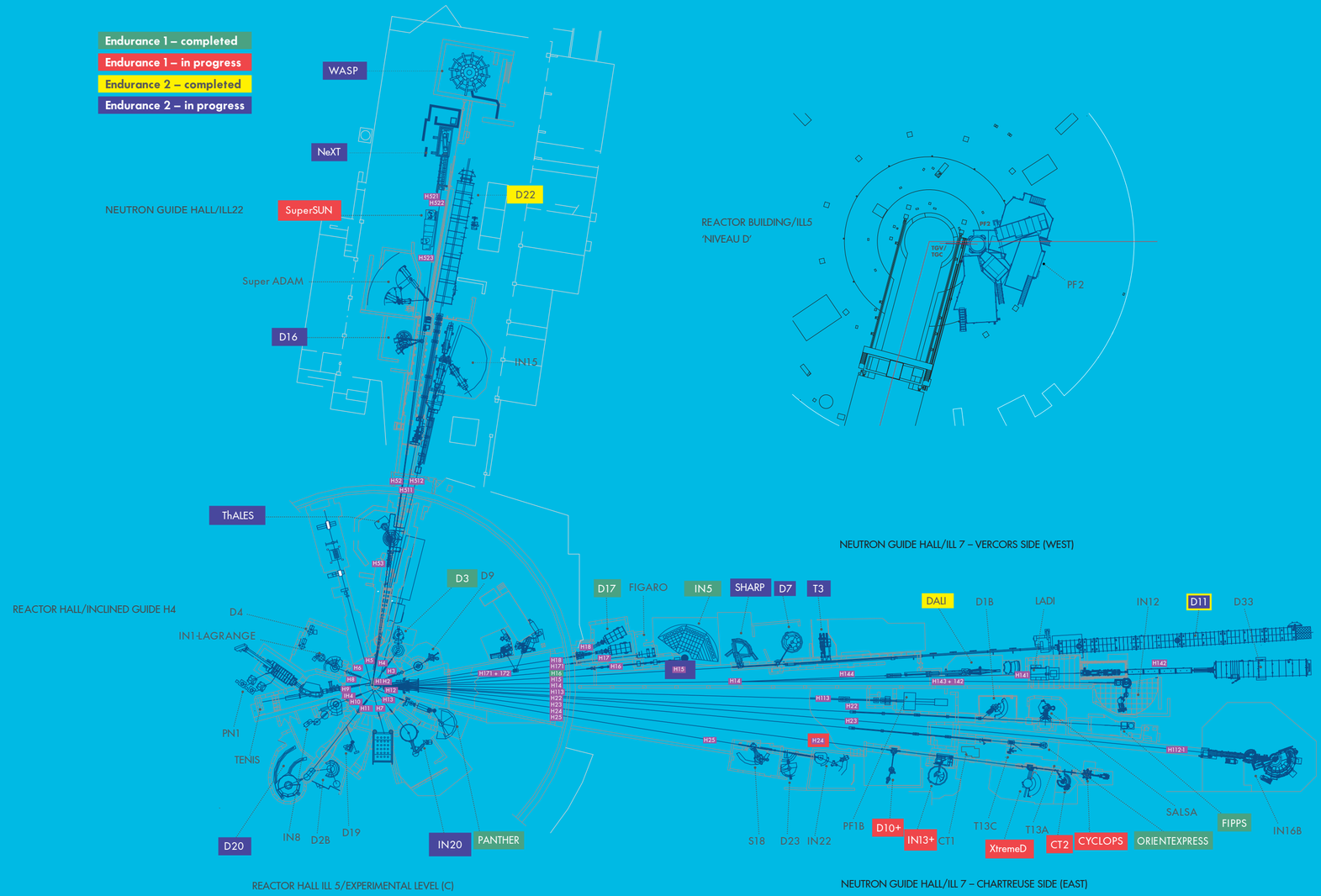

The instrument facilities at the ILL are listed in the Table on the left and shown in the plan on p. 99. In addition to the 28 ILL instruments, there are 10 Collaborative Research Group (CRG) instruments.

CRGs can build and manage instruments at the ILL to carry out their own research programmes.

There can be three different categories of CRG instrument:

- CRG-A category: the external group leases an instrument owned by the ILL. They have access to 50 % of the beamtime; for the remaining 50 % the instrument is made available to the ILL's scientific user programme.
- CRG-B category: the external group owns its instrument and retains 70 % of the available beamtime, supporting the ILL programme for the other 30 %.
- CRG-C category: the instrument is used full time for specific research programmes by the external group, which has exclusive use of the beam.

Details about the framework of operation for CRGs can be found at **https://www.ill.eu/users/instruments/crgs/**

All current CRGs are either A- or B-type. IN15 has special status because it is a joint venture of the ILL and FZ Jülich. The instrument STEREO is jointly funded by the ILL and CEA Saclay, LAPP Annecy, LPSC Grenoble and MPIK Heidelberg.

INSTRUMENT LAYOUT

REACTOR OPERATION

KEEP **UP-TO-DATE**:

- facebook.com/ILLGrenoble
- twitter.com/ILLGrenoble
- linkedin.com/company/institut-laue-langevin

THREE CYCLES AND **176** DAYS OF **OPERATION** IN 2021

58.3 MW

1.5 x 10^{15} n/s cm^2

A SINGLE, HIGHLY ENRICHED URANIUM FUEL ELEMENT

THE ILL's high-flux reactor produces one of the most intense neutron flux in the world: 1.5 x 10^{15} neutrons per second per cm^2, with a thermal power of 58.3 MW. The reactor normally operates three or four reactor cycles per year. At the end of each cycle there is a shutdown period during which the fuel element is changed and checks are carried out. Occasional longer shutdowns are scheduled to allow for maintenance or refurbishment.

The reactor's fuel element can provide 46 days of operation per cycle at maximum power. Over recent years, the ILL's Millennium and Endurance programmes have improved the performance of our instruments by a factor ranging from 20 to 100. However, the current beam tube replacement programme and the installation of more powerful instruments is now preventing us from providing a nominal programme of 180 days per year. We are therefore scheduling the maximum number of days of operation possible in light of the upgrades. We can also adapt the power of the reactor to experimental requirements, providing, for example, slightly lower power but a longer period of beamtime for experimentalists.

Following the nuclear disaster at Fukushima in 2011, the French nuclear safety authority (ASN) ordered additional safety assessments on all French 'basic nuclear installations' (INBs), including the ILL. The ILL's post-Fukushima programme has now ended, and the safety of the reactor is guaranteed even in the event of an extreme earthquake-with-flood combination following breach of the dams upstream. This goes well beyond previous dimensioning standards.

The ASN has also asked the ILL to reorganise its technical procedures *via* the introduction of an Integrated Management System ('SMI' – INB Decree of 2012), to be incorporated into all its essential operating practices. ASN requests are extremely demanding and generate a significant workload. They are nevertheless necessary and have been given top priority by the ILL.

In addition to the above, the ILL has been working since November 2017 on another safety authority requirement—the 10-yearly reactor safety assessment. The results of this examination have just been received and are very positive. This means that the ILL is authorised to continue its operations for a further ten years, as long as it continues to modernise as required by the authorities.

Jérôme Estrade
Head of the Reactor Division

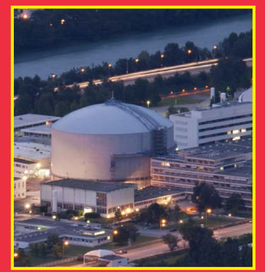

From top:
The Reactor dome.
ILL site view.

REACTOR OPERATION 2021

In light of the public health crisis, the reactor operating schedules for both 2020 and 2021 were adapted in order to optimise, on the one hand, the shutdown periods used to carry out regulatory maintenance operations and install new scientific instruments; and on the other, the reactor operating periods during which we host our scientific users.

In 2021, we ran three cycles (27 January 2021 to 30 March 2021; 11 May 2021 to 14 July 2021; and 24 August to 13 October 2021) before the long H1–H2 shutdown.

It is important to note the excellent results of these three cycles, which as well as absorbing the backlog allowed a large number of experiments to be conducted in spite of the difficult conditions caused by COVID-19. This underscores the high degree of efficiency achieved by ILL staff.

Cycle n°	Start of cycle	End of cycle	Number of days of operation	Number of days scheduled	Power in MW	Number of unscheduled shutdowns
189	27.01.21	30.03.21	62	62	43	0
190	11.05.21	14.07.21	64	64	42	0
191	24.08.21	13.10.21	50	50	54	1
Total			**176**	**176**		**1**

RELATIONS WITH THE FRENCH NUCLEAR SAFETY AUTHORITY (ASN)

Recent ASN inspections have continued to go well. However, we must intensify our efforts and take even greater care to ensure that we maintain our good record, especially as the latest inspection on waste management resulted in new requirements from the ASN.

On 15 October 2021 the chairman of the ASN visited the ILL, accompanied by two members of the ASN Commission and representatives of its Paris and Lyon divisions. The day was devoted to a tour of the facilities and a presentation on the various projects being implemented as a result of commitments made by the ILL under the framework of the periodic safety review. The ultimate purpose of this review is to confirm the ILL's licence to operate until 2027, the date of the next safety review. This visit was important for the ILL and showed the positive interest the ASN is taking in our facility.

REINFORCEMENT OF PHYSICAL PROTECTION (RPP) PROJECT

This project to reinforce our physical security measures is making good progress; despite the pandemic it is only slightly behind schedule. It is being conducted under the supervision of France's security authority, the HFDS (*Haut Fonctionnaire de Défense et de Sécurité – senior defence and security advisor at ministerial level*). The major milestone of 2021 was the first stage of commissioning of the new controlled access zone (ZAC) on 1 August 2021. Following initial feedback some adjustments will be necessary, but these will be completed in 2022. The next step to be completed is further reinforcement by installing additional barriers within an inner protection zone (ZPR).

10-YEAR SAFETY REVIEW

The 10-year safety review by the ASN is to be officially concluded by the beginning of 2022. This will involve two meetings of the ASN Commission (*Collège des commissaires*) and a public consultation.

On 7 September 2021, the ASN Commission (comprising five independent commissioners) examined the draft decisions of the meeting of the *Groupe Permanent* in November 2020. In view of the robustness of the ILL's programme of commitments, the Commission's view on the continuation of ILL operations for another 10 years is likely to be issued soon after the public consultation.

Following the 10-year safety review, the ILL presented the ASN with a comprehensive set of commitments. Based on these, and more recent requirements issued by the ASN, we now have a timeline for the period 2020–2025 for fulfilling these commitments. The programme ensures that all our other essential maintenance operations can be maintained (such as the KRC programme—see below), and that the ILL's scientific programme can progress as planned. The ILL has planned three long shutdowns for this work. The schedule will ensure that time is optimised for the scientific programme (providing the maximum number of beam days possible for science).

REQUALIFICATION OF THE REACTOR VESSEL

At the beginning of October 2020, the reactor was shut down to allow work to be carried out on requalification of the reactor vessel. This crucial obligation was successfully completed in January 2021. The vessel passed the tests and is approved for ten more years of operation.

FIRE PROTECTION

Following changes in the regulations for fire protection, the old fire detectors have been replaced by ion smoke detectors, and the project for installing a sprinkler system at level C and in the different casemates has launched.

KEY REACTOR COMPONENTS PROGRAMME (KRC)

The aim of the KRC programme is to ensure the upgrade and maintenance of the reactor's most important components, thereby guaranteeing the reliability of reactor operations for the future. The main components concerned are the cold-neutron sources, the fire protection equipment and the physical protection equipment.

CLEAN-UP OF THE DETRITIATION FACILITY AND REFURBISHMENT OF SOURCE EQUIPMENT

The detritiation facility is no longer in use and needs to be dismantled. The plan was to rapidly reduce the pressure in the last four tanks containing tritium and deuterium, to avoid falling within the scope of ESPN regulations. We received ASN authorisation for this operation, which has since been successfully performed.

We now intend, in a second phase, to use a recombiner unit to combine the tritium and deuterium with oxygen at very low concentration in order to produce heavy water for the primary circuit. The recombiner will also make it possible to treat the deuterium from the cold sources and to clean the tanks and circuits of the facility. The huge advantage of this solution is that it avoids creating an explosive atmosphere (which is the case with the current burner) and reduces the amount of waste produced.

We will send a request for ASN authorisation for this second stage in 2022.

RADIOACTIVE WASTE AND EFFLUENTS

The ILL's activities in 2021 generated waste and effluents in respect of the regulatory limits applicable to our installation, as follows:

Evacuation of radioactive waste	Quantity
Decay bin (60 L)*	0
5 m^3 pre-concreted crate (low- and intermediate-level waste)	0
5 m^3 crate (low- and intermediate-level waste)	4
HDPE 200 L drums of 'incinerable' waste	62
HDPE 120 L drums (laboratory waste)	7
30 L cylinders (liquid)	2
Radioactive organic liquid from the reactor	0 m^3

** The decay bins contain very active waste. They will be transferred to ANDRA's new storage centre CIGEO after an interim period in special storage.*

Gaseous effluents	Released in 2021 (TBq)
Tritium	10
Rare gas	1
Carbon-14	0.34
Iodine	$9.8\ 10^{-7}$
Aerosols	$4.8\ 10^{-8}$

Liquid effluents	Released in 2021 (TBq)
Tritium	0.15
Carbon-14	$1.9\ 10^{-4}$
Iodine	$3.4\ 10^{-7}$
Other activation products	$1\ 10^{-5}$

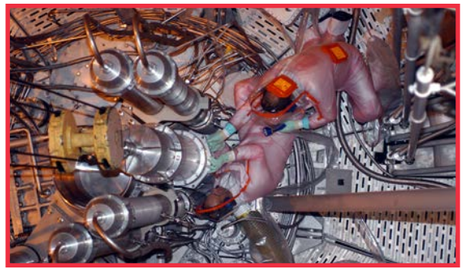

From top:
Fuel element unloaded and being cooled.
The new H1–H2 beam tube.
Maintenance work in the reactor pool.

MORE THAN SIMPLY NEUTRONS

106 SCIENTIFIC SUPPORT LABORATORIES
109 EUROPEAN PROGRAMMES
112 TRAINING AND OUTREACH

ACCESS

TO **13 LABORATORIES**
HOSTING
37 LABORATORY INSTRUMENTS
VIA THE **PSCM**

INVOLVED IN
NO FEWER THAN **17**
EU PROJECTS

Access to **20 technology platforms,** including biological deuteration (macromolecular & small biomolecules), synchrotron X-ray crystallography and SANS/SAXS *via* the **PSB**

TRAINING
GRADUATE SCHOOL
40 **FULL-TIME-EQUIVALENT ILL PHD STUDENTS**

HERCULES SCHOOL
90 **PARTICIPANTS**
OF
33 DIFFERENT NATIONALITIES
WORKING IN
21 DIFFERENT COUNTRIES

KEEP **UP-TO-DATE**:

facebook.com/ILLGrenoble
twitter.com/ILLGrenoble
linkedin.com/company/institut-laue-langevin

IN ORDER to maintain their ranking at international level, European research infrastructures must optimise their resources and develop synergies at every level.

The ILL is firmly committed not only to building high-performance instruments but also to offering the best scientific environment for the user community. Over the years, we have also established successful collaborations with neighbouring institutes and launched successful scientific and support partnerships. Two recent examples are: (i) NI-Matters[1]—a collaboration with UGA and HZB, our main partners for imaging, to develop this technique for materials and energy research; and (ii) the Battery Hub[2]—to promote a synergistic approach to battery research at the ILL and the ESRF with the CEA as the initial scientific partner, all three organisations being part of the BIG-MAP European project.

European collaboration is in the DNA of the ILL, and has been since its inception. In 2021 the Institute was involved in 17 European projects funded either by the H2020 research and innovation framework programme or EURATOM, both of which are administered by the European Commission. The benefits are not merely financial; the ILL also gains from the associated networks and resources, which improve its integration with other facilities and the user community. Until June 2021, the ILL was the co-ordinator and sole beneficiary of **FILL 2030** (with a grant of 4 M€ over four years).

The new research and innovation framework programme 'Horizon Europe' was launched at the beginning of 2021. With the aim of further increasing visibility at a European level, the League of advanced European Neutron Sources (LENS) has teamed up with the League of Advanced European Photons Sources (LEAPS) and five other analytical research infrastructure networks to form ARIE (Analytical Research Infrastructures in Europe).

Local collaboration is equally important. The ILL and the ESRF have transformed their site into what is now the **European Photon and Neutron (EPN) science campus**. The EPN Campus hosts three major European institutes—the EMBL, the ESRF and the ILL—as well as France's IBS (**http://www.epn-campus.eu/**), providing a veritable hub of international science in the Grenoble region.

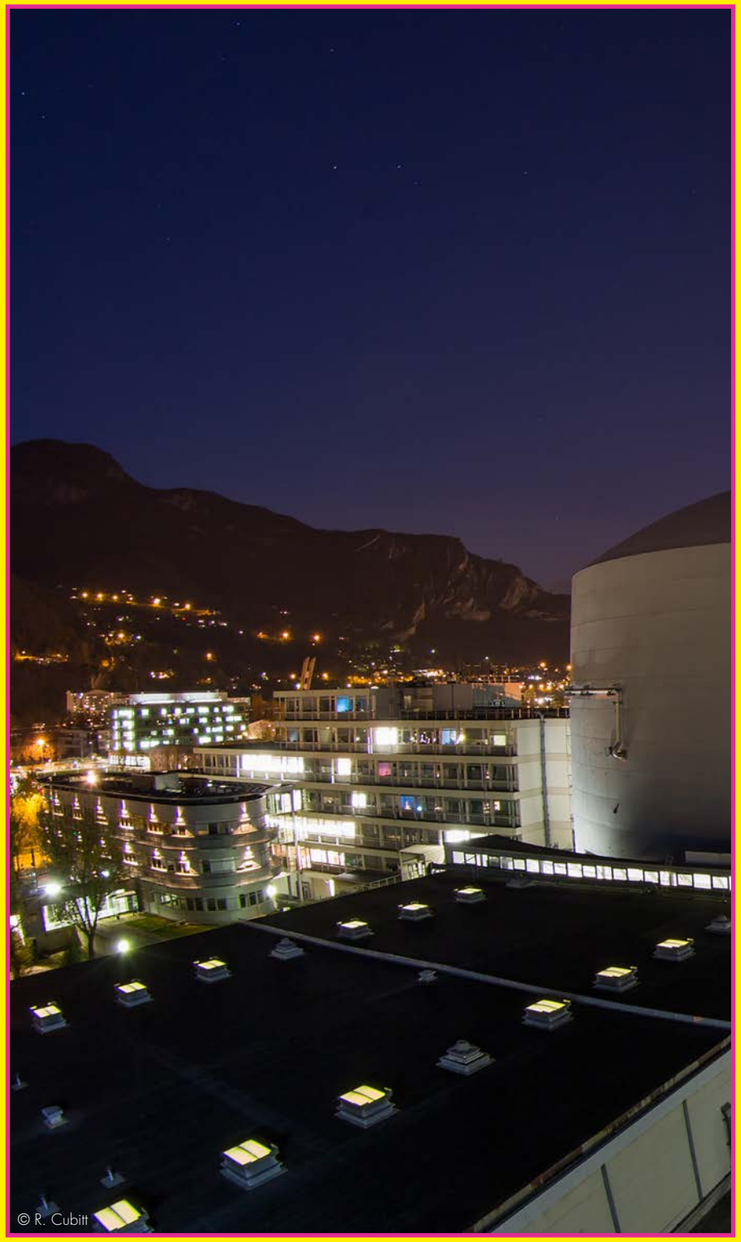
© R. Cubitt

Last but not least, the ILL is committed to training and outreach, which it provides in many different forms. Whilst the ILL Graduate School and the PhD programme are now training future generations of neutron users, we also run neutron schools and other events for MSc and PhD students. In addition, our open days and annual contributions to the local science festival help attract young talent to science and improve the general public's understanding of the science we perform.

1 https://www.ill.eu/about-the-ill/collaborations/international-cooperation/ni-matters-neutron-imaging-for-material-and-energy-research
2 https://www.big-map.eu/

SCIENTIFIC SUPPORT LABORATORIES

PARTNERSHIP FOR SOFT CONDENSED MATTER

The Partnership for Soft Condensed Matter (PSCM) is a joint initiative established by the ILL and the ESRF on the EPN Campus. The PSCM's main mission is to provide support services to ILL and ESRF scientists tackling contemporary challenges in soft matter research (nanomaterials, environmental and energy sciences, biotechnology and related fields). The PSCM provides users with access to 13 laboratories and 37 laboratory instruments, such as multi-angle static and dynamic light scattering machines, rheometers, Langmuir troughs, differential scanning calorimeters, spectrophotometers, optical ellipsometers and a quartz-crystal microbalance, to mention just a few.

It is the Partnership's mission to strengthen the soft matter research community by establishing long-term collaborations to develop specialised instrumentation and sample environment facilities. Six new partnership projects started in 2020, selected through a competitive call for proposals. In 2022, the PSCM will undergo an in-depth review by four selected independent experts in the field of soft condensed matter.

The PSCM is located on the 2nd floor of the EPN Campus Science Building, along with the Soft Matter Science and Support group. Neutron users wishing to use the PSCM laboratories and equipment in conjunction with their neutron measurements should indicate this when submitting their request for beamtime.

https://www.epn-campus.eu/pscm/

PARTNERSHIP FOR STRUCTURAL BIOLOGY

The Partnership for Structural Biology (PSB) operates a powerful set of technology platforms provided and managed by its partner institutes (ILL, ESRF, EMBL, IBS). It provides advanced capabilities that complement the neutron scattering facilities available to ILL users. These include synchrotron X-rays, cryo-electron microscopy, high-field nuclear magnetic resonance, mass spectrometry, high-throughput methods (*e.g.* soluble expression and crystallisation); as well as a range of biophysical techniques such as isothermal calorimetry, surface plasmon resonance and mass photometry. The PSB includes the Deuteration Laboratory (see below), which is operated as a user platform within the ILL's Life Sciences Group, and the joint SANS/SAXS platform. There are strong links and collaboration between the ILL, ESRF life sciences/structural biology and industry groups.

The aim of the PSB is to enhance the interdisciplinary capabilities of each of the facilities located on the site and to widen the scientific scope of external user communities. The Carl-Ivar Brändén Building (CIBB) acts as home to the PSB and its partner organisations.

https://www.psb-grenoble.eu/

THE LIFE SCIENCES GROUP AND ITS DEUTERATION LABORATORY

The Deuteration Laboratory (D-Lab) is located and operated as a PSB platform within the ILL's Life Sciences Group. It was created in the 2000s with major funding from the UK Engineering and Physical Sciences Council (EPSRC), its principal missions being to provide deuterated biomolecules to the user community, innovation and development for biological neutron scattering, and training. The Life Sciences Group works in purpose-designed laboratories in the Carl-Ivar Brändén Building, the centre of the PSB. It has always functioned as a user platform, continuously innovating for novel neutron science in biology, and is embedded in a group that has an active in-house research programme with substantial external funding.

Since the D-Lab platform's inception, deuteration facilities have been set up around the world providing purpose-designed deuterated samples that have revolutionised biological neutron science. Its user programme uses *in vivo* recombinant expression approaches to provide deuterated analogues of proteins, nucleic acids and lipids for studying structure (crystallography, SANS, fibre diffraction, reflection) and dynamics using neutron scattering. The D-Lab is therefore of central importance to all the ILL instrument groups involved in biological research. In terms of development, it is involved in a broad range of activities including novel deuteration regimes, the expression of deuterated proteins using insect and mammalian cell deuteration, and the cultivation of large protein crystals.

The Life Sciences Group is additionally involved in a wide variety of externally-funded programmes exploiting the capabilities of the PSB as well as promoting interdisciplinary structural biology. It also has strong connections with industry. In addition, it is involved in operating and developing the cryo-EM capabilities being established through the installation of Titan Krios at the ESRF, in collaboration with the ESRF, the IBS and the EMBL. The group is also actively engaged in training and each year takes on a number of undergraduate placement students for training in different techniques.

Access to the D-Lab is gained through a rapid peer-review proposal system. The facility is available to all the ILL member countries, regardless of where the neutron scattering study is carried out. It is also available to users from non-member countries—although in such cases a contribution to the costs may be requested.

https://www.ill.eu/users/support-labs-infrastructure/deuteration-laboratory

CHEMISTRY LABORATORIES

The Soft Matter Science and Support Group (SMSS) manages the ILL chemistry laboratories together with the PSCM laboratories. Its main goal is to allow ILL users to prepare and characterise their samples during their neutron experiments, while also supporting the in-house research conducted by instrument scientists and PhD students.

The main facilities are located in the Science Building. In addition, three sample preparation labs are available in the guide halls ILL 7 and ILL 22. The laboratories are equipped with the basic equipment (glassware, consumables and chemicals) necessary to prepare samples for a variety of different neutron experiments, as well as more specific facilities such as high-temperature furnaces and a glovebox or enclosure for handling nano-powders. The PSCM laboratories offer various methods for sample characterisation, such as UV-Vis, FTIR and light scattering.

https://www.ill.eu/users/support-labs-infrastructure/chemistry-laboratories/

MATERIALS SCIENCE SUPPORT LABORATORY

Scientists (local contacts) in our joint ILL–ESRF Materials Science Support Laboratory (MSSL) provide a range of support to our users, from advice on proposals and experiment design to assistance with preparing samples and performing experiments.

The Lab also has shared equipment for load testing:

- 50 kN INSTRON hydraulic rig, which also allows for cyclic testing and induction heating (Tmax < 1 000 °C)
- 15 kN compact load rig, able to be mounted on a cradle
- Other INSTRON rigs at the ESRF: ETMT (combined load and heating, 3 kN, Tmax ~1 500 °C); 4 kN hydraulic; and 25 kN hydraulic.

The ILL also provides facilities for sample polishing, hardness testing and optical microscopy. Furthermore, a co-ordinate measuring machine (CMM) and a portable metrology arm are available for confirming or benchmarking samples' surface dimensions and/or distortion before actual neutron measurements are made and for increasing the speed at which complex/large components can be aligned directly at the beamline. Other lab equipment brought in by users may also be adapted to the beamline upon discussion with the scientists responsible for particular instruments and safety approval.

Local contacts are responsible for working with users to optimise their methodology before the start of an experiment. This can involve standardised specimen mounting and the digitalisation of samples. We invite users to get in touch with ILL scientists well in advance when designing their proposed experiment, and to arrive at the campus a day or two before the start of their beamtime to enable these off-line preparations to be made.

Images © C. Jimenez

L-LAB: A PLATFORM FOR NATURAL DEUTERATED LIPID EXTRACTION WITHIN THE PSCM

Neutron scattering techniques are ideally suited to the study of lipid bilayers, major components of cellular membranes. At the ILL, we have been working for several years to provide our users with well-characterised membrane models for physical and biological studies. These efforts have been recognised and praised by the international community, and many facilities have since followed our example. The considerable interest in working with lipid bilayers and biological membranes at the ILL is confirmed by the numbers of such experiments performed (> 200) and manuscripts published (> 300) in the last five years.

The community's interest in accessing deuterated glycerophospholipids (GPLs) has also been confirmed by the results of a survey conducted within the DEUNET (**https://deuteration.net/**) network set up under the SINE2020 grant. These findings show that GPLs are the species most often requested by soft- and bio-neutron scientists (the targets of the survey). GPL deuteration helps elucidate membrane structure, dynamics and function by providing selective visualisation in neutron scattering. However, studies involving deuterated biomimetic membranes are currently limited by the low availability of several biologically relevant, unsaturated GPL species. To overcome this, facilities such as ANSTO, ISIS and the ESS have achieved some success in chemically synthetising certain mono-unsaturated GPLs for users (but with conditions for their use or at enormous cost). An alternative, and much cheaper, method of obtaining a wide variety of deuterated GPL species (including unsaturated ones) is to extract them from organisms grown under deuterated conditions.

Work pioneered back in 2013 within the PSCM (de Ghellinck *et al.*, 2014), in collaboration with the D-Lab and Hanna Wacklin (now at the ESS), has evolved over the years with the aim of extracting and purifying GPLs from deuterated cell cultures through the following steps: (i) selection of suitable organisms for growth; (ii) optimisation of extraction protocols for GPLs; (iii) development of methods for GPL separation as a function of the head-group; (iv) development of protocols for characterising the prepared GPL mixtures; and (v) 'mass production' for the neutron facilities' user community.

So far, we have successfully investigated methods to characterise and quantify deuterated GPL mixtures after producing them biologically in the oleaginous yeast *P. pastoris* and the bacterium *E. coli* grown on perdeuterated medium. Extensive use of chromatography and mass-spectrometric techniques have been employed for deep compositional analysis of the purified GPL mixtures. In tandem with this we have been developing protocols for preparing mono/bi-layers composed of such mixtures. The lab is also currently focused on isolating cellular organelles in their deuterated forms that could be directly employed in various studies.

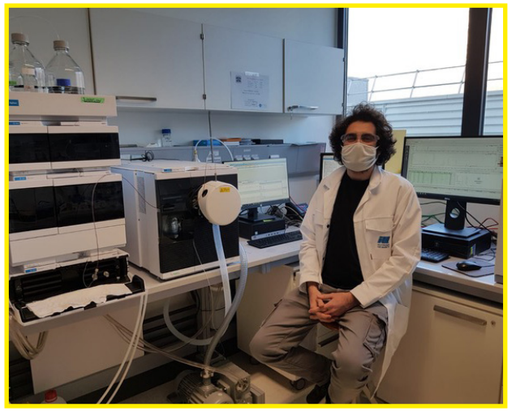

New L-Lab acquisition, a mass spectrometer, with student Giacomo Corucci very happy to use it!

The physico-chemical properties as well as the structure of membrane bilayers have been extensively characterised, initially by techniques available within the PSCM and later by neutron reflectivity techniques. Neutron characterisation of membrane mimics from these lipids include SANS from nano-discs, diffraction from stacked bilayers, reflectometry from mono- and bilayers, and inelastic scattering and spin-echo measurements from multilamellar vesicles. The GPLs currently available to internal scientists/students in quantities appropriate for neutron experiments can be found on the L-Lab website.

Future perspectives include the following: 1) separation of GPLs as a function of their chain length/unsaturation; and 2) extraction/separation of deuterated sugars, TAGs, DAGs and other metabolites. In the short-term, we will pursue these characterisation studies in two ways: 1) through the production of a library of pure PLs for soft matter studies of their properties and use in interactions with a variety of other molecules; and 2) by characterising contrast-matched, natural mixtures of PLs, providing a very physiologically relevant environment for biology studies of membrane proteins.

At the present time, no other facility can provide this service. Nevertheless, there is strong interest in this area and scientists at universities and other neutron centres have asked to collaborate with us. Scientist Krishna Batchu has brought unique expertise on site, and since his arrival three years ago enormous progress has been made. The platform is already handling several internal requests for deuterated GPLs and has been heavily involved in the preparation of samples for COVID19-related science during lockdown and throughout the summer. The service started to entertain requests from users at the beginning of 2021 (the February 2021 proposal round). Finally, it is worth mentioning that this work is part of the activities currently funded by LENS (League of advanced European Neutron Sources).

https://www.ill.eu/L-Lab

European collaborations

European collaboration has been an important part of the ILL's activities since its inception. In 2021, the Institute was involved in 17 European projects funded either by the H2020 research and innovation framework programme or EURATOM, both of which are administered by the European Commission. The benefits are not merely financial; the ILL also gains from the associated networks and resources, which improve its integration with other facilities and the user community.

Table 1 summarises EU project activity at the ILL.

FILL 2030 is a mono-beneficiary project, funded under the European Union's Horizon 2020 research and innovation programme and dedicated to ensuring the long-term sustainability of the ILL business model. Due to the pandemic the project was extended for six months, coming to an end in June 2021. The health crisis also halted several planned activities for reaching out to emerging user communities, with physical meetings found to be unrealistic even with the additional six months. Thus, we adapted our means of outreach and developed more online and digital tools—such as short promotional videos and featured webpages—to promote neutron imaging, remote access at the ILL, and so on.

Our offer to cover open-access fees for scientific publications, has been a huge success. The number of such publications has doubled: from an initial 40 up to 80. This was made possible by lower fees and internal budget shifts.

The newly developed bibliometric tool (PUMA) is a great help to both the management and the scientists at the ILL in terms of analysing the geographical and scientific spread of the user community. The initial target of matching publications linked to ILL experiments was achieved in 2020 and has been extended into 2021, ensuring good use of this statistical tool. PUMA has even been successfully transferred to a neighbouring institute. Both of us are now currently exploring ways to further develop it and eventually extend its use to other European institutions.

Thanks to FILL2030, we can now better identify and follow up new users in order to refuel our user community from new countries and new scientific domains. The number of transnational access days available to users from new non-member countries was fully exploited in 2021, thanks to the project's six-month extension; as a result of the lower number of reactor cycles and the predominant use of remote access mode in 2021, this extension was necessary to achieve our target of 50 days.

Table 1

Overview of EU project activity at the ILL.

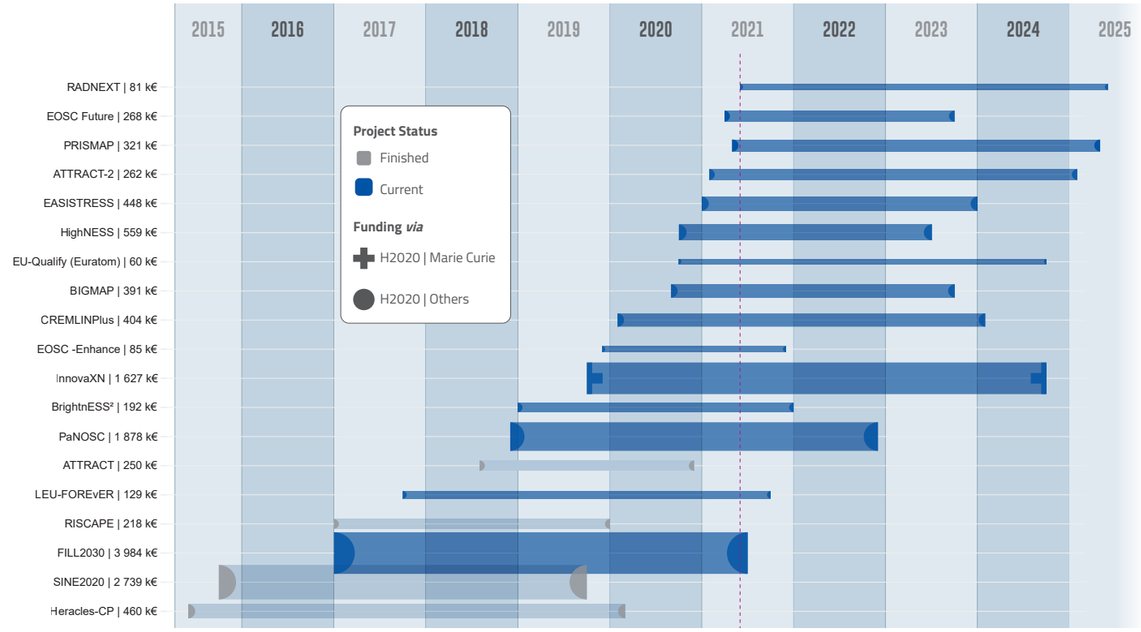

EUROPEAN PROGRAMMES

InnovaXN students on the EPN campus in October 2021. ©ESRF

PaNOSC (Photon and Neutron Open Science Cloud) is funded under the European Union's Horizon 2020 research and innovation programme. It provides joint policies, strategies and solutions for enabling open science through the adoption of FAIR principles. Since the project's start, in December 2018, six strategic European photon and neutron (PaN) sources (the ESRF, CERIC-ERIC, ELI-DC, ESS, XFEL and ILL) and the e-infrastructures EGI and GEANT have been collaborating to make FAIR data a reality at PaN facilities; this is being achieved by developing and providing services for scientific data and connecting them to the European open science cloud (EOSC).

In 2021, the PaNOSC partners started implementing the API (Application Programming Interface) at all PaNOSC partner sites. This search API allows datasets to be found based on relevant, domain-specific metadata. It can be used by third parties to find datasets that have been released from any facility-imposed embargo period or by the original researchers. Work is now underway to produce a joint data catalogue encompassing search results from all the partner sites. As well as providing a data catalogue, each facility will provide access to remote data analysis services, allowing users to analyse experimental data on remote desktops and Jupyter notebooks through a common data portal. A second iteration of the portal was completed at all partner sites during 2021. In addition to the remote desktops and Jupyter notebooks for data analysis purposes, the Virtual Infrastructure for Scientific Analysis (VISA) has been a huge success. VISA provides an effective platform for performing remote experiments at the ILL, using the NOMAD Remote client.

InnovaXN is a doctoral training programme, supported by the H2020 MSCA COFUND Programme, that brings together the expertise of large-scale research infrastructures with the R&D needs of European industry. In September 2021, the second cohort of 20 PhD students, made up of 11 different nationalities, started their projects on the doctoral programme InnovaXN managed by the ILL and the ESRF. Eleven of the students are being co-supervised by ILL scientists, academic partners and industrial researchers in various pre-competitive research projects dealing with chemical engineering, biotechnologies or energy storage. Following this second recruitment wave, 38 PhD students are now working on the EPN campus, while two further recruitment processes are underway.

The League of advanced European Neutron Sources (LENS), the strategic consortium of European neutron sources, acts as guide and advocate for the European neutron user community. It promotes neutron science as a fundamental component of European scientific research and innovation.

The two leagues of analytical infrastructures, LENS and LEAPS, have come together with five other networks—e-DREAM (electrons), LaserLab (lasers), RADIATE (ions), INSPIRE (protons) and EMFL (high-magnetic fields)—to create a new network named ARIE (Analytical Research Infrastructures In Europe). ARIE submitted a proposal in response to one of the additional calls for proposals issued at the end of Horizon 2020. These calls all had a strong link to the Green Deal, this particular one relating to the action 'European Research Infrastructures capacities and services to address European Green Deal challenges'. Unfortunately, the proposal was not accepted. However, this has not discouraged ARIE; learning from this experience it has since submitted another proposal, this one in response to the call for action on 'Research Infrastructures services enabling the development of materials for a circular economy'.

LENS celebrated the handover by the outgoing chair, Helmut Schober, to the incoming chair, Robert McGreevy, in March 2021. The following general assembly was held in June in virtual format. The autumn general assembly has been postponed until 2022, as three new directors have just taken over in the three LENS member facilities.

EIROforum

EIROforum brings together the eight flagship institutions of large-scale European research infrastructures. All EIROs are leaders in their field and work continuously to push back the frontiers, from the infinitely small to the infinitely large, of scientific knowledge. Created in 2002, EIROforum's mission is to enable its eight member organisations—the CERN, EMBL, ESA, ESO, ESRF, European XFEL, EUROfusion and the ILL—to pool their resources and expertise in support of European science. By promoting the exchange of know-how and best practice, EIROforum makes a major contribution to enhancing scientific collaboration in Europe.

The EIROforum DGs meeting was held in Grenoble on 15 and 16 November.

TRAINING AND OUTREACH

STUDENT TRAINING

The ILL Graduate School has grown in strength over the past few years as the ILL PhD programme has evolved and improved. It continues to provide training and finance for the equivalent of about 40 full-time, three-year-PhD students from various member countries. It also receives a number of PhD students with external funding. A total of 20 ILL PhD students began their doctoral work in 2021, 12 of whom were recruited as part of the 'second wave' of the InnovaXN PhD programme financed by the EU *via* the Marie Sklodovska Curie Actions COFUND programme. InnovaXN projects differ from the ILL's regular PhD projects in that each includes an industrial partner, and naturally our InnovaXN projects have *Innova*-tive industrial applications (hence the name). Besides extensive provision for PhD student courses and training (including transferable skills), an important aspect of the programme is that each InnovaXN student spends at least three months of internship working at their industrial partner's site during their PhD work. The five-year InnovaXN programme provides three years of doctoral funding for two recruitment rounds of 10 PhD students each, to both the ILL and the ESRF, meaning that a total of 40 PhD students are currently benefitting from the InnovaXN programme on the EPN campus.

Given the success of InnovaXN, continued constraints as a result of the COVID-19 pandemic, the ILL's budgetary plans and the year-long shutdown of the ILL reactor throughout 2022, we decided not to call for PhD project applications within the regular PhD programme in autumn 2021. Nevertheless, we fully anticipate reinstating our yearly call for PhD projects in autumn 2022. Successful candidates would then begin work at the ILL in autumn 2023, when the first wave of InnovaXN students finishes their work.

The International Summer School for undergraduate students, organised by the ILL and the ESRF every year since 2014, allows undergraduate students from all our member countries to spend a month on site. The students follow a series of lectures and seminars on the fundamentals of X-rays and neutrons and their use in science today. Unfortunately, the 2020 school was cancelled because of the health crisis in Europe.

NEUTRON SCATTERING SCHOOLS

The **Hercules School**, co-ordinated by the Université Grenoble Alpes, has been held every year since 1991. It consists of a five-week course on neutron and synchrotron radiation for condensed matter studies aimed at students and young scientists. The course includes lectures, hands-on practicals and tutorials in small groups, a poster session and visits to partner facilities including the ILL.

The 2021 session took place from 22 February to 26 March and attracted 135 applicants. Of those, 90 students comprising 33 nationalities from 21 countries were selected; most came from Europe, while a few came from India, Iran, Mexico, Pakistan, Russia, Rwanda and Taiwan. Because of the COVID-19 pandemic, the 2021 school was run wholly online and included remote, hands-on practicals and tutorials and virtual visits to large-scale facilities. The practicals and tutorials in Grenoble were held at the ILL, ESRF, CNRS, CEA and/or IBS. During the fourth week of the school, the students were split into four groups to pursue further remote training organised by our partner facilities: ALBA, European XFEL, Elettra/FERMI, SLS/SINQ and KIT. Participants attended about 85 hours of online lectures and 55 hours of online tutorials and practicals in total. Overall feedback on the school was extremely positive. More information is available at: **https://hercules-school.eu/**

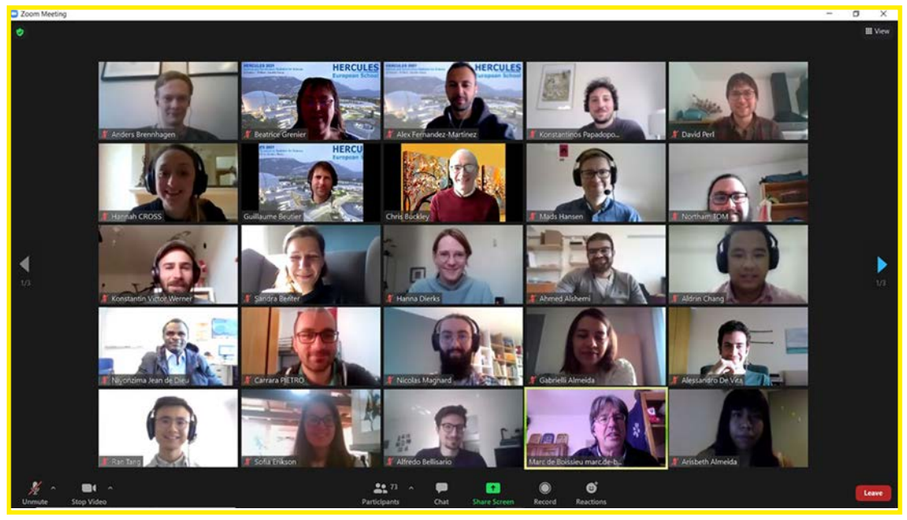

Visit of the ILL facilities during the ILL–ESRF summer school.

The FANs, which stands for 'Formation à la Neutronique', is a popular school dedicated to neutron scattering techniques that has been running for more than twenty years. It is open to any young researcher working in a French laboratory and welcomes mostly PhD students and postdoctoral fellows. The school's programme mainly entails practicals on various neutron instruments, thereby complementing more academic summer schools such as those organised by the Société Française de la Neutronique (SFN). Historically organised at Saclay by the Laboratoire Léon Brillouin (LLB), the FANs practicals were carried out up to 2019 on the neutron scattering instruments installed at the Orphée reactor. The last FANs event was held shortly before the last shutdown of the Orphée reactor, in October 2019. After a one-year break in 2020 due to the COVID-19 pandemic, the FANs was organised again successfully at the ILL in October 2021, thanks to a fruitful collaboration between LLB, the 'Fédération Française de Diffusion Neutronique' (2FDN) and the ILL involving teachers from the three institutes.

During the 2021 FANs event (11–13 October), the two main scientific areas offered to students were Soft Matter and Biology, and Condensed Matter and Magnetism. Neutron beamtime was available for experiments on the ILL's small-angle diffractometer D33 and on three French CRG instruments: the time of flight (TOF) spectrometer SHARP, the powder diffractometer D1B and the three-axis spectrometer IN12. The first day of the school was devoted to a virtual tour of the ILL facility and to general introductory lectures on neutron scattering, for all students. The students were then split into two groups according to their main area of scientific interest and attended lectures on either small-angle scattering and TOF spectroscopy or neutron elastic and inelastic scattering. The last two days were dedicated to practicals performed on the SHARP, D1B and D33 instruments. In all, 15 students attended the school this year. The casual and friendly atmosphere provided an excellent learning environment for students starting their PhD and keen to come back to the ILL or other large-scale neutron facilities!

Participants of the FANs 2021 session at the ILL.

WORKSHOPS AND EVENTS

KEEP **UP-TO-DATE**:

facebook.com/ILLGrenoble
twitter.com/ILLGrenoble
linkedin.com/company/institut-laue-langevin

10
SCIENTIFIC EVENTS
WORKSHOPS
SCHOOLS AND
CONFERENCES

22
GENERAL
SEMINARS
AND
COLLOQUIA **3**

ILL Chronicle **2021**

29–31 MARCH
Subcommittee and ILL Scientific Council virtual meetings

11–12 MAY
Meeting of the Subcommittee on Administrative Questions (SAQ)

17–18 MAY
EIROforum General Assembly
(last one under the ILL's chairmanship)

7–8 JUNE
LENS General Assembly (last one under the ILL's chairmanship)

24 JUNE
Meeting of the ILL Steering Committee

15 SEPTEMBER
Signature of the 6th protocol by the governments of France, Germany and the UK

13 OCTOBER
Meeting of the Subcommittee on Administrative Questions (SAQ)

15 OCTOBER
Visit by the chairman of the ASN (Autorité de sûreté nucléaire)

4 NOVEMBER
ILL Scientific Council virtual meeting

15 NOVEMBER
EIROforum DG Assembly

17 NOVEMBER
Visit by Theo Rycroft, Deputy UK ambassador

24–25 NOVEMBER
Virtual meeting of the ILL Steering Committee

10 DECEMBER
Visit by Mrs Fraise, CNRS Regional Delegate, and her deputy, Mrs Achin

WORKSHOPS AND EVENTS

Scientific events

In 2021, the ILL organised (or co-organised) 10 scientific events (workshops, conferences and schools). In the same year a total of 22 general seminars were organised at the ILL, in addition to three colloquia. Because of the pandemic, most of these events were held remotely.

15–19 FEBRUARY
LENS Machine Learning School

22 FEBRUARY–26 MARCH
HERCULES European School

7–11 JUNE
7th EIROforum School on Instrumentation

5 SEPTEMBER–2 OCTOBER
International Summer Programme on Neutron and X-Ray Science for undergraduate students

11–13 OCTOBER
FAN School at LLB (Formation Annuelle à la Neutronique)

18–20 OCTOBER
Innovative inelastic neutron scattering, I2NS

24 NOVEMBER
Launch of the Grenoble Battery Hub

29–30 NOVEMBER
Mantid user workshop (Manipulation and Analysis Toolkit for Instrument Data)

LECTURE SERIES ON SOFT MATTER

27 MAY
Calorimetric methodologies: principles and applications

3 JUNE
Direct measurement of free energy derivatives: calorimetry and volumetry

10 JUNE
Introduction to classical particle-based simulations of soft matter

17 JUNE
Surfactant self-assembly—fundamentals and applications

24 JUNE
Thermodynamics of interfaces

8 JULY
Atomic Force Microscopy (AFM): working principles, modes of operation and applications

LENS WEBINARS SERIES

The LENS initiative[1] presents one live webinar roughly every month. The webinars are also streamed live to the LENS website, where they are recorded and archived.

Currently, the webinars alternate between two themes: how neutron science contributes to the fight against global health threats; and new directions in neutron instrumentation.

The complete list can be found here

https://www.lens-initiative.org/2020/06/02/lens-webinars/

GLOBAL HEALTH THREATS

4 MARCH 2021
- Elucidating amyloid aggregation mechanisms behind neurodegenerative diseases
- Co-assembly of lipids and the amyloid protein alpha-synuclein
- Structural bases of Huntington's Disease pathological threshold: an integrative structural biology approach

25 MARCH 2021
Drug development & drug delivery systems
- Targeting the heart of a virus: design of SARS-CoV-2 main protease inhibitors using X-rays, neutrons and computation
- Lipid nanoparticles for mRNA delivery: using neutron scattering for their successful redesign

NEW DIRECTIONS IN INSTRUMENTATION

11 FEBRUARY 2021
- Exploring the potential of neutron imaging and diffraction techniques on IMAT instrument at ISIS, UK

27 MAY 2021
- Ultra-high field magnets for neutron scattering: latest developments and possibilities

10 JUNE 2021
- The Wolter optics-based neutron microscope

[1] The League of advanced European Neutron Sources (LENS) is a not-for-profit consortium working to promote co-operation between European-level neutron infrastructure providers offering transnational user programmes to external researchers. More on p.111.

A year in photos

1.


2.


3.


4.


5.


6.


7.


8.

1. The 7th edition of the EIROforum School of Instrumentation was run by the ILL and the ESRF as a virtual event this year.
2. ILL–ESRF international summer school 2021.
3. Participants of the FANs–LLB school, in October.
4. Visit by the Chairman of the ASN on 15 October.
5. The I2NS conference was held in Autrans (Grenoble region) in October.
6. The ILL50 building (left) – the new ILL entry point.
7. The EIROforum DGs meeting.
8. Visit by Theo Rycroft, deputy UK ambassador, on 17 November.

FACTS AND FIGURES

105 M€
ANNUAL INCOME*

* 68 % FROM THE ASSOCIATES AND 19 % FROM SCIENTIFIC MEMBER COUNTRIES

920
DISTINCT VISITORS FROM **27 COUNTRIES** IN 2021

544
PUBLICATIONS RECORDED IN 2021

563
MEMBERS OF STAFF

KEEP **UP-TO-DATE**:

facebook.com/ILLGrenoble
twitter.com/ILLGrenoble
linkedin.com/company/institut-laue-langevin

STAFF ON 31/12/2021

563.2 people, including 76.75 experimentalists in the scientific sector and 56.5 thesis students.

393.5 French; 38.5 German; 28.5 British; 59.5 scientific participating countries; and 43.25 others.

Nationality		**%**
French	393.5	69.86 %
German	38.5	6.84 %
British	28.5	5.06 %
Member countries	59.5	10.56 %
Others	43.25	7.68 %
Total	**563.2**	**100.00 %**

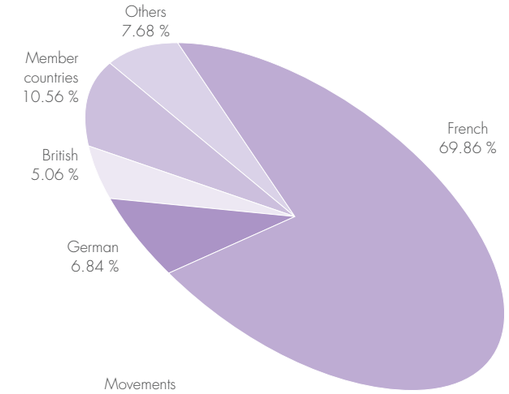

IMPLEMENTATION BUDGET 2021:
105.40 M€ (excluding taxes)

Income	**M€**	**%**
Income from Associates (incl. Endurance Programme and additional nuclear tax and insurance)	71.82	68.14 %
Income from Scientific Members	20.38	19.34 %
Own income	4.37	4.14 %
Carry forward from 2020	0.37	0.35 %
Movements from reserve and use of cash flow	8.22	7.80 %
Contribution from local authority	0.25	0.24 %
Total	**105.40**	**100.00 %**

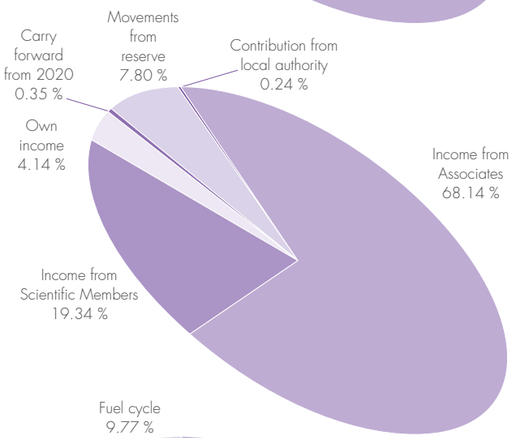

Expenditure	**M€**	**%**
Staff costs	51.60	48.96 %
Operating costs	21.52	20.42 %
Investment costs	21.97	20.85 %
Fuel cycle	10.30	9.77 %
Total	**105.39**	**100.00 %**

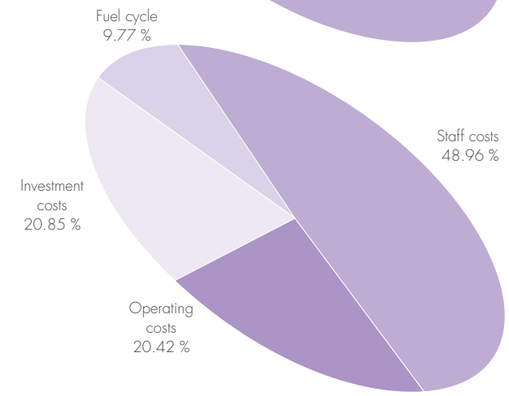

PURCHASING STATISTICS (JANUARY-AUGUST 2021)

	M€	**%**
France	14.06	69.16 %
Germany	1.55	7.62 %
United Kingdom	0.73	3.59 %
Scientific Members	3.50	17.22 %
Others	0.49	2.41 %
Total	**20.33**	**100.00 %**
France captive market	6.12	23.14 %
Total captive/non-captive	**26.45**	**0**

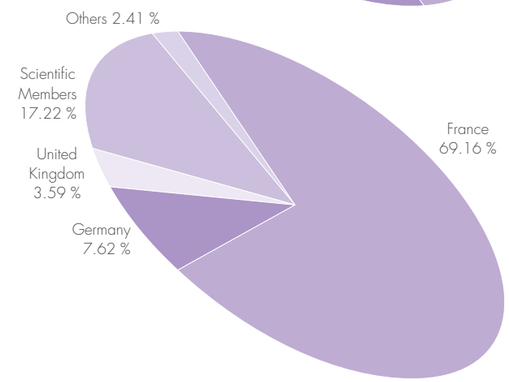

FACTS AND FIGURES

NAME
Institut Max von Laue-Paul Langevin (ILL)

FOUNDED
19 January 1967

Intergovernmental Convention between France, Germany and United Kingdom (19/07/1974)

ASSOCIATES
France

Commissariat à l'Energie Atomique et aux Energies Alternatives (CEA)

Centre National de la Recherche Scientifique (CNRS)

Germany

Forschungszentrum Jülich (FZJ)

United Kingdom

United Kingdom Research & Innovation (UKRI)

COUNTRIES WITH SCIENTIFIC MEMBERSHIP
Spain
MCIN Ministerio de Ciencia e Innovación

Switzerland
Staatssekretariat für Bildung, Forschung und Innovation (SBFI)

Italy
Consiglio Nazionale delle Ricerche (CNR)

Belgium
Belgian Federal Science Policy Office (BELSPOL)

Sweden
Swedish Research Council (VR)

Denmark
Danish Agency for Science and Higher Education

Poland
(NDPN) Consortium of Polish Scientific and Research Institutions

Slovenia
The Slovenian National Institute of Chemistry

CENI (Central European Neutron Initiative)
Consortium composed of:

Austria: Österreichische Akademie der Wissenschaften
Czech Republic: Charles University, Prague
Slovakia: Comenius University, Bratislava

CONTRACTUALLY AGREED BEAMTIME SHARE FOR MEMBER COUNTRIES

Austria	2.500 %	
Czech Republic	0.750 %	
Slovakia	0.184 %	
Belgium	0.550 %	
Sweden	4.500 %	
Denmark	1.570 %	
Italy	1.300 %	
Switzerland	2.372 %	average over 5 years
Spain	4.500 %	average over 5 years
Poland	0.800 %	
Slovenia	0.150 %	

SUPERVISORY AND ADVISORY BODIES
Steering Committee, which meets twice a year

Subcommittee on Administrative Questions, which meets twice a year

Audit Commission, which meets once a year, and statutory auditor

Scientific Council with 9 Subcommittees, which meets twice a year

REACTOR
Operating 3 cycles in 2021
176 days in total, average power (p.102)

EXPERIMENTAL PROGRAMME
1 435 ILL and CRG experiments
(of which 550 accepted by the Subcommittees)
1 413 user visits (920 distinct visitors) from 27 countries

Publications in 2021

In 2021, the ILL received notice of 544 publications (published in 2020 or 2021), 139 of which were published in high-impact journals.

They are listed on the ILL website:
https://www.ill.eu/about-the-ill/documentation/scientific-publications/scientific-publication-list

THE DISTRIBUTION BY SUBJECT IS AS FOLLOWS

Applied Physics, Instrumentation and Techniques	37
Biology	50
Crystallography and Chemistry	56
Liquids and Glasses	20
Magnetic Excitations	39
Magnetic Structures	80
Materials Science and Engineering	52
Medicine	10
Nuclear and Particle Physics	57
Soft Condensed Matter	107
Spectroscopy in Solid State Physics and Chemistry	21
Theory	15

ILL PHD STUDENTSHIPS

Full-time-equivalent ILL-funded PhD projects in 2021	40
PhD students working on ILL PhD projects in 2021	65*
Successfuly defended ILL PhD theses in 2021	15

* includes PhD projects that are co-funded or completely externally funded.

ORGANISATION CHART IN AUTUMN 2021

REVIEW PANELS

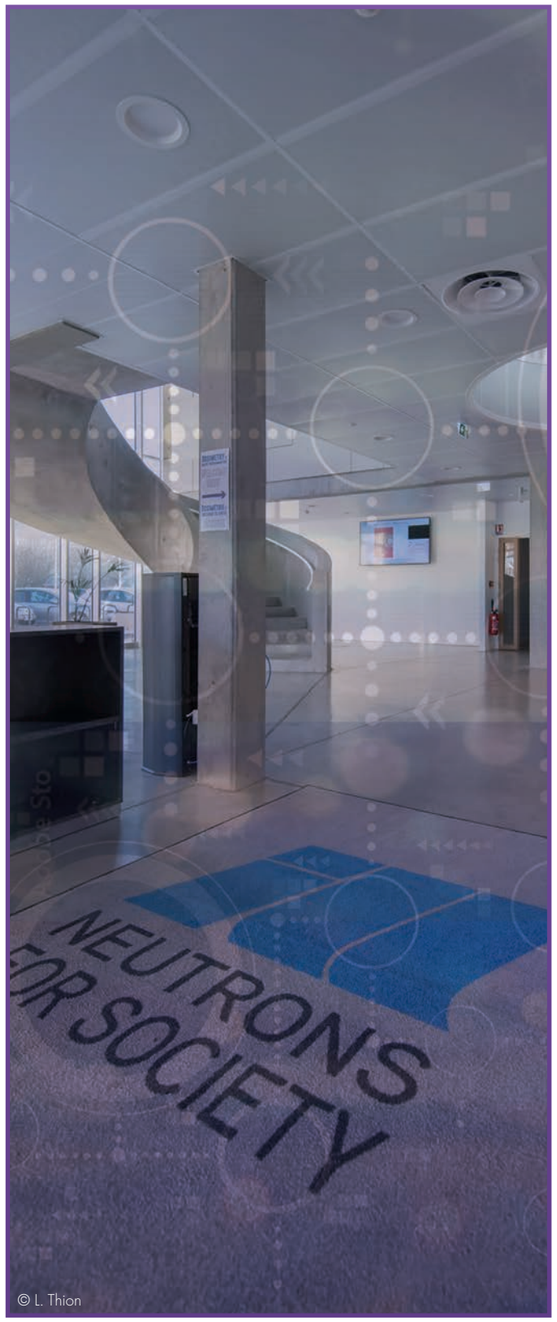

© L. Thion

Key
Chair/focus group Chair
ILL college secretary/focus group secretary
ILL specialist

REVIEW PANELS

APPLIED METALLURGY, INSTRUMENTATION AND TECHNIQUES
M. Strobl (PSI, Switzerland)
L. Helfen
T. Pirling/L. Porcar/G. Cuello/A. Tengattini

NUCLEAR AND PARTICLE PHYSICS
G. Pignol (LPSC, France)
Y.H. Kim
T. Soldner

MAGNETIC EXCITATIONS
H. Walker (STFC, UK)
U.B. Hansen
P. Steffens

CRYSTALLOGRAPHY
M. Widenmeyer (TU Darmstadt, Germany)
L. Cañadillas-Delgado
T. Hansen

MAGNETIC STRUCTURES
A. Gibbs (ISIS, UK)/
D. Lott (GKSS Forschungszentrum, Germany)
K. Beauvois/O. Fabelo Rosa
T. Saerbeck

STRUCTURE AND DYNAMICS OF LIQUIDS AND GLASSES
P. Huber (Hamburg University of Technology, Germany)
M. Appel
M.M. Koza

SPECTROSCOPY IN SOLID STATE PHYSICS AND CHEMISTRY
F. Juranyi (PSI, Switzerland)
J. Ollivier
P. Fouquet

STRUCTURE AND DYNAMICS OF BIOLOGICAL SYSTEMS
J. Lawrence (Manchester University, UK)
O. Matsarskaia
M. Blakeley/J. Peters

STRUCTURE AND DYNAMICS OF SOFT CONDENSED MATTER
E. Dubois (Pierre and Marie Curie University, Paris, France)/
A. Zarbakhsh (University of London, UK)
S. Prevost/A. Maestro
O. Czakkel/P. Gutfreund – R. Schweins (obs)

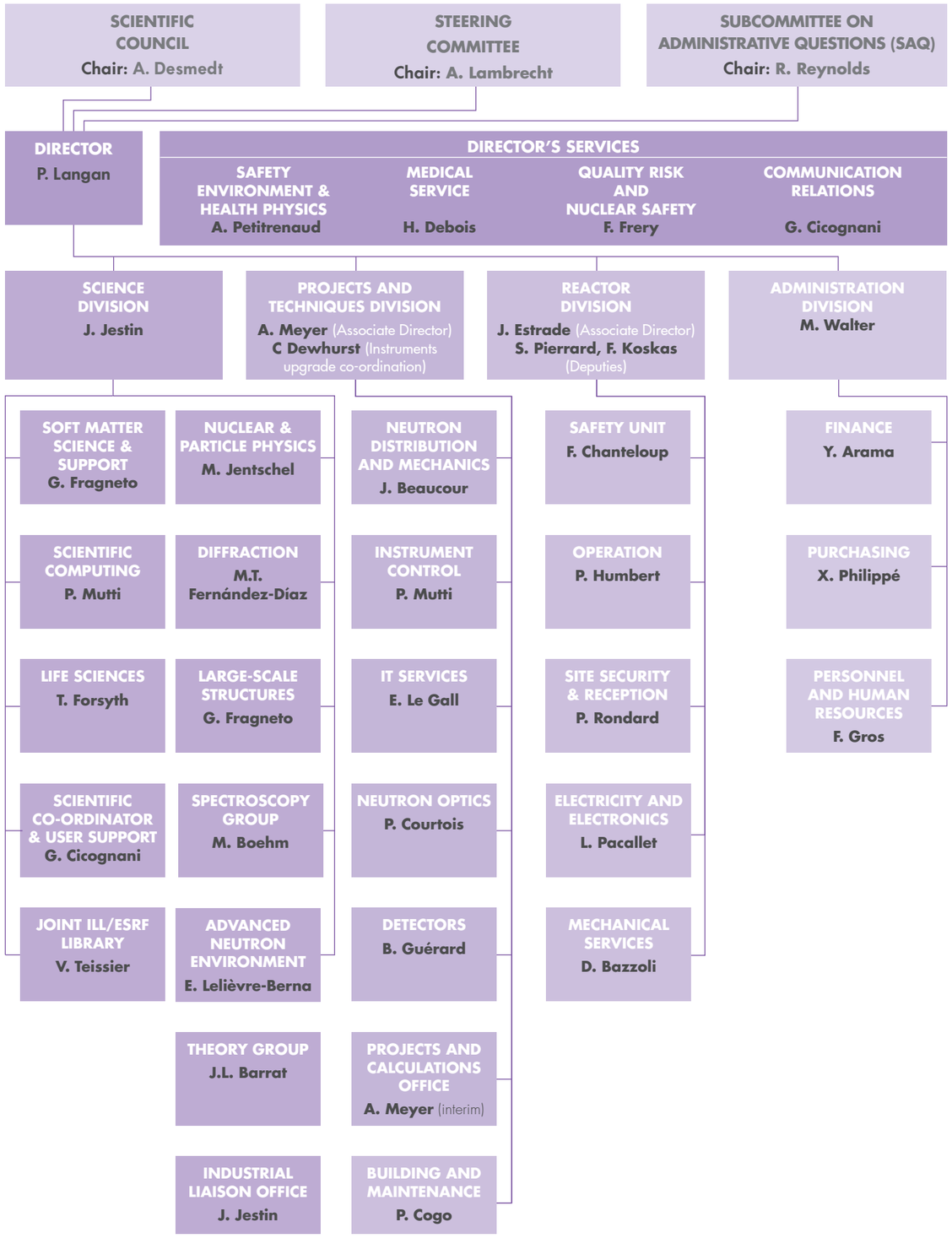

71, avenue des Martyrs
38000 Grenoble
France
www.ill.eu

FSC This report has been printed using FSC certified paper **www.fsc.org**